DISSERTATION

# INVESTIGATING THE SALINITY IMPACTS ON CURRENT AND FUTURE WATER USE AND CROP PRODUCTION IN A SEMI-ARID AGRICULTURAL WATERSHED

Submitted by

Pardis Hosseini Ghasemabadian

Department of Civil & Environmental Engineering

In partial fulfilment of the requirements

For the Degree of Doctor of Philosophy

Colorado State University

Fort Collins, Colorado

Summer 2024

Doctoral Committee:

Advisor: Ryan T. Bailey

Mazdak Arabi
Ryan Smith
Allan Andales

ABSTRACT

INVESTIGATING THE SALINITY IMPACTS ON CURRENT AND FUTURE WATER USE AND CROP PRODUCTION IN A SEMI-ARID AGRICULTURAL WATERSHED

Soil salinity can have a significant impact on agricultural productivity and crop yield, particularly in arid and semi-arid irrigated watersheds wherein irrigation and inadequate drainage often combine to increase salt ion concentrations in soil water. In conjunction with intense irrigation in semi-arid agricultural regions, increasing population resulting in boosted water demand, adverse impacts of climate change on water availability, in other words, water scarcity, future land use and land cover changes, changes in applied irrigation practices, and introducing new point-sources and non-point sources of salinity in the region all can govern the salinity and crop yield consequently. Taking into account the aforementioned impactful components on crop reduction via salinity increase, the overall objective of this dissertation is to provide insights for policymakers to better address the current and future salinity issues to sustain crop production in semi-arid regions under progressive salinity. This will be accomplished by i) investigating the controlling factors on salinity in the soil, groundwater, and river water using the SWAT-Salt model which simulates the reactive transport of 8 major salt ions in major hydrological pathways applied to a 1118 $km^2$ irrigated stream-aquifer system located within the Lower Arkansas River Valley (LARV) in southeastern Colorado, USA ii) Assessing the salinity impacts on crops production blue and green water footprint as a measurable indicator for water being used per unit of a given crop production using the SWAT-MODFLOW-Salt model applied to a 732 $km^2$ irrigated stream-

aquifer system located in the LARV, iii) quantify the impact of environmental factors alteration including changes in climatic and irrigation practices in the LARV on future salinity content and its impact on crop production in the region using the SWAT-MODFLOW-Salt model.

To control salinity, more importantly in semi-arid irrigated areas, the principal step is to identify the key environmental and hydrologic factors that govern the fate and transport of salts in these irrigated regions. To accomplish this objective, global sensitivity analysis was applied to the newly developed SWAT-Salt model (Bailey et al., 2019), which simulates the reactive transport of 8 major salt ions ($SO_4$, Ca, Mg, Na, K, Cl, $CO_3$, and $HCO_3$) in major hydrologic pathways in a watershed system. The model was applied to a saline 1118 $km^2$ irrigated stream-aquifer system located within the Lower Arkansas River Valley in southeastern Colorado, USA. Multiple parameters including plant growth factors, stream channel factors, evaporation factors, surface runoff factors, and the initial mass concentrations of salt minerals $MgSO_4$, $MgCO_3$, $CaSO_4$, $CaCO_3$, and NaCl in the soils and in the aquifer were investigated for control on salinity in groundwater, soils, and streams. The Morris screening method was used to identify the most sensitive factors, followed by the Sobol' variance-based method to provide a final ranking and to identify interactions between factors. Results showed that salt ion concentration in soils and groundwater was controlled principally by hydrologic factors (evaporation, groundwater discharge and up flux, and surface runoff factors) as well as the initial amounts of salt minerals in soils. Salt concentration in the Arkansas River was governed by similar factors, likely due to salt ion mass in the streams controlled by surface runoff and groundwater discharge from the aquifer.

Sustainable agriculture in intensively irrigated watersheds, especially those in arid and semi-arid regions, requires improved management practices to sustain crop production. This depends on factors such as climate, water resources, soil conditions, irrigation methods, and crop types. Of

these factors, soil salinity and climate change are significant challenges to agricultural productivity. To investigate the long-term impact of salinity and climate change on crop production from 1999 to 2100 in irrigated semi-arid regions, we applied the water footprint (WF) concept using the hydro-chemical watershed model SWAT-MODFLOW-Salt, driven by five General Circulation Models (GCMs) and two climate scenarios (RCP4.5 and RCP8.5), to a 732 $km^2$ irrigated stream-aquifer system within the Lower Arkansas River Valley (LARV), Colorado, USA. In this study we estimated the green ($WF_{green}$), blue ($WF_{blue}$), and total ($WF_{total}$) crop production WFs for 29 crops in the region, both with and without considering the impact of salinity on crop yield. The results indicate that during the baseline period (1999-2009), the total annual average $WF_{green}$, $WF_{blue}$, and $WF_{total}$ increased by 7.6%, 4.4%, and 6.5%, respectively, under salinity stress, with crop yields decreasing by up to 4.6%, 1.6%, and 2.3% for green, blue, and total crop yield. The combined impact of salinity and the worst-case climate model (IPSL_CM5A_MR) under the higher emission scenario (RCP8.5) resulted in increases of 3.3%, 1.9%, and 3% in green, blue, and total crop production WFs. Additionally, the study found that the proportion of green, blue, and total crop production WFs in the LARV exceeded the world average. This discrepancy was attributed to various factors, including different spatial and temporal crop distribution, irrigation practices, soil types, and climate conditions. Notably, salinity stress had a more significant impact on green crop yield and green WF compared to blue crop yield and blue WF across all GCM models. This finding highlights the need to prioritize management practices that address salinity-associated challenges in the region.

The adverse effects of salinity on soil health, crop yield, and environmental ecosystem require comprehensive strategies for managing salinity in agricultural watersheds by adopting improved irrigation practices and effective salinity management strategies for mitigating these impacts and

sustaining agricultural productivity in salinity-affected regions. The complex dynamics between various irrigation practices and soil salinity play a pivotal role in shaping agricultural productions and managing soil salinity. In semi-arid regions like the LARV, salinity poses a significant threat to agriculture, exacerbated by climate change and historic irrigation practices. To evaluate the interplay between salinity, climate change, and irrigation management in affecting crop yields within the Lower Arkansas River Valley (LARV), focusing on corn and alfalfa, we utilized the SWAT-MODFLOW-Salt model to examine how changes in irrigation management influence crop production under various scenarios projected through the year 2100. This study addresses the differential responses of corn and alfalfa to the impact of incremental increases and reductions in irrigation efficiency and irrigation water loss (5%, 10%, 15%, and 20%) on corn and alfalfa yields dynamics under salinity stress, utilizing projections from five global climate models under two distinct Representative Concentration Pathway (RCP) scenarios, RCP4.5 and RCP8.5 and two irrigation scenarios.

The findings from irrigation practice scenario (1), maintaining a constant amount of irrigation water, revealed that corn yields improved by up to 13.8% under salinity stress and 16.5% under non-salinity conditions with a 20% increase in irrigation efficiency and a 20% reduction in water loss under RCP4.5. Alfalfa, demonstrating greater salinity tolerance, showed similar benefits, with yield increases of 9.1% under salinity stress and even higher improvements under non-salinity conditions. These results highlight the effectiveness of tailored irrigation practices in mitigating environmental stresses. In contrast, scenario (2), which involved reducing irrigation water by half, resulted in more pronounced negative outcomes. Corn yields exhibited greater sensitivity to salinity stress, with yield reductions ranging from -9.8% under salinity stress to -9.3% under non-salinity conditions, particularly under the RCP8.5 scenario. Alfalfa yields also declined, though

less severely than corn, with reductions ranging from -8.9% under salinity stress to -8.3% under non-salinity conditions. Despite improvements in irrigation efficiency and reduced water loss, the adverse effects of salinity stress were not fully mitigated in scenario (2), emphasizing the need for adequate water availability to sustain crop yields under salinity and climate change pressures. The research highlights the importance of adopting advanced irrigation technologies and practices that not only counteract the adverse effects of salinity but also adapt to evolving climatic conditions. This study offers valuable insights for policymakers and agricultural managers on strategic water resource management to sustain crop yields in salinity-affected and water-limited agricultural systems.

The results of this study can be used in decision-making regarding the most impactful land and water management strategies for controlling salinity transport and build-up in soils, both for this watershed and other similar semi-arid salinity-impacted watersheds for present and future purposes.

# ACKNOWLEDGMENTS

I am immensely grateful for the support and guidance I have received throughout my PhD journey, and I would like to express my deepest appreciation to those who have made this endeavor both possible and rewarding.

First and foremost, I extend my sincere thanks to my advisor, Dr. Ryan T. Bailey, whose expertise and insightful guidance have been instrumental throughout my research. His patience, profound knowledge, and meticulous attention to detail have significantly shaped my academic growth. Dr. Bailey's encouragement has been a steadfast pillar during my PhD studies.

I am also deeply thankful to the members of my committee: Dr. Mazdak Arabi, Dr. Allan Andales, and Dr. Ryan Smith. Their constructive feedback and valuable suggestions have greatly enriched my dissertation. Their willingness to share their time and expertise with me has been crucial to both my academic and personal growth.

My heartfelt gratitude goes to my family, whose love and encouragement have been my constant source of strength. I thank my parents and my brother, Payam, for their unwavering belief in my potential and their boundless support through all my pursuits. Their faith in me has been a continuous source of motivation and resilience.

I would also like to extend my special thanks to my groupmates, Dr. Soheil Nozari and Dr. Fatemeh Aliyari, for their support and camaraderie throughout this journey.

Lastly, I am thankful to my best friend, Ibrahim Bouzaid, for his enduring friendship and support. His companionship and reassurance were comforting and uplifting during the most challenging phases of this journey.

I am immensely thankful to everyone mentioned here, whose support has been vital to my success. This journey would not have been the same without your belief in me and your invaluable encouragement.

TABLE OF CONTENTS

LIST OF TABLES

LIST OF FIGURES

# Chapter 1. INTRODUCTION AND OBJECTIVES

## 1.1 INTRODUCTION

Global population growth, projected to reach 10 billion by 2050, combined with climate change, environmental stressors, human activities, and pollution, will likely reduce water resources and increase freshwater demand by one-third. This trend underscores the necessity for sustainable water resources and food production. Agriculture, which uses 85% of global water consumption, will face heightened pressure, especially in arid and semi-arid regions already experiencing water stress (FAO, 2017; Casella et al., 2019).

To sustain crop production, securing water resources and addressing yield-reducing factors, especially in vulnerable regions, is crucial. In arid and semi-arid areas, soil salinity—worsened by saline irrigation, synthetic fertilizers, and salt minerals—significantly reduces crop yields by accumulating salts in the root zone (Bailey et al., 2019; Gates et al., 2002; Hosseini and Bailey, 2022; Skrzypek et al., 2013; Zörb et al., 2019). Climate change further exacerbate this issue by causing drier conditions and higher temperatures, degrading irrigation water quality, and limiting the flushing of salt from the root zone (Haj-Amor and Bouri, 2020; Mukhopadhyay et al., 2021). The primary drivers of salinity in agricultural regions include using saline water for irrigation, inadequate drainage systems, and high evaporation rates that concentrate salts in the soil. Climate change intensifies these negative factors by altering precipitation patterns, increasing drought frequency, and raising temperatures. Therefore, effective salinity management is essential for sustainable agriculture and securing water resources for future generations. Understanding the physical and chemical characteristics of a watershed system that influence salt movement and salinity levels in soils, aquifers, and rivers is crucial for developing effective salinity management

strategies. Integrated approaches combining efficient irrigation techniques, proper drainage systems, and salt-tolerant crops are essential for mitigating salinity's adverse effects (Munns & Tester, 2008). However, the complex interplay between salinity, water management, and agricultural productivity in semi-arid regions presents significant challenges to sustainable agriculture and effective water resource management. The Lower Arkansas River Valley (LARV) in Colorado, USA, characterized by intensive agricultural activities and a semi-arid climate, is particularly vulnerable to these issues. The region relies heavily on irrigation to support its agriculture, making it susceptible to salinity problems. Climate change adds further threats to the LARV, with projections indicating increased temperatures and altered precipitation patterns that could worsen existing salinity issues by increasing evapotranspiration rates, leading to greater salt accumulation in soils. Therefore, addressing these challenges requires a comprehensive water management approach that integrates modern irrigation practices, climate resilience, and salinity mitigation strategies.

## 1.2. OBJECTIVES

Given the complex challenges outlined, this dissertation aims to deepen the understanding of how improved irrigation management practices can mitigate salinity impacts while enhancing water efficiency and agricultural productivity. The specific objectives are structured to explore strategic interventions that can potentially mitigate the adverse effects of salinity and optimize water use under varying climatic conditions.

1. Identify the key hydrological and environmental system parameters influencing soil salinity, groundwater salinity, and streamwater salinity in a semi-arid irrigated watershed.

2. Assess and quantify the combined impacts of soil salinity and climate change on the green, blue, and total water footprint (WF) of crop production in a semi-arid agricultural watershed using an integrated surface/subsurface hydro-chemical modeling approach.
3. Understanding the interplay between soil and groundwater salinity, climate change, and irrigation practices to provide insights into the most effective management practices for sustaining agricultural productivity of two major crops in the LARV, corn and alfalfa, by utilizing the newly developed comprehensive SWAT-MODFLOW-Salt model.

The study area is located in the Lower Arkansas River Valley (LARV) in southeastern Colorado, covering an area of approximately 732 $km^2$. Due to the semi-arid climate, high evapotranspiration rates, and low average annual precipitation, agriculture in the LARV depends heavily on irrigation. Soil salinity is a major issue in the LARV, caused by the dissolution of existing salt minerals in the soil, irrigation with saline water from the Arkansas River and the aquifer, and the hyper-concentration of salinity in the shallow subsurface brought by groundwater. Excessive irrigation, canal seepage, and inadequate drainage have resulted in shallow groundwater levels, leading to increased soil salinity and reducing crop yields by 20% over the past few decades (Burkhalter et al., 2005; Gates et al., 2002; Morway and Gates, 2012).

Each objective serves as the foundation for a journal article. The first objective is detailed in the article titled " Investigating the controlling factors on salinity in soil, groundwater, and river water in a semi-arid agricultural watershed using SWAT-Salt." published in Science of the Total Environment (STOTEN) Journal (Hosseini and Bailey, 2022). The second objective is covered in the article "Mutual impact of salinity and climate change on crop production water footprint in a

semiarid agricultural watershed: Application of SWAT-MODFLOW-Salt" currently under review by Science of the Total Environment (STOTEN) Journal (Hosseini and Bailey, 2024).

## REFERENCES


Bailey, R.T., Tavakoli-Kivi, S., Wei, X., 2019. A salinity module for SWAT to simulate salt ion fate and transport at the watershed scale. Hydrol. Earth Syst. Sci. 23, 3155–3174.

Burkhalter, J.P., Gates, T.K., 2005. Agroecological impacts from salinization and waterlogging in an irrigated river valley. J. Irrig. Drain. Eng. 131 (2), 197–209.

Casella, P., De Rosa, L., Salluzzo, A., De Gisi, S., 2019. Combining GIS and FAO's crop water productivity model for the estimation of water footprinting in a temporary river catchment. Sustainable Production and Consumption 17, 254–268.

FAO. 2017. The future of food and agriculture – Trends and challenges. Rome., 2017.

Gates, T.K., Burkhalter, J.P., Labadie, J.W., Valliant, J.C., Broner, I., 2002. Monitoring and modeling flow and salt transport in a salinity-threatened irrigated valley. J. Irrig. Drain. Eng. 128 (2), 88–99.

Haj-Amor, Z., Bouri, S., 2020. Use of HYDRUS-1D–GIS tool for evaluating effects of climate changes on soil salinization and irrigation management. Archives of Agronomy and Soil Science 66, 193–207.

Hosseini, P., Bailey, R.T., 2022. Investigating the controlling factors on salinity in soil, groundwater, and river water in a semi-arid agricultural watershed using SWAT-Salt. Science of the Total Environment 810.

Morway, E.D., Gates, T.K., 2012. Regional assessment of soil water salinity across an intensively irrigated river valley. J. Irrig. Drain. Eng. 138 (5), 393–405.

Mukhopadhyay, R., Sarkar, B., Jat, H.S., Sharma, P.C., Bolan, N.S., 2021. Soil salinity under climate change: Challenges for sustainable agriculture and food security. Journal of Environmental Management 280, 111736.

Munns, R., Tester, M., 2008. Mechanisms of Salinity Tolerance. Annual Review of Plant Biology 59, 651–681. https://doi.org/10.1146/annurev.arplant.59.032607.092911.

Skrzypek, G., Dogramaci, S., Grierson, P.F., 2013. Geochemical and hydrological processes controlling groundwater salinity of a large inland wetland of Northwest Australia. Chem. Geol. 357, 164–177.

Zorb, C., Geilfus, C.M., Dietz, K.J., 2019. Salinity and crop yield. Plant Biol. 21, 31–38.

# Chapter 2. INVESTIGATING THE CONTROLLING FACTORS ON SALINITY IN SOIL, GROUNDWATER, AND RIVER WATER IN A SEMI-ARID AGRICULTURAL WATERSHED USING SWAT-SALT[1]

## 2.1. INTRODUCTION

Salinity in arid and semi-arid irrigated watersheds can have a large impact on crop yield (Zorb et al., 2019) due to the adverse effect of soil salinity on crop root water uptake and subsequent crop growth. The degree of yield reduction that occurs depends on crop types, with some crops more salt tolerant than others (Mass and Grattan, 1999). However, the predominant crop species used in modern agriculture are salt sensitive (glycophytes) and can only tolerate limited salt concentration in their growth media: once the salinity thresholds are exceeded, crop yields are affected and productivity is reduced correspondingly (Gates et al., 2002; Singh, 2005; Schoups et al., 2005; Jalali, 2007; Chen et al., 2010; Skrazypek et al., 2013; Panta et al., 2014). Therefore, management strategies to control salinity in watershed systems are essential.

A key to identifying effective salinity management strategies is to understand the physical and chemical features of a watershed system that govern the movement of salt and resulting salinity concentration in soils, aquifers, and rivers. As salinity is composed of salt ions that each have different sources (e.g., various salt minerals) and fate pathways (e.g., chemical reactions), understanding the control on each individual ion can also assist in identifying effective management practices.

---

[1] *As published in*: Hosseini, P., Bailey, R.T., 2022. Investigating the controlling factors on salinity in soil, groundwater, and river water in a semi-arid agricultural watershed using SWAT-Salt. Science of the Total Environment 810. https://doi.org/10.1016/j.scitotenv.2021.152293

Although hundreds of studies have been performed to study the effect of soil salinity on crop yield (e.g., Rogers, 2002; Katerji et al., 2003; Misra and Mishra, 2007; Jalali, 2007; Lorenzen et al., 2012; Xiao et al., 2015; Machado and Serralheiro, 2017; Chidambaram et al., 2018, Zorb et al., 2019; Tomaz et al., 2020), comparatively few studies have investigated the relative control of the system factors (e.g., hydrological inputs, hydrological processes, chemical reactions) on salinity in a watershed system. Of these studies, the majority have used field experiments to determine controls on salinity. These studies found that, depending on the region, the following features can govern groundwater salinity and salinity mobilization: irrigation canals and canal seepage (Misra and Mishra, 2007); groundwater level fluctuations (Lorenzen et al., 2012); evaporation in a dry climate (Jalali, 2007; Misra and Mishra, 2007; Lorenzen et al., 2012; Xiao et al., 2015); chemical reactions such as salt mineral dissolution, ion exchange, and weathering (Jalali, 2007; Xiao et al., 2015; Chidambaram et al., 2018); seawater intrusion (Chidambaram et al., 2018); and anthropogenic sources (Chidambaram et al., 2018).

Some studies on the other hand have focused on investigating the controlling factors in soil water salinity and demonstrated that topography in terms of elevation, climate and hydrological conditions, and land use changes are major factors that govern the transport and accumulation of salts in the soil water in the watershed. Considering irrigated croplands, agricultural irrigation, crop sequences, fertilizer, intensive farming, evaporation and transpiration (Zanchi and Cecchi, 2010; Wang et al., 2018; Zhang et al., 2021), excessive use of groundwater and changes in the groundwater table, increasing use of low-quality water in irrigation, irrigation practices (Morway and Gates, 2012; Machado and Serralheiro, 2017; Zhang et al., 2020), land use type (e.g., farmland, grassland, saline-alkali land) and agricultural land exploitation (Fang et al., 2005; Wang and Li, 2012), drainage systems (Benyamini et al., 2005), and extended periods of rainfall and droughts

(Falloon and Betts, 2010) can all have a strong impact on salinity in the soil water. Apart from the hydrological, climate, cultivating, and management factors, a variety of chemical reactions in the soil layer including anion exchange, oxidation-reduction, ion adsorption, chemical speciation, complex formation, mineral weathering, solubility, and precipitation can also dominate salinity movement in soil water (Rengasamy, 2016).

Studies have also investigated the factors that govern stream water salinity. Identified watershed features include soil type, land use and vegetation (Manon Lax et al., 2017); natural and manmade erosion (Forti et al., 2000; Ballester et al., 2003; Lindell et al., 2010); seasonal variability in river discharge (Rahi and Halihan, 2018); variation in surface runoff (Whitney, 2010); increase in water temperature (Thomas et al., 2004); seasonal snowmelt runoff pulse, intermittent flooding events, and drought events (Cayan, 2002; Huang et al., 2014); river bank characteristics (Ralston et al., 2012); and irrigation return flow (Rahi and Halihan, 2018).

Several studies have used modeling approaches to simulate salinity and salt ion transport in agricultural systems, including models such as CATSALT (Tuteja et al., 2003), SAHYSMOD (Singh and Panda, 2012), MT3DMS (Burkhalter and Gates, 2005), UNSATCHEM (Schoups et al., 2006), UZF-RT3D (Tavakoli-Kivi et al., 2019), and SWAT-Salt (Bailey et al., 2019). However, none have investigated systematically the controlling factors on salinity in soils, aquifers, and rivers within a watershed system.

The objective of this study is to determine the most influential system parameters on soil salinity, groundwater salinity, and streamwater salinity in a semi-arid irrigated watershed system. To accomplish this objective, global sensitivity analysis was applied to the newly developed SWAT-Salt watershed model (Bailey et al., 2019), which simulates the fate and transport of 8 major salt ions ($SO_4$, Ca, Mg, Na, K, Cl, $CO_3$, and $HCO_3$) in soils, aquifers, and streams subject to

equilibrium chemistry reactions of precipitation-dissolution, complexation, and cation exchange. System factors included in the sensitivity analysis are land surface hydrological factors, subsurface hydrological factors, chemical reaction parameters, soil and aquifer content of salt minerals, and initial conditions of salt ion concentrations in soil water and groundwater. The method was applied to a 1118 $km^2$ irrigated region within Arkansas River Valley in southeastern Colorado, USA, for which increasing salinization of the watershed waters have contributed to a decrease in crop yield in recent years. This study uses the SWAT-Salt model of Bailey et al. (2019), which has already been tested in this region against soil salinity, groundwater salinity, and in-stream salinity. The influence of the parameters on salinity, however, has not been investigated.

## 2.2 STUDY REGION AND PREVIOUS MODEL APPLICATIONS

### 2.2.1 Study region

The study area is located in the Lower Arkansas River Valley (LARV) in southeastern Colorado, between the towns of Fowler and Las Animas and occupying an area of 1118 $km^2$ irrigated stream-aquifer system along the Arkansas River (see Figure 2.1). The major tributaries to the Arkansas River in the study region are Timpas Creek and Crooked Arroyo (see Figure 2.1a). The alluvial aquifer thickness ranges between 12 and 15 m with a permeable bedrock consists of Cretaceous shale and limestone located approximately 10-15 m below ground surface (Moore and Wood, 1967; Wei et al., 2018). The watershed is characterized mostly as an agricultural watershed with dominant crop types of alfalfa, melons, corn, beans, sorghum, wheat, grass and pasture, and vegetables. The study region has a semi-arid climate with an average precipitation of 376 mm per year. Monthly average minimum and maximum temperatures range from -12.6 ℃ in January to 35.9 ℃ in July with an annual average of 13.6 ℃ (Holmberg., 2017).

Due to the semi-arid characteristic of the region, high evapotranspiration, and insufficient average annual precipitation, irrigation water always needs to be supplemented by the water diverted from Arkansas River into 6 major irrigation canals or from the alluvial aquifer (Morway et al., 2013). The irrigation season typically occurs between March 15th and November 15th of each year. Approximately 500 pumping wells (Figure 2.1b) are used to supplement surface water irrigation with groundwater irrigation. Groundwater is pumped from a sand-gravel alluvial aquifer along the corridor of Arkansas River, with aquifer thickness ranging from 4 to 34 m. Groundwater level generally ranges between 2 to 3 m of the ground surface in the region. The soils are dominated by calcite ($CaCO_3$) and gypsum ($CaSO_4$).

Soil salinity in the region is high due to a combination of 1) dissolution of existing salt minerals in the soil profile; 2) irrigating with saline water from Arkansas River and the aquifer; and 3) hyper-concentration of salinity brought to the shallow subsurface by groundwater, with shallow groundwater levels occurring due to excessive irrigation, seepage from the canals, and inadequate drainage. These processes have salinized a large portion of the region's soil, resulting in a reduction in crop yield (11%-19%) in decades (Gates et al., 2002; Burkhalter and Gates, 2005; Gates et al., 2006; Mueller Price and Gates, 2008; Gates et al., 2009; Morway and Gates, 2012). Soil salinity is leached to the water table and loaded to the tributaries and the Arkansas River via groundwater discharge.

Field measurements in the region over the past two decades have demonstrated the saline conditions. Average soil water salinity measured by electrical conductivity (EC) of soil from thousands of measurements in cultivated fields is 4.11 dS/m, with a minimum and maximum of 0.9 and 56.5 dS/m, respectively (Morway and Gates, 2012). Groundwater sampling from 82 groundwater monitoring wells in the study region (see Figure 2.1a) between 2006 and 2010 show

that the average total salinity concentration of groundwater ranges between 2,700 to 3,000 mg/L, with a range of 460 mg/L to 44,600 mg/L. The predominant presence of gypsum ($CaSO_4$) in the area resulted in higher concentrations of $SO_4$ with the minimum, maximum, and average of 147 mg/L, 29,457 mg/L, and 1,878 mg/L, making up approximately 56 % of total salinity. The annual salt loading to the Arkansas River from groundwater return flows is approximately 530 kg of salt per irrigated hectare per kilometer of the river (Burkhalter and Gates, 2005), and average salinity and $SO_4$ concentrations in the Arkansas River and its tributaries are 1,145 mg/L and 560 mg/L, respectively (Gates et al., 2009).

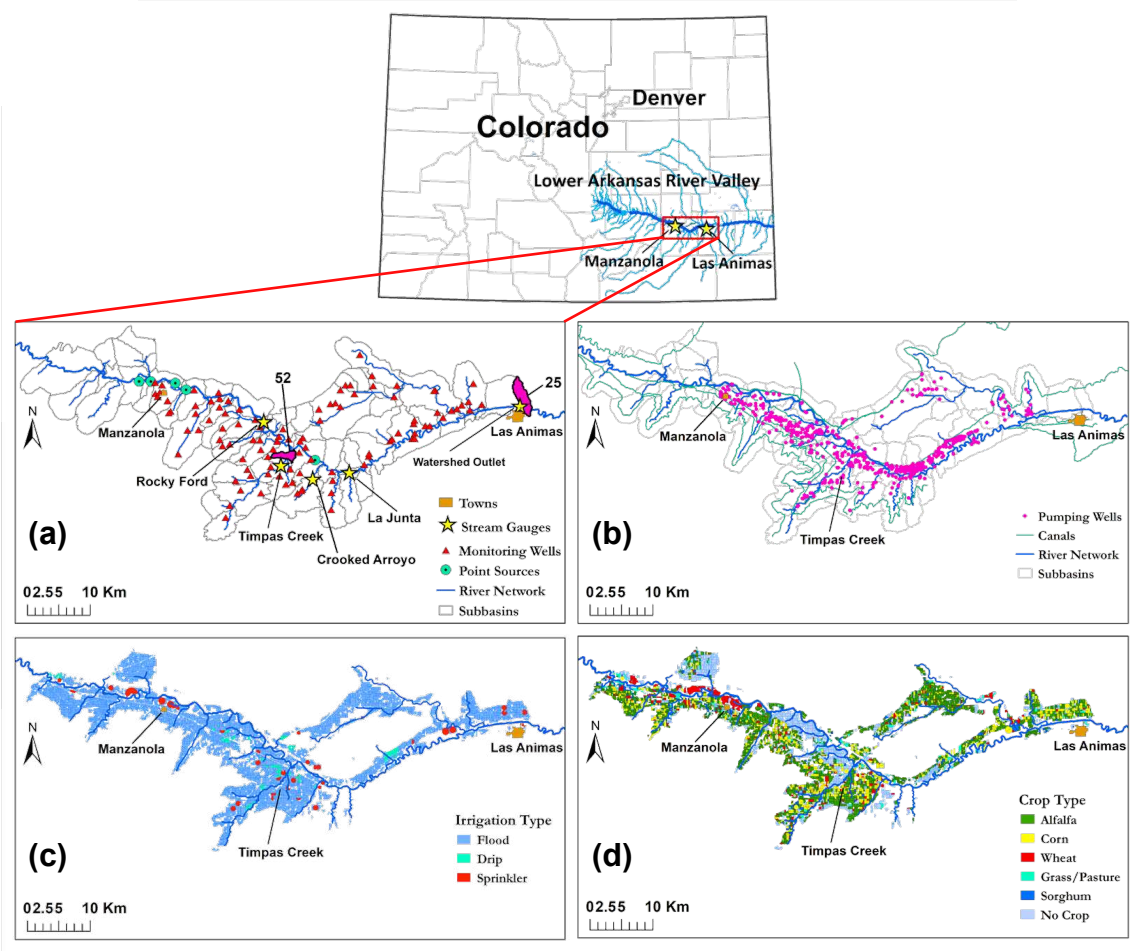


**Figure 2.1.** Location of the study area in the Lower Arkansas River Valley (LARV). Map (a) shows the location of stream gauges, monitoring wells, point sources, and two main subbasins within the watershed. Map (b) shows canal network and the location of pumping wells in the study area. Map (c) shows the irrigation type, and map (d) shows the land use type within the LARV.

### 2.2.2 SWAT model application

The Soil and Water Assessment Tool (SWAT) (Arnold et al., 1998) is a comprehensive continuous-in-time, physically based, hydrologic, and environmental model that simulates water, sediment, and nutrient storage and fluxes within a watershed. SWAT has been used extensively worldwide for a variety of watershed and nutrient management purposes (e.g., Spruill et al, 2000, Grizzetti et al., 2003; Gassman et al., 2010; van Griensven et al., 2012, Bressiani et al., 2015; Worku et al., 2017; Ercan et al., 2020; Gupta et al., 2020; Mosbahi and Benabdallah, 2020). To run SWAT, the study watershed is divided into subbasins, and the subbasins are divided into hydrologic response units (HRUs) with the same land use, soil type, and topographic slope. SWAT solves a daily water balance and nutrient mass balance for the soil profile, the aquifer, and the channel. The balances for the soil profile and the aquifer are simulated for the HRUs within each subbasin, with water and nutrient mass loaded to the stream of the subbasin via surface runoff, soil lateral flow, and groundwater flow. The balances for the channel are performed for each individual subbasin channel, with water and nutrient mass routed through the subbasin streams to the watershed outlet.

Wei et al. (2018) constructed and tested the SWAT model for streamflow in the Arkansas River and several tributaries in the study region, using a USGS 30-m digital elevation model, a STATSGO soil map, a National Hydrography Data Set stream network, climate data from several weather stations of Colorado Agricultural Meteorological Network, and canal diversion data from Colorado Division of Water Resources. The model was run from April 1999 to December 2007. Twenty parameters governing surface and subsurface water responses, snow response, and soil properties were adjusted during the calibration process using SWAT-CUP (Abbaspour et al., 2008) performed for 2001 to 2003 using the observed and simulated monthly averaged streamflow data

at Rocky Ford, Las Animas, and Timpas Creek stations. Of considered parameters, SCS[1] runoff curve number, Manning's *n* value for the main channel, effective hydraulic conductivity of channel, initial depth of water in the shallow aquifer, the delay time for aquifer recharge, and deep aquifer percolation fraction showed strong controls on streamflow. The calibrated model was then tested for 2004 to 2007 streamflow data.

### 2.2.3 SWAT-Salt model application

The new SWAT salinity module (Bailey et al., 2019), imbedded within the original SWAT modeling code (FORTRAN language), simulates the fate and transport of Sulfate ($SO_4$), Calcium (Ca), Magnesium (Mg), Sodium (Na), Chloride (Cl), Potasium (K), Carbonate ($CO_3$), and Bicarbonate ($HCO_3$) in a watershed system. The chemical reactions and salinity flux pathways simulated in the SWAT-Salt model (i.e. SWAT model with the added salinity module) are shown in Figure 2.2. Salinity flux pathways include surface runoff, groundwater flow, streamflow, soil percolation and leaching, groundwater upflux to the soil profile, and soil lateral flow. The module solves for salt ion concentration in 1) soil water of each HRU soil layer, 2) groundwater in each HRU aquifer unit, and 3) surface water in each subbasin stream as a result of these salinity fluxes and equilibrium chemistry reactions (precipitation-dissolution, complexation, cation-exchange), which are solved for each salt ion within each HRU soil layer and each HRU aquifer unit on a daily time step. The module also simulates salt ion mass loadings to the soil profile due to irrigation practices, from both groundwater (pumping) and surface water (canal) sources. For groundwater irrigation, salt ion mass is removed from the respective HRU aquifer unit wherein the groundwater pump is located. For surface water irrigation, the salt ion mass is removed from the respective

[1] Soil Conservation Service

subbasin stream from which the canal water is diverted, as specified in the SWAT management input file for each HRU.

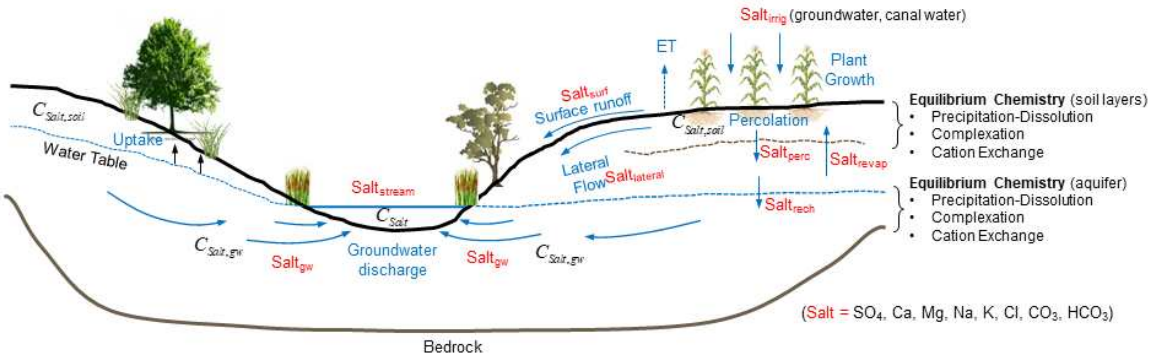


**Figure 2.2.** Schematic of a typical watershed stream-aquifer cross-section in irrigated regions, showing the hydrologic and salinity fluxes simulated by SWAT-Salt. After Bailey et al. (2019).

The mass fate and transport of each salt ion in the soil system is calculated using the following mass balance equation for each HRU soil layer on a daily time step, using $SO_4$ as an example:

$$\frac{dM_{SO_4,soil}}{dt} = M_{irrig,sw} + M_{irrig,gw} + M_{diss} - M_{precip} - M_{lat} - M_{perc} + M_{revap} \qquad (1)$$

where $M$ represent solute mass (kg/ha) and *irrig*, *sw*, *gw*, *diss*, *precip*, *lat*, *perc*, and *revap* represent irrigation, surface water, groundwater, chemical dissolution of salt minerals, precipitation of salt minerals, soil lateral flow, percolation to the shallow aquifer, and upflux from the shallow aquifer, respectively. Equation (1) is repeated for each salt ion and for each soil layer. The mass balance equation for $SO_4$ fate and transport in each HRU aquifer is:

$$\frac{dM_{SO_4,gw}}{dt} = M_{perc} - M_{revap} + M_{diss} - M_{precip} - M_{gwflow} \qquad (2)$$

where *gwflow* represents groundwater flow. Equation (2) is repeated for each salt ion. At each time step, the new salt ion mass storage in each soil layer and aquifer unit is converted to concentrations

$C_{salt,soil}$ and $C_{salt,gw}$ (mg/L) (see Figure 2.2) using the current water storage volume in the soil layer and the aquifer, respectively.

Whereas salt ion mass fluxes in percolation water, lateral flow, groundwater upflux, surface runoff, irrigation water, and groundwater flow are simulated using the hydrologic fluxes calculated from the original SWAT subroutines and algorithms (see details in Bailey et al., 2019), salt ion mass changes associated with salt mineral precipitation and dissolution are computed using mass balance and mass action equations. Salt mineral (e.g., gypsum $CaSO_4$) dissolution is simulated if the solution in the soil layer or aquifer is under-saturated with respect to the two associated salt ions (e.g., $Ca^{2+}$ and $SO_4^{2-}$), whereas salt mineral precipitation is simulated if the solution is super-saturated with respect to these two ions. Salt minerals included in the module are $CaSO_4$, $CaCO_3$, $MgCO_3$, $MgSO_4$, and NaCl. For each daily time step, new concentrations for each salt ion and salt mineral are calculated for each soil layer and aquifer unit using the chemistry reactions, whereupon salt ion mass fluxes via hydrologic fluxes are computed. At the conclusion of all HRU calculations for the daily time step, the salt ion mass added to the subbasin streams is routed through the stream network using SWAT's water and solute routing algorithms. The SWAT-Salt modeling code is available for download at https://github.com/rtbailey8/SWAT_Salinity.

Bailey et al. (2019) applied and tested the new SWAT-Salt model to the current study region, using the calibrated SWAT model from Wei et al. (2018). Observed field data and mapped soils data were used to provide initial concentrations of salt ions in soil water and groundwater and the initial mass of salt minerals $CaCO_3$, $MgCO_3$, $CaSO_4$, $MgSO_4$, and NaCl in soils and aquifer material. The SWAT-Salt model was run from 1 April 1999 to 13 December 2009. Manual calibration was performed from 2006 to 2007 using the solubility product of $CaSO_4$ precipitation-dissolution and the soil fraction of $CaSO_4$, due to the predominant presence of Ca and $SO_4$ among

the salt ions in the region. The model then was tested from 2008 to 2009 against soil salinity from cultivated fields (Morway and Gates, 2012), groundwater salt ion concentrations from groundwater monitoring wells (see Figure 2.1a for locations), in-stream salt ion concentrations at sampling sites in the Arkansas River and tributaries, and groundwater salt ion mass loading to the Arkansas river (Bailey et al., 2019).

## 2.3 METHODOLOGY

### 2.3.1 Overview of method

Sensitivity analysis is a robust and widely used tool for various purposes including analyzing the dominant controls of a system (Pastres et al., 1999; Pianosi et al., 2016), hence, to investigate the controls on salinity in groundwater, soil water, and stream water in the Lower Arkansas River Valley irrigated watershed system, global sensitivity analysis (GSA) was applied to the tested SWAT-Salt model of the study region. GSA was selected since it considers the influence of model parameters over the entire range of possible values and is suitable for nonlinear models (Baroni and Tarantola, 2014; Song et al., 2015). A total of 41 model parameters were selected for the analysis, with each parameter, tested for effect on salt ion concentrations in groundwater, soil water, and stream water. The Morris method (Morris, 1991) was used as a screening tool to determine the most influential model parameters, which were then assessed for influence using the variance-based Sobol' method (Sobol', 1990).

Model parameters include hydrologic parameters from the original SWAT simulation algorithms and salinity parameters from the salinity module. The model parameters and their ranges used in the sensitivity analysis are listed in Table 2.1. The 15 hydrologic parameters included in the analysis are based on previous studies of sensitivity analysis using the SWAT model in other regions (Arabi et al., 2007; Nossent et al., 2011; Zhang et al., 2013; Ahmadi et al., 2014a;

Sarrazin et al., 2016; Khorashadi Zadeh et al., 2017; Neupane et al., 2020), and include groundwater parameters (RCHRG_DP, GWQMN, REVAPMN, ALPHA_BF, GW_REVAP, and GW_DELAY), surface runoff and streamflow parameters (CN2, SURLAG, OV_N, CH_N2), and soil hydrologic parameters (SOL_K, SOL_AWC, EPCO, ESCO, DEP_IMP). Ranges for these hydrologic parameters were selected based on literature review (Arabi et al., 2007; Cibin et al., 2010; Arnold et al., 2011; Nossent et al., 2011; Zhang et al., 2013; Ahmadi et al., 2014b; Sarrazin et al., 2016; Khorashadi Zadeh et al., 2017, Gao et al., 2017; Wei et al., 2018; Tasdighi et al., 2018; Aliyari et al., 2019). The 26 parameters for the salinity module (see Table 2.1) include initial salt ion dissolved concentrations in soil water and groundwater and initial salt mineral fractions in soil and aquifer material. Solubility constants for the five included salt minerals ($CaCO_3$, $MgCO_3$, $CaSO_4$, $MgSO_4$, and NaCl) were not included in the sensitivity analysis since these are natural constants. Initial values for each of the 26 parameters are based on measured salt ion concentrations in soil water and groundwater (Gates et al., 2009) and estimated values from soil surveys of the Natural Resources Conservation Service (NRCS), with the range set to +/- 50% of these values. Of the primary interest is the relative effect of hydrologic parameter and salinity parameters on salinity concentrations in soil water, groundwater, and stream water.

**Table 2.1** List of selected hydrological and salinity parameters from SWAT-Salt model for Morris and Sobol' sensitivity analysis methods in this study. The bold parameters include parameters selected for Sobol' sensitivity analysis after applying Morris sensitivity analysis method.

| No. | Parameter Type | | Parameters | Description | Unit | Initial value | Range LB[2] | Range UB[3] |
|---|---|---|---|---|---|---|---|---|
| 1 | Hydrological parameters | Groundwater | RCHRG_DP | Deep aquifer percolation fraction | - | - | 0 | 1 |
| 2 | | | **GWQMN** | Threshold depth of water level in shallow aquifer for return base flow to occur | mm | - - | 0 | 5000 |
| 3 | | | **REVAPMN** | Threshold depth of water level in shallow aquifer for revap to occur | mm | - | 0 | 1000 |
| 4 | | | **ALPHA_BF** | Base flow alpha factor for recession constant | day | - | 0 | 1 |
| 5 | | | **GW_REVAP** | Groundwater revap coefficient | - | - | 0.02 | 0.2 |
| 6 | | | **GW_DELAY** | Delay time for aquifer recharge | day | - | 0 | 500 |
| 7 | | Surface runoff & streamflow | **CN2** | Initial SCS runoff curve number for moisture condition II | - | - | -25% | +25% |
| 8 | | | **SURLAG** | Surface runoff lag coefficient | day | - | 0.1 | 12 |
| 9 | | | **OV_N** | Manning's n value for overland flow | - | - | 0.01 | 0.6 |
| 10 | | | **CH_N2** | Manning's n value for the main channel | - | - | 0.01 | 0.3 |
| 11 | | Soil hydrology | **SOL_K** | Saturated hydraulic conductivity | mm/hr | - | -50% | +50% |
| 12 | | | **SOL_AWC** | Available water capacity of the soil layer | mm $H_2O$/mm soil | - | -50% | +50% |
| 13 | | | **EPCO** | Plant uptake compensation factor | - | - | 0.01 | 1 |
| 14 | | | **ESCO** | Soil evaporation compensation factor | - | - | 0 | 1 |
| 15 | | | DEP_IMP | Depth to impervious layer in soil profile | | - | | |
| 16 | Salinity parameters | | **$SO_4$_gw** | Initial concentration in groundwater | mg/L | 1878 | 939 | 2817 |
| 17 | | | **Ca_gw** | Initial concentration in groundwater | mg/L | 353 | 176.5 | 529.5 |
| 18 | | | Mg_gw | Initial concentration in groundwater | mg/L | 191 | 95.5 | 286.5 |
| 19 | | | Na_gw | Initial concentration in groundwater | mg/L | 402 | 201 | 603 |
| 20 | | | K_gw | Initial concentration in groundwater | mg/L | 4 | 2 | 6 |
| 21 | | | Cl_gw | Initial concentration in groundwater | mg/L | 95 | 47.5 | 142.5 |

**Table 2.1.** (continued)

[2] Lower bound
[3] Upper bound

| No. | Parameter Type | Parameters | Description | Unit | Initial value | Range | |
|---|---|---|---|---|---|---|---|
| | | | | | | LB | UB |
| 22 | Salinity parameters | $CO_3$_gw | Initial concentration in groundwater | mg/L | 2 | 1 | 3 |
| 23 | | $HCO_3$_gw | Initial concentration in groundwater | mg/L | 410 | 205 | 615 |
| 24 | | **$SO_4$_soil** | Initial concentration in soil water | mg/L | 1878 | 939 | 2817 |
| 25 | | **Ca_soil** | Initial concentration in soil water | mg/L | 353 | 176.5 | 529.5 |
| 26 | | Mg_soil | Initial concentration in soil water | mg/L | 191 | 95.5 | 286.5 |
| 27 | | Na_soil | Initial concentration in soil water | mg/L | 402 | 201 | 603 |
| 28 | | K_soil | Initial concentration in soil water | mg/L | 4 | 2 | 6 |
| 29 | | Cl_soil | Initial concentration in soil water | mg/L | 95 | 47.5 | 142.5 |
| 30 | | $CO_3$_soil | Initial concentration in soil water | mg/L | 2 | 1 | 3 |
| 31 | | $HCO_3$_soil | Initial concentration in soil water | mg/L | 410 | 205 | 615 |
| 32 | | **$CaCO_3$** | Initial fraction of soil for each salt mineral in soil | - | 0.1 | 0.05 | 0.15 |
| 33 | | **$MgCO_3$** | Initial fraction of soil for each salt mineral in soil | - | 0.01 | 0.005 | 0.015 |
| 34 | | **$CaSO_4$** | Initial fraction of soil for each salt mineral in soil | - | 0.01 | 0.005 | 0.015 |
| 35 | | **$MgSO_4$** | Initial fraction of soil for each salt mineral in soil | - | 0.01 | 0.005 | 0.015 |
| 36 | | **NaCl** | Initial fraction of soil for each salt mineral in soil | - | 0.01 | 0.005 | 0.015 |
| 37 | | **$CaCO_3$** | Initial amount for each salt mineral in aquifer | - | 0.1 | 0.05 | 0.15 |
| 38 | | **$MgCO_3$** | Initial amount for each salt mineral in aquifer | - | 0.01 | 0.005 | 0.015 |
| 39 | | **$CaSO_4$** | Initial amount for each salt mineral in aquifer | - | 0.01 | 0.005 | 0.015 |
| 40 | | **$MgSO_4$** | Initial amount for each salt mineral in aquifer | - | 0.01 | 0.005 | 0.015 |
| 41 | | **NaCl** | Initial amount for each salt mineral in aquifer | - | 0.01 | 0.005 | 0.015 |

### 2.3.2 Preliminary screening investigation: Morris method

The Morris screening method or Elementary Effect $(EE)$ method (Morris, 1991) is a well-established one-factor-at-a-time $(OAT)$ sensitivity analysis method, often used for models with a high number of uncertain input factors and for models with high simulation costs. This method is used to identify non-influential factors with a small number of model simulations. This method classifies the input factors into three different categories; a) factors with negligible effects b) factors with large linear effects but without interactions, and c) factors with large non-linear interaction effects (Saltelli et al., 2004) and ranks them based on their influence on model outputs with a limited number of model simulations (based on the number of input factors, but generally smaller than 1000).

For a given model with $n$ parameters $X=(X_1, X_2, \ldots, X_n)$ and corresponding model output $Y(X)$, the elementary effect of the $i^{th}$ parameter is estimated as the change in the model output due to a change in the model factor:

$$d_i(\mathrm{X}) = \frac{Y(X_1, \ldots, X_{i-1}, X_i + \Delta, X_{i+1}, \ldots, X_n) - Y(X)}{\Delta} \qquad (3)$$

where $\Delta$ is a value in the set $\{1/(p-1), 2/(p-1), \ldots, 1-1/(p-1)\}$ which specifies the optimal increment to be used in Equation 3 and defined as $\Delta = p/[2(p-1)]$, and $p$ is the number of levels, normally between 4 and 8 (Saltelli et al., 1999). The $p$ value generally is taken 4 which means that $\Delta$ is equal to $2/3 = 0.76$. To estimate the overall influence of each input factor on a given model output and the higher order effects due to nonlinearity or interactions between input factors, two sensitivity measures, the mean $(\mu)$ and standard deviation $(\sigma)$ are used in this method, respectively and defined as:

$$\mu_i = \frac{1}{r}\sum_{k=1}^{r} d_i(k) \tag{4}$$

$$\sigma_i = \sqrt{\frac{1}{r-1}\sum_{k=1}^{r}\left[d_i(k) - \mu_i\right]^2} \tag{5}$$

where $d_i(k)$ is the elementary effect $(EE)$ of input factor $k, k = 1,2,\ldots,r$, and $r$ is the number of samples. Campolongo et al. (2007) introduced $\mu^*$, the absolute value of the mean of the $EE$, to prevent opposite signs from lowering the $\mu$ value of a factor:

$$\mu_i^* = \frac{1}{r}\sum_{k=1}^{r}\left|d_i(k)\right| \tag{6}$$

A large $\mu_i$ or $\mu_i^*$ value indicates that the $i^{th}$ factor has a greater overall influence on the output, and a large $\sigma_i$ value implies that the $i^{th}$ input factor has an interaction with other factors or has a nonlinear effect on the output. To perform sensitivity analysis by Morris method, the number of model executions needed to be run is $r \times (n+1)$ times. In this regard, the SIMLAB software v2.2 (Saltelli et al., 2004) was used to generate the input sample file of size $n = 420$ for the 41 primary model input factors (see Table 2.1) by Latin hypercube sampling (LHS) method considering uniform distribution for all the variables and the number of level of $p = 4$. The SWAT-Salt model was then run 420 times, with each run using a different parameter set, whereupon $\mu^*$ and $\sigma_i$ were calculated by SIMLAB.

The SWAT-Salt system-response variables assessed in this study include salinity loads (percolation, surface runoff, soil lateral flow, groundwater flow, groundwater upflux); in-stream salt ion concentrations; groundwater salt ion concentrations; and soil water salt ion concentrations.

### 2.3.3 Secondary investigation: Sobol' method

Sobol' method (Sobol', 1990) is a variance-based, model-independent global sensitivity analysis method based on variance decomposition. It can be applied to non-linear and non-monotonic models (Looss and Lemaitre, 2015). Given a model output $Y$ and $X = (X_1, X_2, \ldots, X_n)$ a set of the $n$ model parameters, the corresponding function $f(X)$ can be decomposed into terms of increasing order as follows:

$$Y = f(X) = f(X_1, X_2, \ldots, X_n) \tag{7}$$

$$f(X_1, \ldots, X_n) = f_0 + \sum_{i=1}^{n} f_i(X_i) + \sum_{i=1}^{n} \sum_{j=i+1}^{n} f_{ij}(X_i, X_j) + \ldots + f_{1,\ldots,n}(X_1, \ldots, X_n) \tag{8}$$

The total unconditional variance of the model output $V(Y)$ is defined as:

$$V(Y) = \int f^2(X)\, dX - f_0^2 \tag{9}$$

where all integrals are multiple integrals with limits $[0,1]$ on each dimension. The unconditional variance Equation 9 can be decomposed into partial variances as:

$$V(Y) = \sum_{i=1}^{n} V_i + \sum_{i=1}^{n-1} \sum_{j=i+1}^{n} V_{ij} + V_{1,\ldots,n} \tag{10}$$

where $V_i$ and $V_{ij}$ represent the variances of $f_i$ and $f_{ij}$ which are the variance contribution of individual parameter $X_i$ to the total variance and part of the total variance resulted by the interaction between $X_i$ and $X_j$, respectively, and $V_{1,\ldots,n}$ is the variance caused by the interaction among $n$ model parameters (Nossent et al., 2011). Several sensitivity indices can be defined using the partial variances in this method. The first-order index (or 'main effect') quantifies the influence of each individual parameter on the output without considering the interaction with other parameters:

$$S_i = \frac{V_i}{V(Y)} = \frac{V_{Xi}\left[E_{X\sim i}(Y|X_i)\right]}{V(Y)} \quad (11)$$

where $E$ stands for expected value, $V$ denotes the variance, and $X \sim i$ denotes all input parameters but the $i_{th}$. The total-order (or 'total effect') index quantifies the contribution of the input parameter and all other interactions, i.e., the contribution of the first-order effect and the sum of all higher-order interaction effects (Sobol', 2001; Saltelli et al., 2008; Owen, 2013):

$$ST_i = 1 - \frac{V_{\sim i}}{V(Y)} = \frac{E_{X\sim Xi}\left[V_{Xi}(Y|X_{\sim Xi})\right]}{V(Y)} \quad (12)$$

First-order indices are often used for ranking the parameters so that the input parameters with the highest main effects are the most influential ones, and the total-order indices are used for screening as the input factor with $ST$ equal to zero means the parameter is non-influential and can be discarded from the analysis (Jaxa-Rozan and Kwakkel, 2018). In addition, the difference between the total effect and the main effect implies the degree of interaction between the individual parameter $X_i$ and the other parameters (Yang, 2011). In this article, the total effect indices were used for ranking purposes. To estimate the number of model simulations needed for a given number of input parameters, Saltelli and Tarantola (2002) introduced a method to calculate the number of runs in the range of $m(n+2)$ which is used to calculate only the first and the total order indices and $m(2n+2)$ to calculate the first, second, and the total order indices where $m$ represents the sample size and $n$ is the number of parameters (Yang, 2011; Nossent et al., 2011). In this study, the Sobol' quasi-random sampling approach was used for generating a sample input file of size $n = 1147$ for 27 final input factors (bold factors in Table 2.1, found to be sensitive in the Morris Method; see Section 4.2.1) to be used for Sobol' sensitivity analysis, resulting in 28,672 model

simulations. Similar to the Morris Method, the SIMLAB software was used to generate parameter sets and evaluate model output.

## 2.4 RESULTS AND DISCUSSION

### 2.4.1 General model results from output files

Results are presented for one of the simulations of the ensemble used in the sensitivity analysis, to provide insights into typical salinity concentrations and loadings in the watershed system. Figure 2.3 shows temporally averaged $SO_4$, Cl, Mg, and Ca concentrations (mg/L) in groundwater and in soil water for each HRU, and in-stream loadings (kg/day) for each subbasin stream over the 13-year simulation period. These results indicate the high spatial variability in salinity concentrations and loadings. Due to the large groundwater salinity loadings to the stream system, the in-stream loadings increase with distance downstream, resulting in maximum loading at the outlet near Las Animas (a3, b3, c3, and d3). Also notice that the subbasin stream just upstream of Manzanola has higher in-stream loadings for each of the salt ions than the next downstream subbasin stream. This is due to the removal of salt from this stream as river water is diverted to canals for irrigation (see Figure 2.1b for location of diversions). In addition, the in-stream loadings show high values right before Manzanola due to the inclusion of a point source, representing the inflow from the Arkansas River upstream of the study region. The overall pattern of salt loadings within the watershed indicates moderate contributions from tributary subbasin streams, such as Timpas Creek (see Figure 2.1b for location), due to high soil water (a2, b2, c2, d2) and groundwater (a1, b1, c1, d1) salt ion concentrations that control salt loading to streams via soil lateral flow and groundwater discharge.

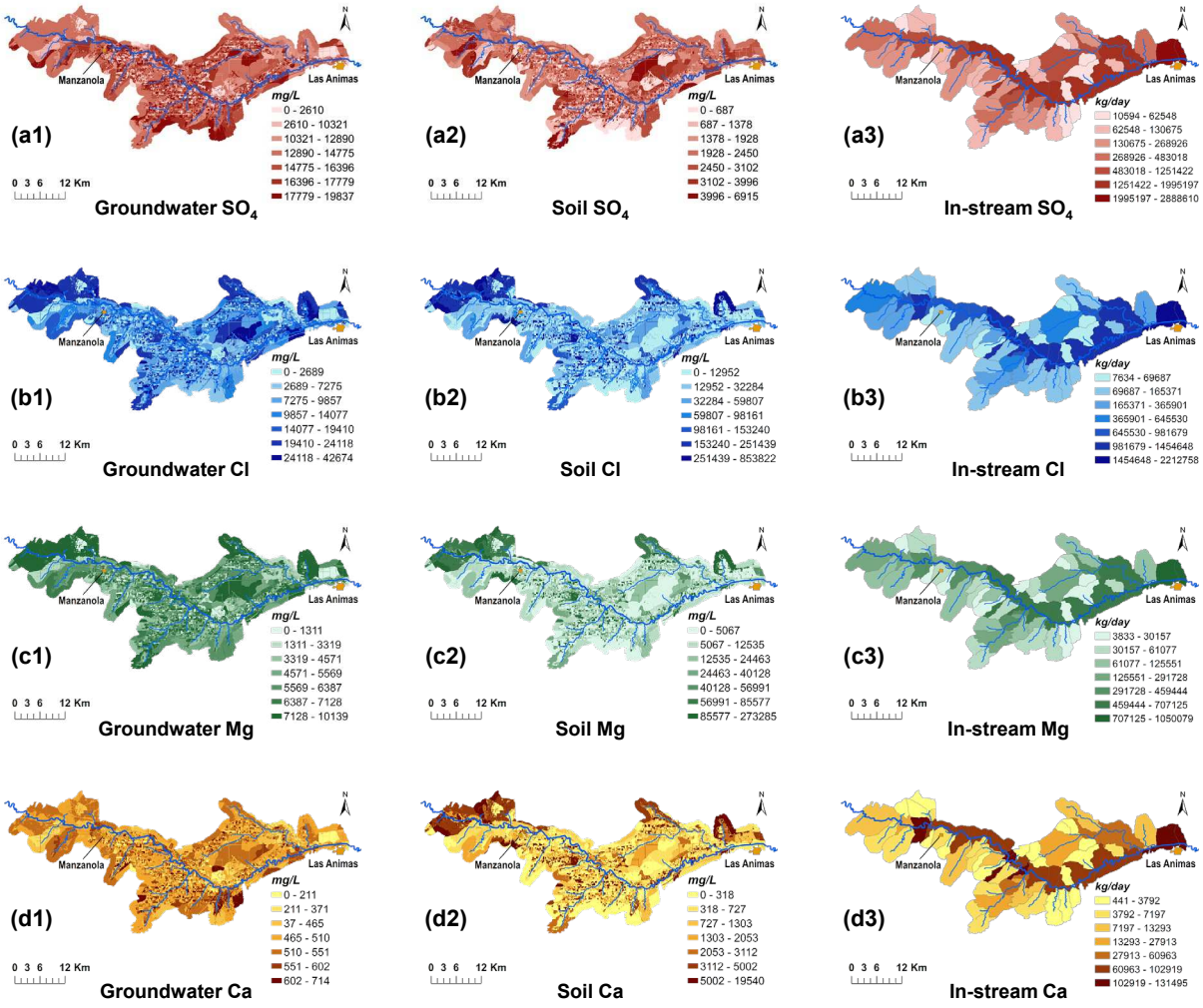


**Figure 2.3.** HRU and Stream-wide averaged concentrations and loadings of 4 predominant salt ions in the LARV study region created based on a randomly selected simulation within the 13-year model execution. Maps (a1, b1, c1, d1) show groundwater concentrations (mg/L) of $SO_4$, Cl, Mg, and Ca ions, maps (a2, b2, c2, d2) show mentioned ions' concentrations (mg/L) in soil water, and maps (a3, b3, c3, d3) show in-stream loadings (kg/day) of the ions in the study area, respectively.

As can be seen in Figure 2.4, which shows the salt ion composition of soil water and groundwater during the 13-year simulation period, $SO_4$ and Cl ions in groundwater and Cl and Mg in soil water are the dominant ions, due to the presence of salt minerals and saline irrigation water throughout the region.

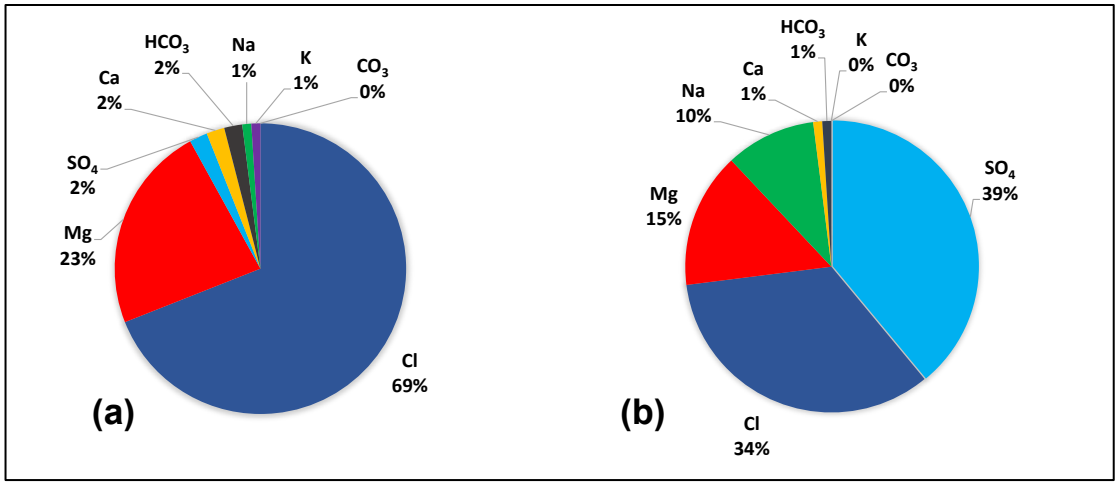


**Figure 2.4.** Percentage of average concentration of each salt ion in (a) soil water and (b) groundwater in the watershed within the 13-year model simulation.

Figure 2.5 shows histograms of average concentrations of $SO_4$, Cl, Mg, and Ca in stream water at the watershed outlet (Figure 2.5a), in groundwater (Figure 2.5b), and in soil water (Figure 2.5c), showing that $SO_4$ is the dominant ion in stream water and in groundwater, and Cl is dominant in soil water, similar to the results shown in Figure 2.4.

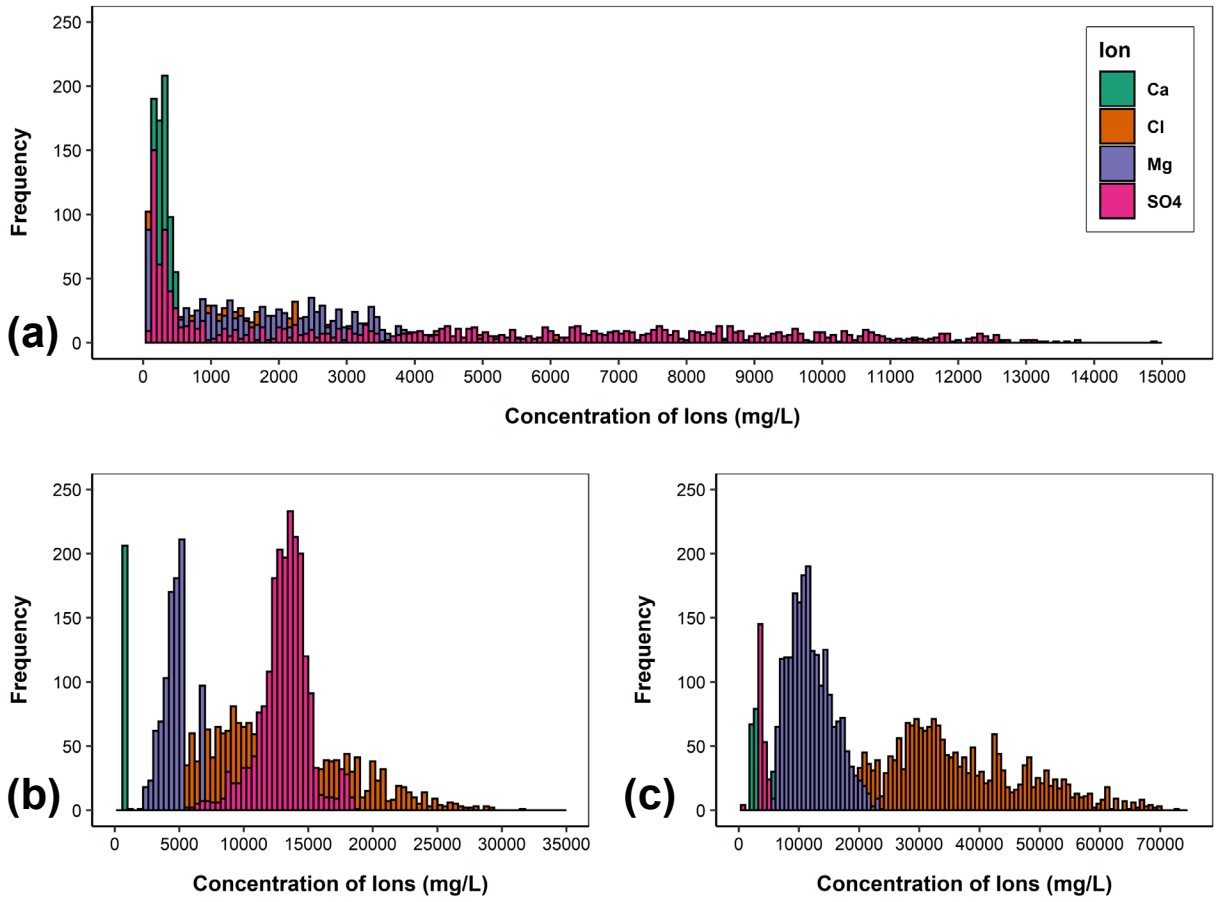


**Figure 2.5.** Concentration frequency histogram of 4 dominant ions in the LARV area within the 13-year simulation period (a) at the watershed outlet, (b) in the groundwater, and (c) in the soil water, respectively.

The simulated daily concentrations (mg/L) and loadings (kg) of the four selected ions in stream water at the watershed outlet are presented in Figure 2.6. Loadings in 1999 have the highest magnitude compared to the following years due to wet climate conditions. Notice that the concentrations during 1999 are low, due to the dilution of river water. A major drought in the region occurred during 2002-2005, resulting in small salinity loads (Figure 2.6b) and associated high concentrations (Figure 2.6a). Both time series plots show that salinity loading from the watershed is composed mainly of $SO_4$, although both $SO_4$ and Cl have high concentrations.

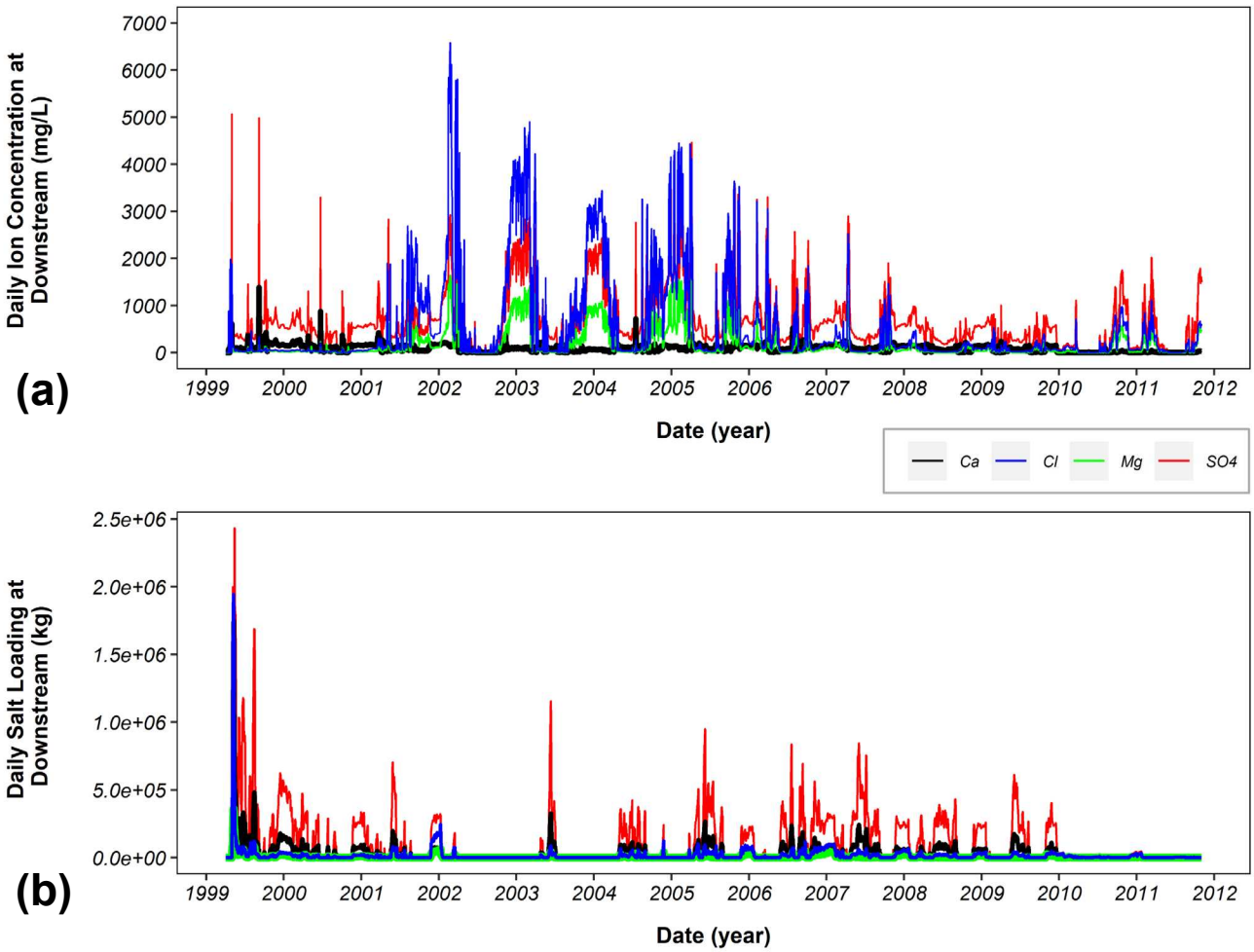


**Figure 2.6.** Time series of 13-year simulation of (a) daily in-stream concentration (mg/L) and (b) daily loading (kg) for each of the four dominant salt ions in the watershed at the Las Animas site.

## 2.4.2 Identifying the controls on watershed salinity

### 2.4.2.1 Morris method

The results of the Morris sensitivity analysis are presented in Figure 2.7 for 16 SWAT-Salt model output variables including 4 hydrological factors of salt loading in soil lateral flow (Latsalt), groundwater discharge (Saltgw), surface runoff (Surqsalt), groundwater upflux (Revapsalt), and concentrations of $SO_4$, Cl, Mg, and Ca ions in groundwater, soil water, and in the watershed

subbasin. Results indicate that the hydrological factors influence salinity response more strongly than salinity factors. For hydrologic factors, GWQMN, EPCO, GW_REVAP, CH_N2 and SOL_AWC are highly sensitive, and ESCO, REVAPMN and GW_DELAY are moderately sensitive. For salinity factors, the initial concentrations of $SO_4$ and Cl in the soil and the initial fractions of salt minerals in soil and the aquifer are moderately sensitive. These 27 factors (bolded in Table 2.1) are included in the Sobol' SA method.

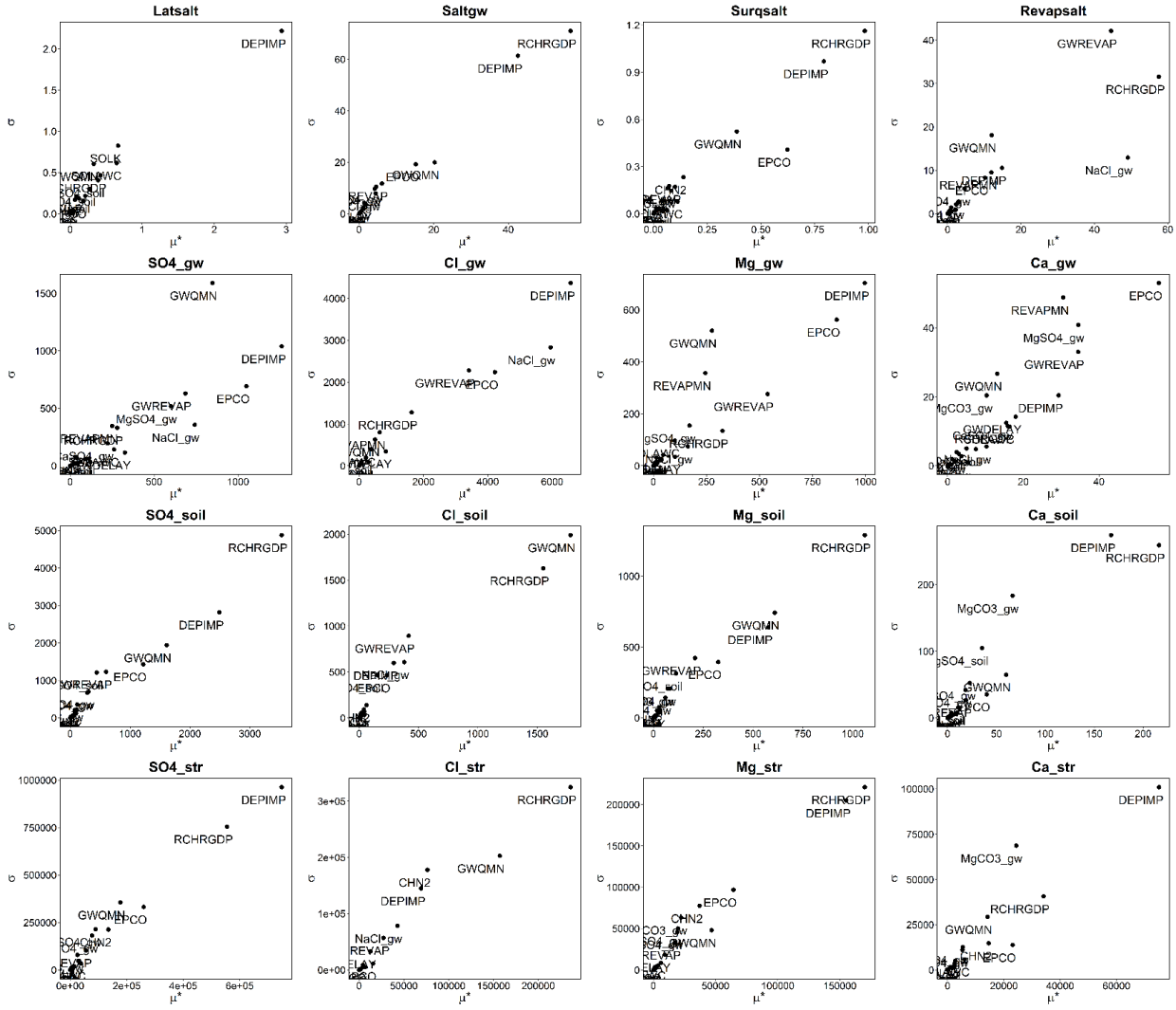


**Figure 2.7.** Scatter plots of the Morris screening method results for 16 selected output variables of the SWAT-Salt model (see Table 2.2) including hydrological factors, concentrations of 4 dominant ions in groundwater, soil water, and in the stream (gw, soil, and str stand for groundwater, soil water, and stream, respectively). Each plot shows the relevancy of selcted model output to the 41 model input parameters. Higher $\mu^*$ represents higher sensitivity of the parameter.

### 2.4.2.2 Sobol' method

The sensitivity analysis results for 27 factors selected by Morris sensitivity analysis method analyzed by Sobol' method is shown in Figure 2.8. Model output parameters shown in Figure 2.8 are defined in Table 2.2 as follows.

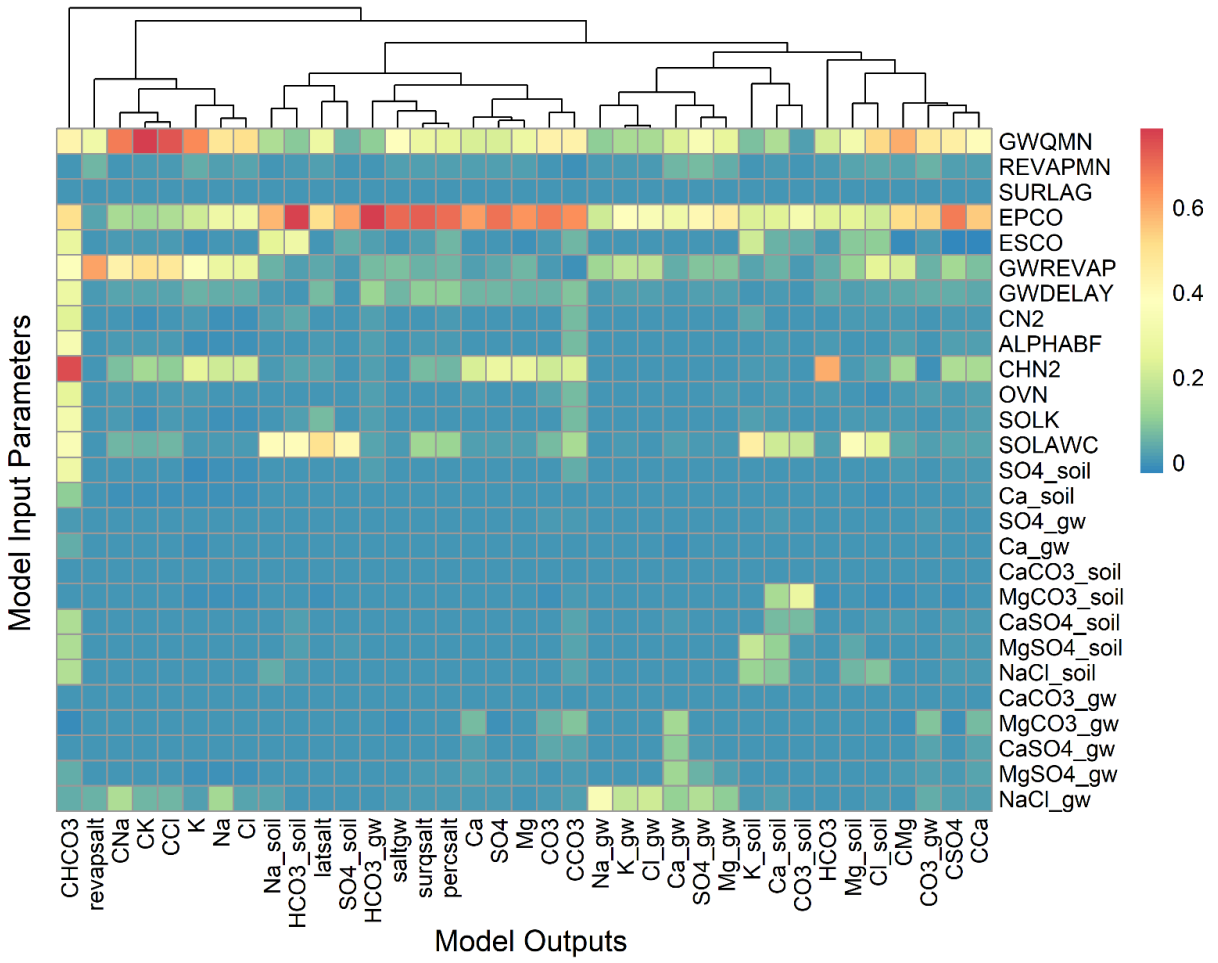


**Figure 2.8.** The above heatmap illustrating Sobol' total order sensitivity indices for 27 selected model input parameters resulted from the Morris screening method (bolded parameters in Table 2.1). In this figure, the term "C" before model outputs' names denotes the concentration of a given ion in the watershed system.

**Table 2.2** List of SWAT-Salt model outputs used for sensitivity analysis by Morris and Sobol' methods in this study. Selected subbasins for the analysis include subbasins 25 and 52 that contain watershed outlet (Las Animas) and main tributary (Timpas Creek), respectively

| No. | Parameter Type | Parameters | Description | Unit |
|---|---|---|---|---|
| 1 | Watershed-wide parameters | latsalt | Total salt load transferred by lateral flows to the streams | kg |
| 2 | | saltgw | Total salt load transferred by groundwater to the streams | kg |
| 3 | | surqsalt | Total salt load from surface runoff to the streams | kg |
| 4 | | percsalt | Total salt load transferred by percolation to groundwater | kg |
| 5 | | revapsalt | Total salt load from groundwater to the soil water | kg |
| 6 | Subbasin-wide parameters | $SO_4$ | Total $SO_4$ load reaching each subbasin | kg |
| 7 | | Ca | Total Ca load reaching each subbasin | kg |
| 8 | | Mg | Total Mg load reaching each subbasin | kg |
| 9 | | Na | Total Na load reaching each subbasin | kg |
| 10 | | K | Total K load reaching each subbasin | kg |
| 11 | | Cl | Total Cl load reaching each subbasin | kg |
| 12 | | $CO_3$ | Total $CO_3$ load reaching each subbasin | kg |
| 13 | | $HCO_3$ | Total $HCO_3$ load reaching each subbasin | kg |
| 14 | | $CSO_4$ | Total $SO_4$ concentration at each subbasin | mg/L |
| 15 | | CCa | Total Ca concentration in each subbasin | mg/L |
| 16 | | CMg | Total Mg concentration in each subbasin | mg/L |
| 17 | | CNa | Total Na concentration in each subbasin | mg/L |
| 18 | | CK | Total K concentration in each subbasin | mg/L |
| 19 | | CCl | Total Cl concentration in each subbasin | mg/L |
| 20 | | $CCO_3$ | Total $CO_3$ concentration in each subbasin | mg/L |
| 21 | | $CHCO_3$ | Total $HCO_3$ concentration in each subbasin | mg/L |
| 22 | HRU-wide parameters | $SO_4$_gw | Total $SO_4$ concentration in groundwater | mg/L |
| 23 | | Ca_gw | Total Ca concentration in groundwater | mg/L |
| 24 | | Mg_gw | Total Mg concentration in groundwater | mg/L |
| 25 | | Na_gw | Total Na concentration in groundwater | mg/L |
| 26 | | K_gw | Total K concentration in groundwater | mg/L |
| 27 | | Cl_gw | Total Cl concentration in groundwater | mg/L |
| 28 | | $CO_3$_gw | Total $CO_3$ concentration in groundwater | mg/L |
| 29 | | $HCO_3$_gw | Total $HCO_3$ concentration in groundwater | mg/L |
| 30 | | $SO_4$_soil | Total $SO_4$ concentration in soil water | mg/L |

**Table 2.2.** (continued)

| No. | Parameter Type | Parameters | Description | Unit |
|---|---|---|---|---|
| 31 | HRU-wide parameters | Ca_soil | Total Ca concentration in soil water | mg/L |
| 32 | | Mg_soil | Total Mg concentration in soil water | mg/L |
| 33 | | Na_soil | Total Na concentration in soil water | mg/L |
| 34 | | K_soil | Total K concentration in soil water | mg/L |
| 35 | | Cl_soil | Total Cl concentration in soil water | mg/L |
| 36 | | $CO_3$_soil | Total $CO_3$ concentration in soil water | mg/L |
| 37 | | $HCO_3$_soil | Total $HCO_3$ concentration in soil water | mg/L |

*Controls on Surface Water Salinity Loading to Streams*

To identify the controls on surface water salinity loadings, the total salt transferred by lateral flows to the streams (latsalt) and the total load from surface runoff to the streams (surqsalt) are considered. For total salt transferred to the streams by lateral flow, there are three highly sensitive hydrological parameters: plant uptake compensation factor (EPCO), available water capacity of the soil layer (SOL_AWC), and threshold depth of the water level in the shallow aquifer for return base flow to occur (GWQMN). These are followed by moderately sensitive parameters: delay time for aquifer recharge (GW_DELAY), saturated hydraulic conductivity of the soil (SOL_K), groundwater revap coefficient for groundwater moving from the aquifer to the soil profile (GW_REVAP), and threshold depth of water level in the shallow aquifer for revap to occur (REVAPMN). For the second output parameter indicating the total salinity loadings to the streams by surface water, there are two highly sensitive parameters including plant uptake compensation factor (EPCO) and threshold depth of water level in the shallow aquifer for return base flow to occur (GWQMN), and there is less but considerable sensitivity to the available water capacity of the soil layer (SOL_AWC), delay time for aquifer recharge (GW_DELAY), Manning's n value for the main channel (CH_N2), threshold depth of water level in the shallow aquifer for revap to occur (GW_REVAP), soil evaporation compensation factor (ESCO), and threshold depth of water level in the shallow aquifer for revap to occur (REVAPMN).

The identified parameters, such as SOL_AWC and EPCO, control the amount of soil water, and hence salt ion mass, in the soil profile, and SOL_K and GW_DELAY control the rate at which water and salt ion mass move through the soil profile and leach to the aquifer. GW_REVAP also controls the amount of salt ion mass in both the aquifer and the soil profile. These parameters have a strong influence on the amount of soil lateral flow, and hence salt ion mass loading in lateral

flow, to subbasin streams. For this study region, these parameter sensitivities indicate that salinity loading to streams is controlled mainly by hydrological parameters, and particularly by soil and groundwater hydrological factors which govern the amount and retention time of water in the soil layer.

*Controls on Groundwater Salinity Loading to Streams*

The total salt loadings transported to the streams by groundwater (saltgw) is highly sensitive to plant uptake compensation factor (EPCO) and threshold depth of the water level in the shallow aquifer for return base flow to occur (GWQMN) followed by threshold depth of water level in shallow aquifer for revap to occur (GW_REVAP), delay time for aquifer recharge (GW_DELAY), and the threshold depth of water level in shallow aquifer for revap to occur (REVAPMN). The total salt load transfers by percolation to the groundwater (percsalt) is greatly sensitive to the plant uptake compensation factor (EPCO), threshold depth of water level in the shallow aquifer for return base flow to occur (GWQMN), and available water capacity of the soil layer (SOL_AWC) followed by delay time for aquifer recharge (GW_DELAY), soil evaporation compensation factor (ESCO), manning's "n" value for the main channel (CH_N2), threshold depth of water level in the shallow aquifer for revap to occur (GW_REVAP), and threshold depth of water level in shallow aquifer for revap to occur (REVAPMN), respectively. The total salt load from groundwater to the soil water (revapsalt) is highly sensitive to threshold depth of water level in the shallow aquifer for revap to occur (GW_REVAP) and the threshold depth of water level in the shallow aquifer for return base flow to occur (GWQMN), and less but still sensitive to threshold depth of water level in shallow aquifer for revap to occur (REVAPMN), plant uptake compensation factor (EPCO), and the initial amount of NaCl salt in the aquifer. The hydrological factors govern groundwater salt loadings to the stream through re-evaporation, percolation, and groundwater recharge are almost

the same as the parameters control salt loadings to the stream through soil lateral flow except for the inclusion of soil evaporation compensation factor (ESCO) which controls the range of soil depth to meet the soil evaporative demand.

Regarding the salt ion concentrations and loadings, the total $SO_4$ load to the Timpas Creek and the main watershed outlet (see Figure 2.1a) is controlled principally by hydrologic factors (EPCO, CH_N2, GWQMN, GW_DELAY, and GW_REVAP), with a variety of surface runoff (CH_N2), soil (EPCO), and groundwater (GWQMN, GW_DELAY, and GW_REVAP) factors. The total Ca load to the main watershed outlet (Las Animas—subbasin 25) and the main tributary in the study area (Timpas Creek— subbasin 52) is controlled by hydrologic factors (EPCO, GWQMN, CH_N2, and GW_DELAY) and salinity factor of the initial amount of $MgCO_3$ in the aquifer. The total Na, K, Mg, and Cl loads to the outlet of the watershed and Timpas Creek are similarly controlled by hydrological factors (GWQMN, EPCO, CH_N2, GW_REVAP, and GW_DELAY) and the salinity factor of the initial amount of NaCl salt in the aquifer.

And lastly, the total loads of $CO_3$ and $HCO_3$ to the Las Animas and Timpas Creek are mainly controlled by similar hydrological factors including plant uptake compensation factor (EPCO), threshold depth of water level in the shallow aquifer for return base flow to occur (GWQMN), manning's "n" value for the main channel (CH_N2), delay time for aquifer recharge (GW_DELAY), and groundwater revap coefficient (GW_REVAP), whereas $CO_3$ also showed sensitivity to the salinity factor of the initial amount of $MgCO_3$ in groundwater. In general, results imply that salinity loadings from groundwater to the stream network are controlled mainly by groundwater and soil hydrological factors (Misra and Mishra, 2007) and the initial amount of NaCl salt in groundwater.

*Controls on Surface Water In-Stream Salinity Concentrations*

For the total $SO_4$ concentration in the watershed outlet (Las Animas) and Timps Creek, the hydrological factors (EPCO, GWQMN, GW_REVAP, REVAPMN, CH_N2, GW_DELAY, and SOL_AWC) control $SO_4$ in-stream concentration. The total Ca concentration is controlled by the same hydrological factors as for $SO_4$ in addition to the salinity factor of the initial amount of $MgCO_3$ in the aquifer material. The influence of the salt mineral $MgCO_3$ on in-stream Ca is due to the relationship between $MgCO_3$, which can release $CO_3$ into groundwater, and $CaCO_3$, which releases both Ca and $CO_3$ into groundwater. The in-stream concentration of the other four major ions including Na, K, Mg, and Cl are controlled by the same hydrological factors as $SO_4$ and Cl in addition to the salinity factor of the initial amount of NaCl in the aquifer material. The results indicate that in-stream salinity is controlled primarily by groundwater and soil hydrological factors, in addition to the initial amount of NaCl and $MgCO_3$ mineral fractions in the aquifer.

*Controls on Groundwater Salinity Concentrations*

The total $SO_4$ concentration in groundwater is controlled primarily by hydrologic factors (EPCO, GWQMN, GW_REVAP, and REVAPMN) and salinity factors (initial amount of NaCl and $MgSO_4$ in groundwater). For the total Ca concentration in groundwater, hydrological factors including plant uptake compensation factor (EPCO), threshold depth of water level in the shallow aquifer for return base flow to occur (GWQMN), threshold depth of water level in shallow aquifer for revap to occur (REVAPMN), and threshold depth of water level in the shallow aquifer for revap to occur (GW_REVAP), as well as salinity factors including the initial amounts of NaCl, $MgSO_4$, $MgCO_3$, and $MgSO_4$ in groundwater are the most sensitive factors controlling Ca concentration in groundwater. For the total concentration of Na, K, and Cl, hydrological factors (EPCO, GWQMN, GW_REVAP, and REVAPMN) and salinity factor (the initial amount of NaCl in groundwater) control salt concentrations in groundwater. The total concertation of $CO_3$ and $HCO_3$ in

groundwater is mainly controlled by hydrological factors including plant uptake compensation factor (EPCO), threshold depth of water level in the shallow aquifer for return base flow to occur (GWQMN), groundwater revap coefficient (GW_REVAP), and delay time for aquifer recharge (GW_DELAY), however; the total concentration of $CO_3$ is also sensitive to the salinity factor of the initial amount of NaCl and $MgCO_3$ in groundwater. Result shows that although ion concentrations in groundwater are controlled predominantly by groundwater and soil hydrological factors associated with evaporation (Jalali, 2007) and groundwater upflux (Burkhalter and Gates, 2006), respectively, the initial amount of NaCl and $MgSO_4$ in the aquifer also has a strong impact on controlling salinity fate and transport in groundwater, particularly for gypsum ($CaSO_4$).

*Controls on Soil Water Salinity Concentrations*

The total $SO_4$ concentration in soil water is controlled mainly by hydrologic factors including plant uptake compensation factor (EPCO), available water capacity of the soil layer (SOL_AWC), threshold depth of water level in the shallow aquifer for return base flow to occur (GWQMN), soil evaporation compensation factor (ESCO), and groundwater revap coefficient (GW_REVAP). The total concentration of Ca in soil water is controlled by the same hydrological factors in addition to salinity factors including the initial amount of NaCl, $MgCO_3$, $MgSO_4$, and $CaSO_4$ in soil water. For the other major ions in the study area including Na, K, Mg, Cl, $CO_3$, and $HCO_3$, controlling hydrological factors are similar to Calcium's hydrological controlling factors with salinity controlling factors including the initial amount of NaCl and $MgSO_4$ in soil water. The sensitivity analysis results indicate that changes and transport of soil salinity are primarily driven by soil water content and the presence of salt minerals, which can dissolve into the soil water (Utset and Borroto, 2001; Wang et al., 2018), land use type and soil properties that alter soil infiltration rate and soil water leaching to groundwater (Fang et al., 2005; Wang et al., 2008), groundwater upflux to the

soil profile (Qadir et al., 2000; Singh, 2005; Misra and Mishra, 2007; Jolly et al., 2008; Morway and Gates, 2012; Wichelns and Qadir, 2015), and groundwater depth (Morway and Gates, 2012) in addition to the initial amount of NaCl, $MgSO_4$, and $MgCO_3$ in soil water. As can be seen, since groundwater and soil water in shallow aquifers have interaction, the controlling factors on salinity fate and transport in groundwater and soil water are similar (Latif et al., 2009).

### 2.4.3 Limitations of study and modeling approach

This paper focuses on investigating hydrological and salinity factors that control salinity transport in a semi-arid irrigated stream-aquifer system. Limitations of this study include:

1. *Simplified groundwater flow processes inherent in the SWAT modeling code*. SWAT uses a combination of steady-state, lumped assumptions in simulating groundwater storage and groundwater discharge to streams. This shortcoming could be addressed by using the SWAT-MODFLOW (Bailey et al., 2016) model. However, SWAT-MODFLOW does not account for salt ion fate and transport.
2. *Neglecting forcing terms* (precipitation, temperature, irrigation amount) in the sensitivity analysis. These terms likely have an influence on salinity in soils, groundwater, and streams, but we focused on system properties and parameters in this study. The inclusion of forcing terms can be investigated in further work.
3. *Short time scale*. The study period covered a single decade. Ideally, the sensitivity analysis could be applied to a simulation of several decades; however, the time period used in this study included an extremely wet year (1999) and an extreme drought period (2002-2003).

## 2.5. SUMMARY AND CONCLUSIONS

In this paper, Morris and Sobol' sensitivity analysis methods were used to investigate controlling factors on salt ions fate and transport in soil water, groundwater, and stream water of

the irrigated stream-aquifer system located in the Lower Arkansas River Valley, Colorado, USA using the SWAT-Salt model. The results of the SA methods indicate that, generally, hydrologic factors such as evaporation coefficients, soil available water content, soil hydraulic conductivity, surface runoff curve numbers, and groundwater discharge coefficients have a relatively stronger influence on salt ion concentrations and fluxes in the watershed system than do salinity factors such as initial soil and groundwater salt ion concentrations and salt mineral presence, although salt minerals do have a moderate influence. Results indicate that salinity control measures for this watershed, and similar irrigated watershed in semi-arid regions (Schoups et al., 2006; Qureshi et al., 2008; Lorenzen et al., 2012), likely should focus on hydrologic conditions and fluxes. In addition, these hydrologic features of the watershed system should be addressed and focused on in future field-sampling campaigns, to decrease uncertainty in their specific model values and to provide additional model testing and corroboration. These results can help policymakers and water resources managers to decide on the best management practices in similar large agricultural watersheds to control salt concentrations and loadings in these regions.

# REFERENCES


Abbaspour, K. C., Yang, J., Reichert, P., Vejdani, M., Haghighat, S., and Srinivasan, R., 2008. SWAT-CUP: SWAT calibration and uncertainty programs, Swiss Federal Institute of Aquatic Science and Technology, Zurich, Switzerland.

Ahmadi, M., Ascough II, J.C., Dejonge, K.C., Arabi, M., 2014a. Multisite-multivariable sensitivity analysis of distributed watershed models: Enhancing the perceptions from computationally frugal methods. Ecological Modeling 279, 54-67.

Ahmadi, M., Arabi, M., Ascough II, J.C., Fontane, D.G., Engel, B.A., 2014b. Toward improved calibration of watershed models: multisite multiobjective measures of information. Environmental Modelling & Software 59, 135-145.

Aliyari, F., Bailey, R.T., Tasdighi, A., Dozier, A., Arabi, M., Zeiler, K., 2019. Coipled SWAT-MODFLOW model for large-scale mixed agro-urban river basin. Environmental Modelling & Software 115, 200-210.

Arabi, M., Govindaraju, R.S., Hantush, M.M., 2007. A probabilistic approach for analysis of uncertainty in the evaluation of watershed management practices. Journal of Hydrology 333 (2-4), 459-471.

Arnold, J.G., Srinivasan, R., Muttiah, R.S., Williams, J.R., 1998. Large area hydrologic modeling and assessment part I: model development1. J. Am. Water Resour. Assoc. 34 (1), 73e89.

Arnold, J.G., Kiniry, J.R., Srinivasan, R., Williams, J.R., Haney, E.B., Neitsch, S.L., 2011. Soil and water assessment tool. Input/output File Documentation, Version 2012. Texas Water Resources Institute.

Bailey, R.T., Wible, T.C., Arabi, M., Records, R.M. and Ditty, J., 2016. Assessing regional-scale spatio-temporal patterns of groundwater–surface water interactions using a coupled SWAT-MODFLOW model. *Hydrological Processes*, *30*(23), pp.4420-4433.

Bailey, R.T., Tavakoli-Kivi, S., Wei, X., 2019. A salinity module for SWAT to simulate salt ion fate and transport at the watershed scale. Hydrology and Earth System Sciences 23, 3155–3174.

Ballester, M.V.R., Victoria, D.D., Krusche, A.V., Coburn, R., Victoria, R.L., Richey, J.E., Logsdon, M.G., Mayorga, E., Matricardi, E., 2003. A remote sensing/GIS-based physical template to understand the biogeochemistry of the Ji-Parana River basin (Western Amazonia). Remote Sens. Environ. 87, 429–445

Baroni, G., Tarantola, S., 2014. A general probabilistic framework for uncertainty and global sensitivity analysis of deterministic models: a hydrological case study. Environ. Modell. Softw. 51, 26–34.

Benyamini, Y., Mirlas, V., Marisj, S., Gottesman, M., Fizik, E., Agassi, M., 2005. A survey of soil salinity and groundwater level control systems in irrigated fields in the Jezre'el Valley, Israel. Agricultural Water Management 76, 181-194.

Bressiani, D.D.A., Gassman, P.W., Fernandes, J.G., Garbossa, L.H.P., Srinivasan, R., Bonuma, N.B., Mendiondo, E.M., 2015. Review of soil and water assessment tool (SWAT) applications in Brazil: challenges and prospects. Int. J. Agric. Biol. Eng. 8 (3), 9-35.

Burkhalter, J. P., and Gates, T. K., 2005. Agroecological impacts from salinization and waterlogging in an irrigated river valley. J. Irrig. Drain. Eng. 131(2), 197–209.

Burkhalter, J. P., and Gates, T. K., 2006. Evaluating regional solutions to salinization and waterlogging in an irrigated river valley. J. Irrig. Drain. Eng. 132(1), 21-30.

Campolongo, F., Cariboni, J., Saltelli, A., 2007. An effective screening design for sensitivity analysis of large models. Environmental Modelling & Software 22, 1509-1518.

Cayan, D.R., 2002. Potential effects of global warming on the Sacramento/San Joaquin watershed and San Fransisco estuary. Geophysical Research Letters 29 (18), 1891.
Cibin, R., Sudheer, K.P., Chaubey, I., 2010. Sensitivity and identifiability of stream flow generation parameters of the SWAT model. Hydrological Processes 24, 1133-1148.
Chen, W., Hou, Z., Wu, L., Liang, Y., Wei, C., 2010. Evaluating salinity distribution in soil irrigated with saline water in arid regions of northwest China. Agric. Water Manage. 97 (12), 2001–2008.
Chidambaram, S., Sarathidasan, J., Srinivasamoorthy, K., Thivya, C., Thilagavathi, R., Prasanna, M.V., Singaraja, C., Nepolian, M., 2018. Assessment of hydrogeochemical status of groundwater in coastal region of Southeast coast of India. Applied Water Science, 8-27.
Ercan, M.B., I., Maghami, B.D., Bowes, M.M., Morsy, and J.L., Goodall. 2020. Estimating Potential Climate Change Effects on the Upper Neuse Watershed Water Balance Using the SWAT Model. Journal of the American Water Resources Association 56 (1): 53–67.
Falloon, P., Betts, R., 2010. Climate impacts on European agriculture and water management in the context of adaptation and mitigation—The importance of an integrated approach. Science of the Total Environment 408, 5667-5687.
Fang, H.L., Liu, G.H., Kearney, M., 2005. Georelationl analysis of soil type, soil salt content, landform, and land use in the Yellow River delta, China. Environmental Management 35, 72–83.
Forti, M.C., Boulet, R., Melfi, A.J., Neal, C., 2000. Hydrogeochemisty of a small catchment in Northeastern Amazonia: a comparison between natural with deforested parts of the catchment (Serra do navio, Amapá state, Brazil). Water Air Soil Pollut. 118, 263–279.
Gao, J., Sheshukov, A.Y., Yen, H., White, M.J., 2017. Impacts of alternative climate information on hydrologic processes with SWAT: A comparison of NCDC, PRISM, and NEXRAD datasets. CATENA 156, 353-364.
Gassman, P.W., Arnold, J.J., Srinivasan, R., Reyes, M., 2010. The worldwide use of the SWAT Model: technological drivers, networking impacts, and simulation trends (p. 1). In: In 21st Century Watershed Technology: Improving Water Quality and Environment Conference Proceedings, 21-24 February 2010, Universidad EARTH. American Society of Agricultural and Biological Engineers, Costa Rica.
Gates, T.K., Burkhalter, J.P., Labadie, J.W., Valliant, J.C., Broner, I., 2002. Monitoring and modeling flow and salt transport in a salinity-threatened irrigated valley. J. Irrig. Drain. Eng. 128 (2), 88–99.
Gates, T. K., Garcia, L. A., and Labadie, J. W., 2006. Toward optimal water management in Colorado's Lower Arkansas River Valley: Monitoring and modeling to enhance agriculture and environment. Colorado Water Resource Research Institute Completion Rep. No. 205, Colorado Agricultural Experimental Station Tech. Rep. TR06-10, Colorado State Univ., Fort Collins, CO.
Gates, T. K., Cody, B. M., Herting, A. W., Donnelly, J. P., Bailey, R. T., and Mueller Price, J., 2009. Assessing selenium contamination in the irrigated stream-aquifer system of the Arkansas River, Colorado. J. Environ. Qual. 38(6), 2344–2356.
Grizzetti, B., Bouraoui, F., Granlund, K., Rekolainen, S., Bidoglio, G., 2003. Modelling diffuse emission and retention of nutrients in the Vantaanjoki watershed (Finland) using the SWAT model. Ecological Modeling 169, 25-38.
Gupta A., Himanshu S.K., Gupta S., Singh R., 2020. Evaluation of the SWAT model for analyzing the water balance components for the upper Sabarmati basin. In: AlKhaddar R., Singh R.,

Dutta S., Kumari M. (eds) Advances in Water Resources Engineering and Management. Lecture Notes in Civil Engineering, vol 39. Springer, Singapore.

Holmberg, M.J., 2017, Hydrogeologic characteristics and geospatial analysis of water-table changes in the alluvium of the lower Arkansas River Valley, southeastern Colorado, 2002, 2008, and 2015: U.S. Geological Survey Scientific Investigations Map 3378, pamphlet, 9 p., 3 sheets, scale 1:130,000 and 1:575,000.

Huang, J., Huang, Y., Zhang, Z., 2014. Coupled effects of natural and anthropogenic controls on seasonal and spatial variations of river water quality during baseflow in a coastal watershed of southeast China. PLoS ONE 9 (3): e91528.

Jalali, M., 2007. Salinization of groundwater in arid and semi-arid zones: an example from Tajarak, western Iran. Environ. Geol. 52 (6), 1133–1149.

Jaxa-Rozen, M., Kwakkel, J., 2018. Tree-based ensemble methods for sensitivity analysis of environmental models: A performance comparison with Sobol and Morris techniques. Environmental Modeling and Software 107, 245-266.

Jolly I.D., McEwan, K.L., Holland, K.L., 2008. A review of groundwater-surface water interactions in arid/semi-arid wetlands and the consequences of salinity for wetland ecology. Ecohydrol. 1, 43-58.

Katerji, N., van Hoorn, J.W., Hamdy, A., Mastrorilli, M., 2003. Salinity effect on crop development and yield, analysis of salt tolerance according to several classification methods. Agricultural Water Management 62, 37-66.

Khorashadi Zadeh, F., Nossent, J., Sarrazin, F., Pianosi, F., Griensven, A., Wagener, T., Bauwens, W., 2017. Comparison of variance-based and moment-independent global sensitivity analysis approaches by application of the SWAT model. Environmental Modelling & Software 91, 210-222.

Latif, M., Ahmad, M.Z., 2009. Groundwater and soil salinity variations in a canal command area in Pakistan. Irrigation and Drainage 58, 456-468.

Lindell, L., Astrom, M., Oberg, T., 2010. Land-use change versus natural controls on stream water chemistry in the Subandean Amazon, Peru. Applied Geochemistry 25, 485-495.

Looss, B., Lemaitre, P, 2015. A review on global sensitivity analysis methods, in: Uncertainty Management in Simulation-Optimization of Complex Systems, Springer, 2015, pp. 101–122.

Lorenzen, G., Sprenger, C., Baudron, P., Gupta, D., Pekdeger, A., 2012. Origin and dynamics of groundwater salinity in the alluvial plains of western Delhi and adjacent territories of Harayana State, India. Hydrological Processes 26, 2333-2345.

Maas, E.V., and Grattan, S.R., 1999. Crop Yields as Affected by Salinity. In: Skaggs, R.W. and van Schilfgaarde, J., Eds., Agricultural Drainage Agronomy Monograph 38, ASA, Madison, 55-108.

Machado, R.M.A., Serralheiro, R.P., 2017. Soil Salinity: Effect on Vegetable Crop Growth. Management Practices to Prevent and Mitigate Soil Salinization. *Horticulturae 3,* 30.

Manon Lax, s., Wade Peterson, E., Van der Hoven. S.J., 2017. Stream chloride concentrations as a function of land use: A comparison of an agricultural watershed to an urban agricultural watershed. Environ. Earth Sci. (76), 708.

Misra, A.K., Mishra, A., 2007. Study of quaternary aquifers in Ganga Plain, India: Focus on groundwater salinity, fluoride and fluorosis. Journal of Hazardous Materials 144, 438-448.

Moore, J. E., Wood, L, A., 1967. Data requirement and preliminary results of an analog-model evaluation—Arkansas River Valley in eastern Colorado. Groundwater 5(1), 20-23.

Morris, M.D., 1991. Factorial sampling plans for preliminary computational experiments. Technometrics 33, 161–174.
Morway, E.D., Gates, T.K., 2012. Regional assessment of soil water salinity across an intensively irrigated river valley. Journal of Irrigation and Drainage engineering 138 (5), 393-405.
Morway, E.D., Gates, T.K., Niswonger, R.G., 2013. Appraising options to reduce shallow groundwater tables and enhance flow conditions over regional scales in an alluvial aquifer system. J. of Hydrol. 495, 216-237.
Mosbahi, M., Benabdallah, S., 2020. Assessment of land management practices on soil erosion using SWAT model in a Tunisian semi-arid catchment. J Soils Sediments 20**,** 1129–1139.
Mueller Price, J., and Gates, T. K., 2008. Assessing uncertainty in mass balance calculation of river nonpoint source loads. J. Environ. Eng. 134(4), 247–258.
Neupane, P., Bailey, R.T., Tavakoli-Kivi, S., 2020. Assessing controls on selenium fate and transport in watersheds using the SWAT model. Science of the Total Environment 738, 140318.
Nossent, J., Elsen, P., Bauwens, W., 2011. Sobol's sensitivity analysis of a complex environmental model. Environmental Modelling & Software 26, 1515-1525.
Owen, A.B., 2013. Variance components and generalized sobol' indices. SIAM/ASA Journal on Uncertainty Quantification 1, 19–41.
Panta, S., Flowers, T., Lane, P., Doyle, R., Haros, G., Shabala, S., 2014. Halophyte agriculture: Success stories. Environmental and Experimental Botany 107, 71-83.
Pastres, R., Chan, K., Solidoro, C., Dejak, C., 1999. Global sensitivity analysis of a shallow-water 3D eutrophication model. Comput. Phys. Commun. 117, 62-74.
Pianosi, F., Beven, K., Freer, J., Hall, J.W., Rougier, J., Stephenson, D.B., Wagener, T., 2016. Sensitivity analysis of environmental models: A systematic review with practical workflow. Environmental Modelling & Software 79, 214-232.
Qadir, M., Ghafoor, a., Murtaza, G., 2000. Amelioration strategies for saline soils: A review. Land Degradation & Development 11, 501-521.
Qureshi, A.S., McCornick, P.G., Qadir, M., Aslam, Z., 2008. Managing salinity and waterlogging in the Indus Basin of Pakistan. Agric. Water Manage. 95 (1), 1–10.
Rahi, K.A., Halihan, T., 2018. Salinity evolution of the Tigris River. Regional Environmental Change 18, 2117-2127.
Ralston, D.K., Geyer, W.R., Warner, J.C., 2012. Bathymetric controls on sediment transport in the Hudson river estuary: Lateral asymmetry and frontal trapping. Journal of Geophysical Research 117, C10013.
Rengasamy, P., 2016. Soil chemistry factors confounding crop salinity tolerance—A review. Agronomy 6, 53.
Rogers, M.E., 2002. Irrigation perennial pasture with saline water: effect on soil chemistry, pasture production and composition. Australian Journal of Experimental Agriculture 42, 265-272.
Saltelli, A., Tarantola, S., Chan, K., 1999. Quantitative model-independent method for global sensitivity analysis of model output. Technometrics 41 (1), 39-56.
Saltelli, A., Tarantola, S., 2002. On the relative importance of input factors in mathematical models: safety assessment for nuclear waste disposal. J. Am. Stat. Assoc. 97, 702–709.
Saltelli, A., Tarantola, S., Campolongo, F., and Ratto, M., 2004. Sensitivity analysis in practice: A guide to assessing scientific models. Chichester, U.K.: John Wiley and Sons, ISBN-9780470870938.

Saltelli, A., Ratto, M., Andres, T., Campolongo, F., Cariboni, J., Gatelli, D., Saisana, M., and Tarantola, S., 2008. Global Sensitivity analysis: The Primer, John Wiley & Sons, SBN-978047005997.

Sarrazin, F., Pianosi, F., Wagener, T., 2016. Global sensitivity analysis of environmental models: Convergence and validation. Environmental Modeling & Software 79, 135-152.

Schoups, G., Hopmans, J.W., Young, C.A., Vrugt, J.A., Wallender, W.W., Tanji, K.K., Panday, S., 2005. Sustainability of irrigated agriculture in the San Joaquin Valley, California. PNAS 102 (43), 15352–15356.

Schoups, G., Hopmans, J.W., Tanji., K.K., 2006. Evaluation of model complexity and space-time resolution on the prediction of long-term soil salinity dynamics, western San Joaquin Valley, California. Hydrological Processes 20, 2647-2668.

Singh, N.T., 2005. Irrigation and soil salinity in the Indian subcontinent: Past and present. Lehigh Univ. Press, Bethlehem, PA.

Singh, A., Panda, S.N., 2012. Integrated salt and water balance modeling for the management of waterlogging and salinization; I: Validation of SAHYSMOD. Journal of Irrigation and Drainage Engineering 138, 955-963.

Skrzypek, G., Dogramaci, S., Grierson, P.F., 2013. Geochemical and hydrological processes controlling groundwater salinity of a large inland wetland of northwest Australia. Chem. Geol. 357, 164–177.

Sobol', I.M., 1990. Sensitivity estimates for nonlinear mathematical models. *Matematicheskoe Modelirovanie* **2**, 112–118 (in Russian). [Transl. (1993) Sensitivity analysis for non-linear mathematical models. *Math. Modelling & Comp. Exp*. 1, 407–414.]

Sobol', I.M., 2001. Global sensitivity indices for nonlinear mathematical models and their Monte Carlo estimates, Math. Comput. Simul. 55 (1–3), 271–280.

Song, X.M., Zhan, C.S., Zhang, J., Xuan, Y.Q., Ye, M., Xu, C.G., 2015. Global sensitivity analysis in hydrological modeling: Review of concepts, methods, theoretical framework, and application. Journal of Hydrology 523, 739-757.

Spruill, C.A., Workman, S.R., and Taraba, J.L., 2000. Simulation of Daily and Monthly Stream Discharge from Small Watersheds Using the SWAT Model. Biosystems and Agricultural Engineering Faculty Publications. 156.

Tasdighi, A., Arabi, M., Harmel, D., 2018. A probabilistic appraisal of rainfall-runoff modeling approached within SWAT in mixed land use watersheds. J. Hydrol 564, 476-489.

Tavakoli-Kivi, S., Bailey, R.T., Gates, T.K., 2019. A salinity reactive transport and equilibrium chemistry model for regional-scale agricultural groundwater systems. Journal of Hydrology 572, 274-293.

Thomas, S.M., Neill, C., Deegan, L.A., Krusche, A.V., Ballester, V.M., Victoria, R.L., 2004. Influences of land use and stream size on particulate and dissolved materials in a small Amazonian stream network. Biogeochemistry 68, 135–151.

Tomaz, A., Palma, P., Alvarenga, P., Conceicao Goncalves, M., 2020. Chapter 13 – Soil salinity risk in a climate change scenario and its effect on crop yield. Climate Change and Soil Interactions, 351-396.

Tuteja, N.K., Beale, G., Dawes, W., Vaze, J., Murphy, B., Barnett, P., Rancic, A., Evans, R., Geeves, G., Rassam, D., Miller, M., 2003. Predicting the effects of landuse change on water and salt balance—a case study of a catchment affected by dryland salinity in NSW, Australia.
Journal of Hydrology 283, 67-90.

Utset, A., Borroto, M., 2001. A modeling-GIS approach for assessing irrigation effects on soil salinization under global warming conditions. Agricultural Water Management 50, 53-63.
van Griensven, A., Ndomba, P., Yalew, S., Kilonzo, F., 2012. Critical review of SWAT applications in the upper Nile basin countries. Hydrology Earth Syst. Sci. 16 (9), 3371e3381.
Wang, Y., Xiao, D., Li, X., 2008. Soil salinity evolution and its relationship with dynamics of groundwater in the oasis of inland river basins: case study from Fubei region of Xinjianf Province, China. Environ, Monit. Assess. 140, 291-302.
Wang, Y., Li, Y., 2012. Land exploitation resulting in soil salinization in a desert-oasis ecotone. Catena 100, 50-56.
Wang, Y., Deng, C., Liu, Y., Niu, Z., Li, Y., 2018. Identifying change in spatial accumulation of soil salinity in an inland river watershed, China. Science of the Total Environment 621, 177-185.
Wei, X., Bailey, R.T., Tasdighi, A., 2018. Using the SWAT model in intensively managed irrigated watersheds: Model modification and application. Journal of Hydrologic Engineering 23 (10): 04018044.
Whitney, M.M., 2010. A study on river discharge and salinity variability in the Middle Atlantic Bight and Long Island Sound. Continental Shelf Research 30, 305-318.
Wichelns, D., Qadir, M., 2015. Achieving sustainable irrigation requires effective management of salts, soil salinity, and shallow groundwater. Agric. Water Manag. 157, 31–38.
Worku, T., Khare, D., Tripathi, S.K., 2017.Modeling runoff–sediment response to land use/land cover changes using integrated GIS and SWAT model in the Beressa watershed. Environ Earth Sci 76, 550.
Yang, J., 2011. Convergence and uncertainty analyses in Monte-Carlo based sensitivity analysis. Environmental Modelling & Software 26, 444-457.
Xiao, J., Jin, Z.D., Wang, J., Zhang, F., 2015. Hydrochemical characteristics, controlling factors and solute sources of groundwter within the Tarim River Basin in the extreme arid region, NW Tibetan Plateau. Quaternary International 380-381, 237-246.
Zanchi, C., Cecchi, S., 2010. Soil salinization in the Grosseto Plain (Maremma, Italy): An environmental and socio-economic analysis of the impact on the agro-ecosystem. In: Scapini F., Ciampi G. (eds) Coastal Water Bodies. Springer, Dordrecht. https://doi.org/10.1007/978-90-481-8854-3_5.
Zhang, C., Chu, J., Fu, G., 2013. Sobol's sensitivity analysis for a distributed hydrological model of Yichun River Basin, China. Journal of Hydrology 480, 58-68.
Zhang, J., Du, D., Ji, D., Bai, Y., Jiang, W., 2020. Multivariate analysis of soil salinity in a semi-arid irrigated district of China: Concern about a recent water project. Water 12(8), 2104.
Zhang, J., Zhang, Z., Chen, J., Chen, H., Jin, J., Han, J., Wang, X., Song, Z., Wei, G., 2021. Estimating soil salinity with different fractional vegetation cover using remote sensing. Land Degradation & Development 32, 597-612.
Zorb, C., Geilfus, C.M., Dietz, K.J., 2019. Salinity and crop yield. Plant Biology 21, 31-38.

# Chapter 3. MUTUAL IMPACT OF SALINITY AND CLIMATE CHANGE ON CROP PRODUCTION WATER FOOTPRINT IN A SEMI-ARID AGRICULTURAL WATERSHED: APPLICATION OF SWAT-MODFLOW-SALT

## 3.1. INTRODUCTION

A constant increase in the world's population, which is expected to reach approximately 10 billion by 2050 ("FAO. 2017. The future of food and agriculture – Trends and challenges. Rome.," 2017) along with climate change, environmental stressors, human activities, and anthropogenic pollution is expected to escalate further reduction in water resources and demand for freshwater by one-third, thereby emphasizing the need for sustainable water resources and food production worldwide. This rapid population increase additionally boosts permanent demand for water in the agricultural sector, which accounts for 85% of global water consumption, placing a steady burden on water use in irrigated areas, specifically in arid and semi-arid agricultural regions which are already subject to water stress and scarcity to provide secure water supplies for agricultural activities (Casella et al., 2019) .

To sustain crop production, in conjunction with opting for securing available water resources, it is crucial to address detrimental factors that can adversely impact crop yields, particularly in regions vulnerable to climatic, hydrological, and environmental changes (Xiang et al., 2020). Among the environmental factors that negatively impact available water resources and agricultural production in the arid and semi-arid regions, soil salinity can lead to a reduction in crop yields as a result of the accumulation of salts in the root zone by over-application of saline irrigation water, synthetic fertilizers, and the presence of salt minerals (Bailey et al., 2019; Gates et al., 2002; Hosseini and Bailey, 2022; Skrzypek et al., 2013; Zörb et al., 2019). Soil salinity can also be

affected by climate change, as drier conditions and increasing air temperature can lead to degradation of irrigation water quality and limit the flushing of salts from the root zone (Haj-Amor and Bouri, 2020; Mukhopadhyay et al., 2021). However, the occurrence of extreme rainfall events can positively affect soil salinity, with soil flushing events.

To assess the impact of salinity under climate change on crop yields, the concept of water footprint (WF) introduced by Hoekstra in 2002 (Hoekstra and Hung, 2002) can be applied to provide valuable insights for future management practices aimed at sustaining food production and preserving available water in the agricultural sector of arid and semi-arid watersheds. WF serves as a quantifiable measure of freshwater utilization and is applicable for assessing water usage across the entire production supply chain (Hoekstra et al., 2011). In the agricultural sector, the WF of crop production (expressed as $m^3 ton^{-1}$) is defined as the volume of water consumption per unit crop yield of a given crop and can be used as practical method for evaluating both present and anticipated crop water usage, particularly in arid and semi-arid irrigated watersheds, where the preservation of crop yields in the face of increasing water scarcity poses a significant challenge and requires deliberate water resource management policies (Masud et al., 2018).

Crop WF comprises three distinct components: green ($WF_{green}$), blue ($WF_{blue}$), and grey ($WF_{grey}$) (Mekonnen and Hoekstra, 2011). The green WF component is determined by the effective precipitation retained in the root zone in the form of soil moisture. The blue WF is based on the freshwater stored in surface and groundwater reservoirs such as rivers, lakes, and aquifers. The grey WF is defined as the amount of freshwater needed to assimilate pollutant loads to freshwater bodies to meet particular water quality standards (Hoekstra and Chapagain, 2007).

To quantify the crop WF, most studies have employed the two primary methods outlined by Hoekstra et al. (2011). These approaches have been widely utilized to calculate WF and examine

how factors such as climate change, crop type, water management strategies, and socio-economic variables affect crop water usage. The first approach, known as the "crop water requirement" method (Cao et al., 2014; Sun et al., 2013) simulates the actual crop evapotranspiration (ET) under optimal conditions utilizing the potential ET calculated by the Penman-Monteith Equation (Allan, 1998) and the effective precipitation calculation provided by the US Department of Agriculture Soil Conservation Service (USDA SCS) (Döll and Siebert, 2002). The second method, termed the “irrigation schedule method”, quantifies WF using an empirical formula model such as the CROPWAT model (Chapagain and Hoekstra, 2011; Mekonnen and Hoekstra, 2011), CropSyst (Bocchiola et al., 2013; Garofalo et al., 2019), and AquaCrop model (Chukalla et al., 2015; Zhuo et al., 2016a; Zhuo and Hoekstra, 2017).

Based on an extensive literature review, a variety of studies have explored different aspects of WF assessment, with some focusing solely on quantifying the WF of predominant crops in specific regions (Chapagain and Hoekstra, 2011, 2007; Gerbens-Leenes and Hoekstra, 2012; Luan et al., 2018; Musa Ahmed and Ribbe, 2011; Shrestha et al., 2013; Zhuo et al., 2016b). Others have evaluated the impact of changing crop selections on the regional-scale crop production WF (Wang et al., 2015), while certain studies have examined the effects of altering irrigation techniques, strategies, and agricultural management practices on changes in the crop production WF (Chukalla et al., 2015; Zhuo and Hoekstra, 2017). Furthermore, several studies have estimated the influence of climate change on the WF of crop production (Elbeltagi et al., 2020; Garofalo et al., 2019; Masud et al., 2018; Shrestha et al., 2017; Zheng et al., 2020), however, no study has addressed the impact of salinity and climate change on crop production WF. Since the salinity increase in soils and shallow groundwater can decrease crop yield and agricultural production due to salt build-up in the root zone (Bailey et al., 2019; Gates et al., 2002; Hosseini and Bailey, 2022; Skrzypek et al.,

2013; Zörb et al., 2019), actual crop yield may be lower than the simulated by models, and hence the WF may be different than expected. This can have a significant impact on future water use, particularly in regions where soil salinization is increasing.

Moreover, among the previous studies, to the best of our knowledge, none have used a coupled surface/subsurface hydrological modeling approach to quantify crop WF under salinity stress and climate change. SWAT model as a physically based, hydrological, and environmental model simulates water, sediment, and nutrient storage and fluxes within a watershed and solves a daily water balance and nutrient mass balance for the soil profile and stream-aquifer system, however, this model does not simulate groundwater head, storage, and flow in a physically based manner, instead using steady-state, linear reservoir equations to route groundwater from the aquifer to nearby streams. Therefore, it becomes imperative to integrate a physically based groundwater model such as MODFLOW in conjunction with a surface water hydrological model like SWAT to comprehensively simulate spatial and temporal variations in groundwater storage which often controls irrigation amount and frequency and allows for a holistic consideration of all hydrological pathways encompassing surface water, soil, and groundwater, in the calculation of crop WFs. This is particularly significant in areas heavily dependent on groundwater for irrigation purposes.

The primary objective of this study is to evaluate and quantify the reciprocal impacts of soil salinity and climate change on the green, blue, and total WF of crop production in a semi-arid agricultural watershed using an integrated surface/subsurface hydro-chemical modeling approach. To achieve this aim, we employed the SWAT-MODFLOW-Salt model (Bailey and Hosseini, 2023), an updated version of the SWAT-MODFLOW model (Bailey et al., 2016). The model simulates the movement and distribution of eight major salt ($SO_4^{2-}$, $Cl^-$, $CO_3^{2-}$, $HCO_3^-$, $Ca^{2+}$, $Na^+$, $Mg^{2+}$, $K^+$) within the soil profile, aquifer, and stream network of a specific watershed as well as

accounting for soil-groundwater and groundwater-stream salt ion mass exchange. The model was applied to a 732 $km^2$ irrigated region within the Arkansas River Valley in southeastern Colorado, the USA, for which recent studies in this region have reported a decline in crop yield attributed to the salinization of watershed waters resulting from historical irrigation practices, the ubiquitous presence of salt minerals, and inadequate drainage (Burkhalter et al., 2005; Gates et al., 2002; Morway and Gates, 2012). We note that the SWAT-MODFLOW-Salt model used in this study has been previously calibrated and validated in this region against datasets of soil salinity, groundwater salinity, and in-stream salinity (see Bailey and Hosseini, 2023 for results).

## 3.2. MATERIALS AND METHODS

### 3.2.1 Study area

The study area is located in the Lower Arkansas River Valley (LARV) in southeastern Colorado, encompassing an area of 732 $km^2$ (see Figure 3.1). The region has a semi-arid climate, characterized by average monthly temperatures that ranges from -12.6 ℃ in January to 35.9 ℃ in July. The annual mean temperature is approximately 13.6 ℃, and the average annual precipitation measures 376 mm (Holmberg, 2017). The major cultivated crops in this area are alfalfa, melon, corn, beans, sorghum, wheat, onion, and pepper (as depicted in Fig. 3.1b & Fig. 3.2). Figure 3.2 illustrates the proportional contribution of each crop to the total annual average crop yield spanning from 1999 to 2009 in the Lower Arkansas River Valley. Alfalfa (ALFA), corn (CORN), and pasture/grass (PAST) collectively account for approximately 80% of the total crop yield during the 1999-2009 period. In contrast, rangeland (RNGE), grain sorghum (GRSG), hay (HAY), spring wheat (SWHT), sorghum hay (SGHY), sunflower (SUNF), onion (ONIO), oats (OATS), cabbage (CABG), soybean (SOYB), generic agricultural land (AGRL), and celery (CELR) contribute to

around 20% of the overall crop yield. The remaining 0.2% is distributed among winter wheat (WWHT), green beans (GRBN), spring barley (BARL), bell pepper (PEPP), honeydew melon (HMEL), tomato (TOMA), sweet corn (SCRN), asparagus (ASPR), sugar beet (SGBT), cantaloupe (CANT), forest-evergreen (FRSE), timothy (TIMO), watermelon (WMEL), and cucumber (CUCM). Given the semi-arid climate of the area, along with the high rates of ET and the inadequacy of precipitation, the cultivation of these crops necessitates the use of surface water irrigation sourced from six canals originating from the Arkansas River, complemented by 575 pumping wells (as shown in Fig. 3.1d) that supply water from an alluvial aquifer primarily composed of sand and gravel and situated along the course of the Arkansas River with an average thickness of approximately 16 m. The typical irrigation period spans from March 15th to November 15th annually. The primary method of irrigating fields in this area is flood irrigation (as depicted in Fig. 3.1c), although there are specific localized areas where sprinkler and drip irrigation methods are employed. The dominant soil salt minerals found in this area consist of calcite ($CaCO_3$) and gypsum ($CaSO_4$).

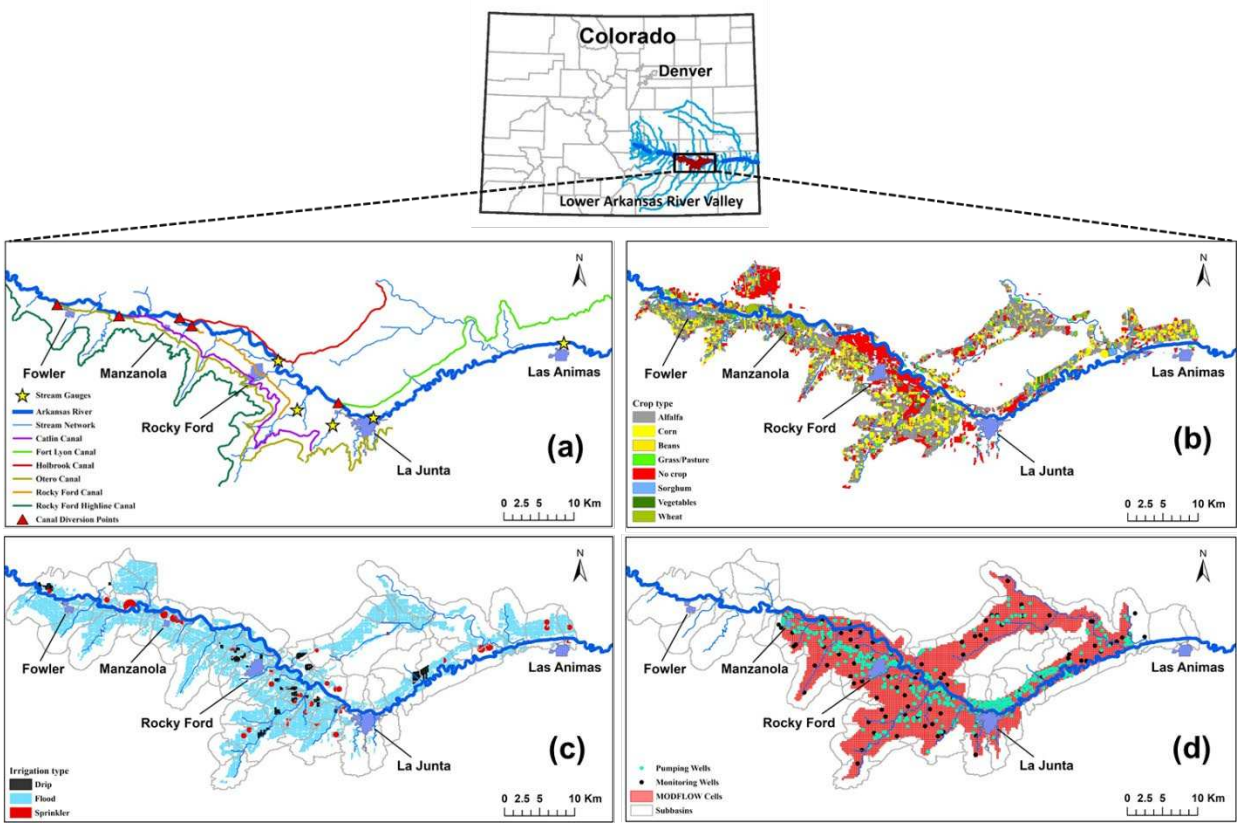


**Figure 3.1.** Study area in the Lower Arkansas River Valley (LARV). (a) Map of the location of stream gauges, stream network, canals, and canal diversion points within the watershed. (b) Map of crop type distribution in the study area. (c) Map of the irrigation type and (d) shows MODFLOW model cells, monitoring wells and pumping wells locations within the study area.

Historically, a combination of factors has contributed to elevated salinity levels in the area including the dissolution of salt minerals within the soil profile, the use of saline water for irrigation sourced from both the Arkansas River and the aquifer, and the salinization of the shallow subsurface due to groundwater associated with the proximity of shallow groundwater levels which has been affected by excessive irrigation, seepage from the canals, and inadequate drainage measures. Several studies conducted in recent years have reported a reduction in crop yields ranging from 11% to 19% within the region attributed to soil salinization (Burkhalter et al., 2005; Gates et al., 2002; Morway and Gates, 2012).

The significance of agriculture in the area, coupled with the prevalent issue of high salinity, has prompted nearly twenty years of ongoing field measurements. This comprehensive data collection effort included the sampling of groundwater from 75 monitoring wells (as shown in Fig. 3.1d) during the period from 2006 to 2010. The findings indicated that the mean concentration of groundwater salinity within the watershed ranged from 2,700 to 3,000 mg/L. The prevalent presence of gypsum ($CaSO_4$) in the region led to elevated levels of sulfate ($SO_4$), with minimum, maximum, and average concentrations of 147 mg/L, 29,457 mg/L, and 1,878 mg/L, respectively, which constitute 56% of the total salinity. Additionally, the estimated mean concentrations of Total Dissolved Solids (TDS) and $SO_4$ in the Arkansas River and its tributaries stands at 1,145 mg/L and 560 mg/L, respectively (Morway and Gates, 2012).

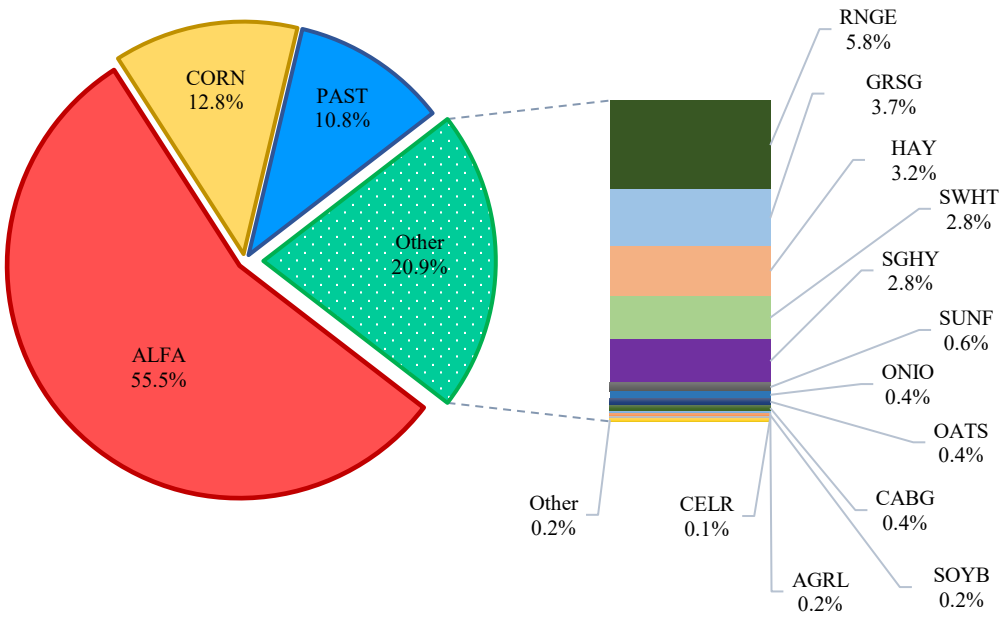


**Figure 3.2.** Contribution of each crop type in annual average crop yield from 1999 to 2009 in the LARV, with abbreviations used for clarity: ALFA (Alfalfa), CORN (corn), PAST (pasture/grass), RNGE (rangeland), GRSG (grain sorghum), HAY (hay), SWHT (spring wheat), SGHY (sorghum hay), SUNF (sunflower), ONIO (onion), OATS (oats), CABG (cabbage), SOYB (soybean), AGRL (generic agricultural land), CELR (celery), WWHT (winter wheat), GRBN (green beans), BARL (spring barley), PEPP (bell pepper), HMEL (honeydew melon), TOMA (tomato), SCRN (sweet corn), ASPR (asparagus), SGBT (sugar beet), CANT (cantaloupe), FRSE (forest-evergreen), TIMO (timothy), WMEL (watermelon), and CUCM (cucumber).

### 3.2.2 SWAT-MODFLOW-Salt overview

In this study, the recently developed and calibrated SWAT-MODFLOW-Salt model (Bailey and Hosseini, 2023) was used to quantify the WFs (including green, blue, and total) of crop production and assess the impact of salinity and climate change on these water footprints. The SWAT-MODFLOW-Salt model code was developed by Bailey and Hosseini (2023) by integrating the SWAT-MODFLOW code (with RT3D functionality for nutrient transport in the groundwater system) (Wei and Bailey, 2019) and the SWAT-Salt code (Bailey et al., 2019) to account for the fate and transport of eight significant salt ions ($SO_4^{2-}$, $Cl^-$, $CO_3^{2-}$, $HCO_3^-$, $Ca^{2+}$, $Na^+$, $Mg^{2+}$, $K^+$) within the soil, groundwater, and stream systems. This integrated model provides comprehensive modeling of salt transport in all major hydrological pathways: surface runoff, streamflow, soil lateral flow, soil percolation and groundwater recharge, groundwater pumping and applied irrigation, canal diversions and applied irrigation, groundwater flow within the aquifer system, and exchanges between groundwater and streams for each HRU, grid cell, and stream channel.

The original SWAT-MODFLOW model code (Bailey et al., 2016) integrates the SWAT watershed modeling code (originally developed by Arnold et al., 1998) with the MODFLOW-NWT groundwater flow modeling code (developed by Niswonger et al., 2011). In the context of the SWAT-MODFLOW framework, SWAT simulates land surface and soil profile processes and fluxes (e.g., surface runoff, evapotranspiration, crop growth, percolation, soil lateral flow, recharge, and stream discharge), and MODFLOW simulates groundwater head, storage, flow, and groundwater-surface water exchange within a heterogeneous, multi-layer aquifer system. SWAT provides recharge from hydrologic response units (HRUs) to the grid cells of MODFLOW, while MODFLOW provides groundwater-stream exchange rates between grid cells and subbasin streams. These exchanges occur at a daily time resolution during the model simulation period. The SWAT-MODFLOW model has been tested for a variety of watersheds worldwide to characterize

water supply, groundwater-surface water interactions, and impact of climate change on hydrological processes (e.g., (Aliyari et al., 2019; Chunn et al., 2019; Molina-Navarro et al., 2019; Wei and Bailey, 2019).

The salt transport processes within the land surface (i.e., hydrologic response units or HRUs), soil layers, and stream channels are based on the SWAT-Salt model presented by Bailey et al. (2019). The SWAT-Salt model simulates the fate and transport of 8 major ions, including Sulfate ($SO_4^{2-}$), Calcium ($Ca^{2+}$), Magnesium ($Mg^{2+}$), Sodium ($Na^{+}$), Chloride ($Cl^{-}$), Potassium ($K^{+}$), Carbonate ($CO_3^{2-}$), and Bicarbonate ($HCO_3^{-}$), within a watershed system. The salinity flux pathways encompass multiple processes, such as surface runoff, groundwater flow, streamflow, soil percolation and leaching, groundwater upflux to the soil profile, and soil lateral flow. The model calculates the concentration of salt ions in three main compartments: 1) soil water in each HRU soil layer, 2) groundwater in each HRU aquifer unit, and 3) surface water in each subbasin stream. These concentrations result from salinity fluxes and equilibrium chemistry reactions, including precipitation-dissolution, complexation, and cation exchange. The model solves for each salt ion within each HRU soil layer and each HRU aquifer unit on a daily time step. Additionally, the salinity module simulates the mass loading of salt ions to the soil profile due to irrigation practices. This includes salt ion mass removal from the HRU aquifer unit for groundwater irrigation and salt ion mass removal from the subbasin stream for surface water irrigation.

The salt transport processes associated with groundwater are based on the salinity module developed by (Tavakoli-Kivi et al., 2019) for the groundwater solute transport code RT3D (termed RT3D-Salt), particularly for irrigated groundwater systems. The modeling code solves for mass balance and equilibrium chemistry, including precipitation-dissolution of salt minerals, for each aquifer grid cell for each of the 8 salt ions.

For SWAT-MODFLOW-Salt, the Fortran codes of SWAT-MODFLOW, SWAT-Salt, and RT3D-Salt are merged into a single code, with the routines from SWAT-Salt performing salt mass balance and chemistry for land surface, soils, and channels, and the routines from RT3D-Salt performing salt mass balance and chemistry for the groundwater system. Salt leaching from the soil profile is provided to RT3D grid cells as incoming salt mass, and exchange salt ion loads between groundwater and streams is performed using the product of flow rates (from MODFLOW) and concentrations (from RT3D-Salt). Salt ion loads within the streams are routed downstream using SWAT's routing algorithm. If MODFLOW simulates groundwater head (water table) within the soil profile of an HRU, then water and associated salt mass are transferred from the aquifer system to the soil system (Bailey and Hosseini, 2023).

Moreover, the code simulates the influence of salinity stress on crop yield. This is achieved through the application of the relative yield equation formulated by Maas (1993), which considers threshold and slope parameters pertinent to various crop types. For a more comprehensive understanding of the theoretical underpinnings and mass balance equations of the SWAT-MODFLOW-Salt model, detailed information can be found in the work by Bailey and Hosseini (2023).

### 3.2.3 Study region model

The SWAT-MODFLOW-Salt model used in this study is the same version introduced by Bailey and Hosseini (2023) in the initial presentation and exposition of the new modeling code. The SWAT-MODFLOW model applied for the study area, as detailed in (Wei and Bailey, 2019), is an integration of the SWAT model (Wei et al., 2018) and MODFLOW model (Morway et al., 2013) developed for the region. The original SWAT model of the study area (Wei et al., 2018) was constructed using soil, land used, topographic, meteorological, and canal diversion data (Table

3.1). The irrigation mode employed is automatic irrigation, while the Penman-Monteith method is utilized to compute crop potential evapotranspiration (PET). Additionally, various management practices, such as planting, harvesting, and tillage, are configured to address both rainfed and irrigated conditions (Wei et al., 2018). The model encompasses a total of 72 subbasins (see Fig. 3.1d for subbasin boundaries). Within these subbasins, there are 5270 HRUs, with each individual cultivated field designated as a distinct HRU. The model's performance was tested against streamflow data collected from multiple monitoring sites along the Arkansas River and tributaries.

The MODFLOW model relies on a dataset encompassing aquifer properties, pumping rates, and groundwater head (Table 3.1). Bailey et al. (2019) developed the SWAT-Salt model to include the fate and transport of 8 major salt ions in the soil, groundwater, and stream system, and subsequently, Bailey and Hosseini (2023) developed the SWAT-MODFLOW-Salt model by integrating the constructed SWAT-MODFLOW modeling code with SWAT-Salt modeling code for the study region applying salt mineral fractions, soil water salt ion concentrations, and groundwater salt ion concentrations data derived from SSURGO and field measurements (Table 3.1). The model was executed over the period spanning from 1999 to 2009 and tested against groundwater salt ion concentrations, soil salinity, in-stream salt ion loading, and crop yield.

**Table 3.1** List of input data used to set up the SWAT-MODFLOW-Salt model.

| Base Model | Data type | Resolution | Sources |
|---|---|---|---|
| SWAT | Soil data | 1:250,000 | US Digital General Soil Map (STATSGO) from National |
| | Land use | 30 m × 30 m | Resources Conservation Service, National Agricultural Statistics Service (NASS) |
| | Meteorological data | 1999-2010 | Colorado Agricultural Meteorological Network (CoAgMet) |
| | Canal diversion | 1999-2010 | Colorado's Decision Support Systems (CDSS) |
| | Streamflow | 1999-2010 | Colorado Division of Water Resources |
| SWAT + MODFLOW | Topography (DEM) | 30 m × 30 m | The National Map System, US Geological Survey |
| | Stream network | 30 m × 30 m | National Hydrography Data Set, US Geological Survey |
| MODFLOW | Aquifer properties | 250 m × 250 m | (Morway et al., 2013) |
| | Pumping rates | Monthly | Colorado Division of Water Resources |
| | Groundwater head | 1999-2010 | US Geological Survey (NWIS) |
| Salinity module | CaCO3 + CaSO4 | 1:250,000 | SSURGO |
| | Groundwater salt ion concentrations | 1999-2010 | Field data (Gates et al., 2016, 2009) |
| | In-stream salt ion concentrations | 1999-2010 | Field data (Gates et al., 2016, 2009) |

### 3.2.4 Climate change scenarios and projection

In this study, the calibrated and validated SWAT-MODFLOW-Salt model for the study region was employed in conjunction with projected climate data from 2021 to 2100 to investigate the impact of climate change on salinity fate and transport and to quantify the crop production water footprints under the coupled stresses of salinity and climate change over the course of the 21$^{st}$

century. We considered five climate models and two Representative Concentration Pathway (RCP) emission scenarios, 4.5 and 8.5.

Due to the coarse spatial resolution of Global Climate Models (GCMs), model output often requires downscaling, through dynamic or statistical methods. Among these two, the statistical method has gained broader utilization due to computational efficiency, the practicality of directly integrating observations into the method, and the capacity to deliver climatic projections at a finer, point-specific scale derived from the broader GCM level (Fowler et al., 2007; Shiru et al., 2022).

In this study, we use the Multivariate Adaptive Constructed Analogs (MACA) statistical method, used for downscaling climate model output within the continuous United States (Abatzoglou and Brown, 2012). This process entails downsizing of data sourced from twenty GCMs from the Coupled Model Inter-Comparison Project Phase 5 (CMIP5) which offers higher meteorological data resolution compared to earlier CMIPs (Shiru et al., 2022; Song et al., 2022), transforming them from their initial resolutions to either 4 or 6 kilometers. These adjustments are made for RCP4.5 and RCP8.5, spanning the period from 2006 to 2100. RCPs signify potential future scenarios regarding greenhouse gas and $CO_2$ emissions considering socio-economic potential future changes and are categorized based on their projected radiative forcing levels by the year 2100 (Aliyari et al., 2021). In a relatively moderate and optimistic environmental scenario, RCP4.5, the change in radiative forcing by 2100 raises to 4.5 watts per square meter ($Wm^{-2}$) and 550 ppm $CO_2$. In the more extreme and pessimistic scenario, RCP8.5, this change increases significantly to 8.5 $Wm^{-2}$ and 1000 ppm $CO_2$ by the year 2100.

To comprehensively assess the impact of projected climate change on salinity fate and transport and quantify the mutual impact of salinity and climate change on crop production WFs in the LARV, we used the combination of five distinct MACA climate models under the RCP4.5 and

RCP8.5 emission scenarios. The chosen climate models for this investigation (Table 3.2), consist of widely utilized GCMs, each representing the least warm projection (WARM), hottest projection (HOT), driest projection (DRY), wettest projection (WET), and a moderate (MODERATE) projection that signifies the midpoint in terms of temperature and precipitation variability among all the other models at a regional scale (Heidari et al., 2020; Joyce and Coulson, 2020). The MACA climate dataset comprises essential meteorological variables, including maximum daily near-surface temperature (tasmax), minimum daily near-surface temperature (tasmin), daily surface-level precipitation (pr), daily eastward wind component near the surface (uas), and daily northward wind component near the surface (vas) (Heidari et al., 2020). In this study, we refer to the period from 1999 to 2009 as the "baseline" to serve as a reference for comparison with future climate scenarios by 2100. The projected downscaled MACA climate dataset from five GCM models were inserted into the SWAT weather input file, and accordingly, each individual GCM was separately simulated in the calibrated and validated SWAT-MODFLOW-Salt model, considering both the present baseline and the future climate scenarios defined by the two Representative Concentration Pathways (RCP4.5 and RCP8.5).

**Table 3.2** List of selected GCM models from MACA climate models (Aliyari et al., 2021; Heidari et al., 2020; Joyce and Coulson, 2020)

| GCM model | Climatic projection | Emission scenarios | Model agency |
|---|---|---|---|
| HadGEM2-ES365 | HOT | RCP4.5, RCP8.5 | Met Office Hadley Center, UK |
| MRI-CGCM3 | WARM | RCP4.5, RCP8.5 | Meteorological Research Institute, Japan |
| IPSL-CM5A-MR | DRY | RCP4.5, RCP8.5 | Institute Pierre Simon Laplace, France |
| NorESM1-M | MODERATE | RCP4.5, RCP8.5 | Norwegian Climate Center, Norway |
| CNRM-CM5 | WET | RCP4.5, RCP8.5 | National Centre of Meteorological Research, France |

### 3.2.5 Estimating crop production water footprints

We used the calibrated and tested SWAT-MODFLOW-Salt model to quantify crop production water footprint under the combined influences of salinity stress and climate change. The $WF_{green}$ $\left(m^3 ton^{-1}\right)$ is defined as the ratio of the volume of green water (derived from precipitation), denoted as $CWU_{green}$, utilized in crop production to crop yield (Y) $\left(ton\, ha^{-1}\right)$ considering that $CWU_{green}$ is equal to the actual crop ET under the condition that soil does not receive any additional moisture through irrigation ($ET_a^{no-irrig}$). To calculate $WF_{green}$, we summed up the total ET values (in millimeters) during the crop growth period for each Hydrologic Response Unit (HRU) and divided this sum by the crop yield. This computation was performed using Equation 1, following the approach outlined by (Mekonnen and Hoekstra, 2011):

$$WF_{green} = \frac{CWU_{green}}{Y} = \frac{ET_a^{no-irrig}}{Y} \quad (1)$$

To calculate $CWU_{green}$ ($ET_a^{no-irrig}$), the SWAT-MODFLOW-Salt code was modified to deactivate irrigation practices within the model simulations, effectively eliminating irrigation from the computational processes. This approach allows the simulation to consider scenarios of only rain-fed cultivation. Subsequently, the model output was used to extract $ET_a$ and crop yield (Y) for each individual HRU.

The concept of $WF_{blue}$ $\left(m^3 ton^{-1}\right)$ centers on the consumption of freshwater resources, including water from rivers, aquifers, and lakes, specifically for irrigation in crop production, following the definition provided by Mekonnen and Hoekstra (2011), and is quantified by dividing the blue crop water use ($CWU_{blue}$) by the crop yield (Y). $CWU_{blue}$, in turn, is derived by subtracting $CWU_{green}$ from the actual evapotranspiration ($ET_a^{irrig}$) that occurs under irrigation practices and was calculated using Equation 2 for each individual HRU:

$$WF_{blue} = \frac{ET_a^{irrig} - CWU_{green}}{Y} \quad (2)$$

The $WF_{total}$ $\left(m^3 ton^{-1}\right)$ is determined by summing the values of $WF_{green}$ and $WF_{blue}$. This calculation was executed separately for each HRU and for each year within the simulation period, spanning from 1999 to 2100. The simulations were conducted under two distinct scenarios, one incorporating the salinity stress routines within the SWAT-MODFLOW-Salt code, and the other without these routines to investigate the combined effects of salinity and climate change on the WFs of crop production.

Each simulation was run with and without the influence of soil salinity on crop yield, to quantify the impact of salinity on calculated WFs.

## 3.3. RESULTS AND DISCUSSION

We first present water footprint results for the historical period (1999-2009), under both salinity and without the influence of soil salinity. Subsequently, we delve into the findings illustrating the combined effects of salinity and climate change on crop yields and crop production water footprints.

### 3.3.1 Salinity impact on crop production water footprints (historical period)

Figure 3.3 shows the annual average green, blue, and total crop yields, along with corresponding green, blue, and total WFs for the primary crops, alfalfa, and corn, in the LARV within the 1999-2009 period encompassing calculations with and without factoring in the influence of salinity on crop yield and WF assessments. Simulated crop yields under rainfed and irrigated conditions considering the salinity conditions for each year during the 1999-2009 period for alfalfa and corn are shown in Figure 3.3a,b,c.

Over the 11-year simulation period, alfalfa's annual average green, blue, and total crop yields, when not influenced by salt stress, are estimated at 1.2, 7.0, and 8.2 $\left(ton\,ha^{-1}\right)$, while for corn, the estimates are 1.1, 3.4, and 4.5$\left(ton\,ha^{-1}\right)$, respectively. Conversely, when subjected to salinity stress, the annual average green, blue, and total crop yields for alfalfa decrease to 1.0, 6.8, and 7.8 $\left(ton\,ha^{-1}\right)$, while corn's yields reduce to 0.95, 3.3, and 4.25 $\left(ton\,ha^{-1}\right)$. The corresponding reductions in green, blue, and total crop yield for alfalfa due to salinity impact are 9.6%, 3.2%, and 4.2%, while in the case of corn, these declines are 13.6%, 2.4%, and 5.3%, respectively.

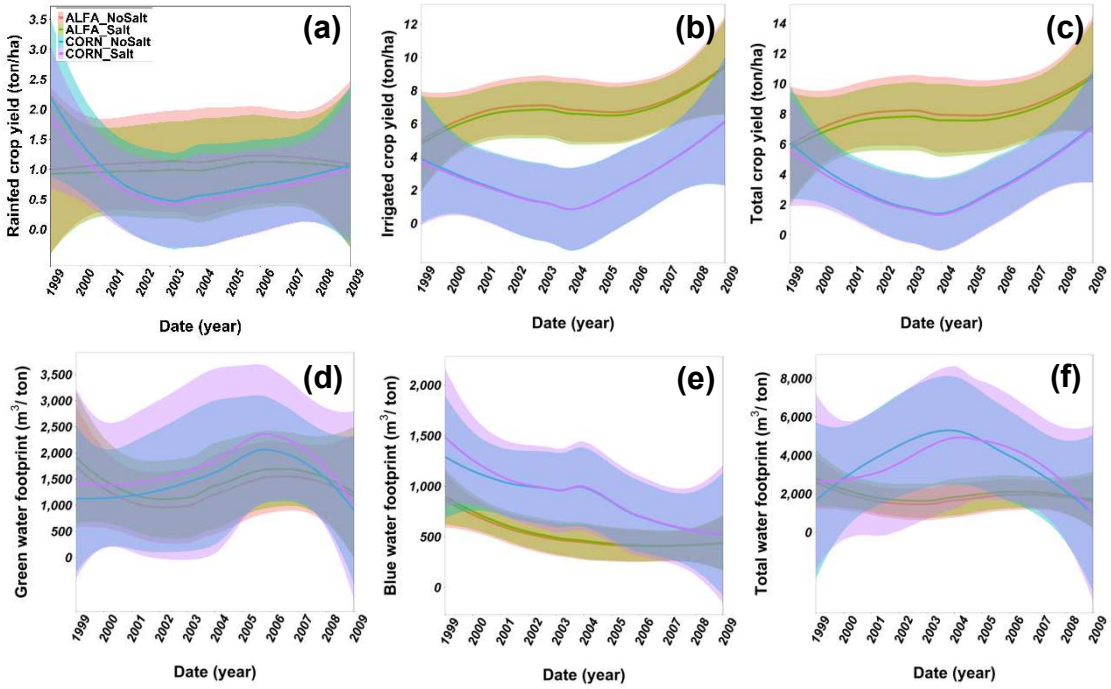


**Figure 3.3.** Area plots above show (a) green crop yield, (b) blue crop yield, (c) total crop yield, (d) green water footprint, (e) blue water footprint, and (f) total water footprint of alfalfa and corn as major crops in the LARV under the salinity stress and without salinity impact between 1999-2009.

The simulated $WF_{green}$, $WF_{blue}$, and $WF_{total}$ for alfalfa and corn, taking into account both salinity and non-salinity conditions are presented in Figure 3.3d,e,f for each year from 1999 to 2009. Among the two dominant crops in the area, the green, blue, and total WFs of alfalfa rise from 1114, 473, and 1587 $\left(m^3 ton^{-1}\right)$ to 1233, 487, and 1720 $\left(m^3 ton^{-1}\right)$ indicating a 10.7%, 2.8%, and 8.4% increase in WFs under salinity conditions. For corn, the green, blue, and total WFs increase from 1292, 724, and 2016 $\left(m^3 ton^{-1}\right)$ to 1497, 739, and 2236 $\left(m^3 ton^{-1}\right)$, showing a 16%, 2.1%, and 11% increase in crop production WFs due to the salinity impact.

As can be seen in Figure 3.3a,b,c, the influence of salinity is more pronounced on green (rainfed) crop yield, resulting in a 3% greater reduction compared to blue crop yield. Correspondingly, the green WF for both crops experienced a 3.13% higher increase compared to the blue WF. Considering that the green WF represents a larger proportion of the total WF (making

up 68% of the total WF), therefore, the decrease in green WF due to salinity has a more noticeable impact on the total WF (Figure 3.3f).

**Table 3.3** The estimated green (WFgreen), blue (WFblue), and total (WFtotal) water footprints under salinity stress condition for selected crops in the study area and comparison to other studies from the literature are provided in the table

| Crop | GWF $\left(m^3 ton^{-1}\right)$ | | BWF $\left(m^3 ton^{-1}\right)$ | | TWF $\left(m^3 ton^{-1}\right)$ | |
|---|---|---|---|---|---|---|
| | This study | Other studies | This study | Other studies | This study | Other studies |
| Alfalfa | 1233 | - | 487 | - | 1720 | - |
| Corn | 1497 | 947 (Mekonnen and Hoekstra, 2011) | 739 | 81 (Mekonnen and Hoekstra, 2011) | 2236 | 1028<br>942-1174 (Luan et al., 2018) |
| Pasture | 1176 | - | 439 | - | | - |
| Oats | 3127 | 1479 (Mekonnen and Hoekstra, 2011) | 1128 | 181 (Mekonnen and Hoekstra, 2011) | 4255 | 1660 (Mekonnen and Hoekstra, 2011) |
| Spring Wheat | 3323 | 1277 (Mekonnen and Hoekstra, 2011) | 670 | 342 (Mekonnen and Hoekstra, 2011) | 3993 | 1619 (Mekonnen and Hoekstra, 2011)<br>1380-2888 (Luan et al., 2018)<br>1751 (Zhuo et al., 2016) |
| Onion | 2549 | 176 (Mekonnen and Hoekstra, 2011) | 662 | 44 (Mekonnen and Hoekstra, 2011) | 3211 | - |
| Sunflower | 3769 | 3017 (Mekonnen and Hoekstra, 2011) | 940 | 148 (Mekonnen and Hoekstra, 2011) | 4709 | 3165 (Mekonnen and Hoekstra, 2011)<br>2095-4855 (Luan et al., 2018)<br>1241 (Zhuo et al., 2016) |
| Grain Sorghum | 3019 | 3945 (Mekonnen and Hoekstra, 2011) | 871 | 125 (Mekonnen and Hoekstra, 2011) | 3890 | 4070 (Mekonnen and Hoekstra, 2011) |

Figure 3.4 illustrates the percentage changes in the average annual green, blue, and total crop yields along with the percentage changes in green, blue, and total WFs of 29 crops in the LARV attributed to salinity stress over the period from 1999 to 2009. The simulated green, blue, and total WFs under salinity impact between 1999 and 2009, along with the comparable estimated WFs from other studies for selected crops are reported in Table 3.3. According to Table 3.3, the

estimated green, blue, and total WFs affected by salinity conditions for the selected crops in the LARV are notably higher compared to the global average WFs documented by Mekonnen and Hoekstra (2011) and the WFs reported in various regions worldwide. Several factors besides salinity can contribute to these variations, including the spatial and temporal distribution of crops in the region, climate conditions, soil types, topography, planting and harvesting schedules, growing periods, crop parameters, irrigation practices, water regulations, the WF estimation model employed, model resolution (spatial and temporal), and the accuracy of the data used in the estimation process.

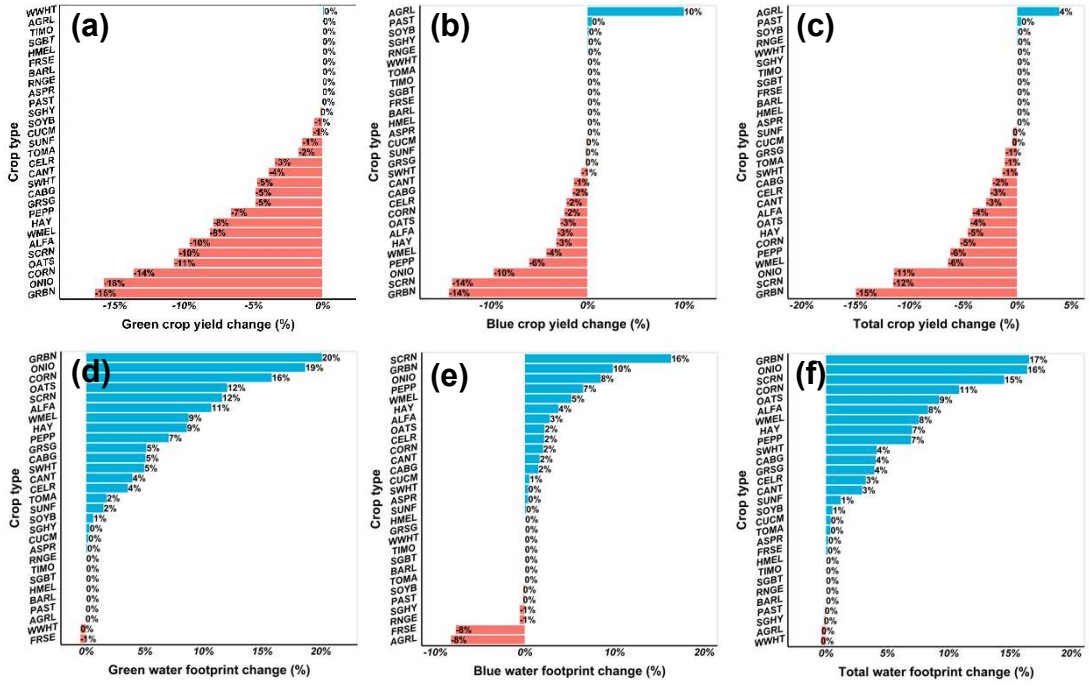


**Figure 3.4.** Average percentage changes in (a) green crop yield, (b) blue crop yield, (c) total crop yield, (d) green water footprint, (e) blue water footprint, and (f) total water footprint of 29 crops in the LARV under the salinity stress from 1999 to 2009.

As depicted in Figure 3.4, providing a comprehensive overview of the salinity impact on $WF_{green}$, $WF_{blue}$, and $WF_{total}$, along with green, blue, and total crop yield for 29 crop types in the LARV from 1999 to 2009, it is evident that certain crops such as green beans (16%), onion (16%), corn (14%), oats (11%), sweet corn (10%), and alfalfa (10%) experienced notable reductions in

green yield compared to other crops. Consequently, the $WF_{green}$ for these crops increased by 20%, 19%, 16%, 12%, 12%, and 11%, respectively. Conversely, green beans (14%), sweet corn (14%), onion (10%), pepper (6%), watermelon (4%), hay (3%), alfalfa (3%), and corn (2%) exhibited the highest reductions in blue yield due to salinity stress. The $WF_{blue}$ for these crops increased by 10%, 16%, 8%, 7%, 5%, 4%, 3%, and 2%, respectively. Correspondingly, the total WF of green beans (17%), onion (16%%), sweet corn (15%), corn (11%), oats (9%), alfalfa (8%), watermelon (8%), and hay (7%) witnessed the most substantial increments, and the total yield of green beans (15%), sweet corn (12%), onion (11%), watermelon (6%), corn (5%), hay (5%), alfalfa (4%), oats (4%)—as the predominant crops—experienced the most significant reduction. Considering that alfalfa and corn collectively contribute to 70% of the total crop yield in the LARV, any reductions in their total crop yield and increases in total WF will exert the most significant impact on the overall annual average crop yield in the region. Ultimately, the estimated annual average green crop yield without salinity impact is 4.5 tons, and the annual average blue crop yield is 14.3 tons. Under salinity conditions, these values decrease to 4.3 and 14 tons, respectively, resulting in a 5.1%, 1.8%, and 2.6% reduction in green, blue, and total crop yield in tons in the LARV.

The average annual contributions of green and blue crop yields, unaffected by salinity stress, account for 18% and 82% of the total crop yield, respectively, while the average annual $WF_{total}$ is composed of 67% $WF_{green}$ and 33% $WF_{blue}$. When salinity stress is introduced, the average annual green and blue crop yields contribute to 17% and 83% of the total crop yield, respectively. The corresponding proportions of $WF_{green}$ and $WF_{blue}$ to the average annual crop production $WF_{total}$ are 68% and 32%, respectively. In the absence of salinity stress, the average annual green crop yield is estimated at 0.62 $\left(ton\,ha^{-1}\right)$, while under salinity stress, it decreases to 0.59 $\left(ton\,ha^{-1}\right)$, reflecting an approximately 4.6% reduction in green crop yield due to salinity impact. The average

annual blue crop yield, unaffected by salt stress is 2.0 $\left(ton\,ha^{-1}\right)$, and under salinity conditions, it reduces to 1.97 $\left(ton\,ha^{-1}\right)$, indicating about a 1.6% decline in blue crop yield. The total annual average crop yield, without salinity stress, is 2.62 $\left(ton\,ha^{-1}\right)$, while under salinity stress, it reduces to 2.56 $\left(ton\,ha^{-1}\right)$, indicating 2.3% reduction in total annual crop yield in the area as detailed in Table 3.5.

The annual average $WF_{green}$, $WF_{blue}$, and $WF_{total}$ for 29 crops in the region without salinity stress are 88366, 43651, and 132018 $\left(m^3ton^{-1}\right)$, respectively. Under salinity stress condition, these values rise to 95058, 45592, and 140650 $\left(m^3ton^{-1}\right)$ indicating a 7.6%, 4.5%, and 6.5% rise in crop production WFs in the area, as reported in Table 3.5. As indicated in Equations 1 and 2, which outline the method for computing green and blue water footprints, a decline in crop yield results in an elevation of crop production water footprints. This is the case even when evapotranspiration (ET) remains constant or decreases to a lesser extent than the reduction observed in crop yield. Consequently, the ratio of ET to yield increases, contributing to a rise in water footprints per unit of crop produced. Additionally, the estimated green and blue WFs for the 29 crops suggest that, for most crop types, $WF_{green}$ constitutes a larger proportion, approximately two to three times that of $WF_{total}$ compared to $WF_{blue}$. This trend aligns with findings from other studies examining crop WFs, as denoted in Table 3.3. Similarly, the ratios of green and blue crop yields mirror the overall crop yield pattern, albeit in reverse. The predominance of $WF_{green}$ over $WF_{blue}$, and blue crop yield over the green crop yield is influenced by the semi-arid nature of the LARV, characterized by an average annual precipitation of 273 mm (Wei and Bailey, 2019), necessitating irrigation to support sustainable crop production. Consequently, the green crop yield, reliant on precipitation-supplied water, results in lower yields and, subsequently, higher $WF_{green}$.

### 3.3.2 Mutual impact of climate change and salinity on crop production water footprints

Figure 3.5 illustrates the projected annual average maximum and minimum temperatures in ℃, and precipitation in mm under RCP4.5 and RCP8.5 for all five GCM models. The comparison includes the annual average of minimum and maximum temperatures and precipitation in the baseline period at three weather stations—Fowler, Rocky Ford, and La Junta—as depicted in Fig. 3.1 within the LARV. The changes in average minimum and maximum temperatures and precipitation compared to the baseline in Fowler range between +25.2% (projected by MRI-CGCM3-4.5) and 119.1% (projected by IPSL-CM5A-MR-8.5), +1.85% (projected by MRI-CGCM3-4.5) and +16.5% (projected by HadGEM2-ES365-8.5), and -15% (projected by IPSL-CM5A-MR-8.5) and +13.7% (projected by MRI-CGCM3-8.5), respectively. In Rocky Ford, the changes in average minimum and maximum temperatures and precipitation compared to the baseline range between +23.6% (projected by MRI-CGCM3-4.5) and 114% (projected by IPSL-CM5A-MR-8.5), +1.93% (projected by MRI-CGCM3-4.5) and +16.2% (projected by HadGEM2-ES365-8.5), and -17.3% (projected by IPSL-CM5A-MR-8.5) and +12.3% (projected by MRI-CGCM3-8.5), respectively. Similarly, in La Junta, the changes in average minimum and maximum temperatures and precipitation compared to the baseline range between +20.9% (projected by MRI-CGCM3-4.5) and 104.3% (projected by IPSL-CM5A-MR-8.5), +2.13% (projected by MRI-CGCM3-4.5) and +16.6% (projected by IPSL-CM5A-MR-8.5), and -19.6% (projected by IPSL-CM5A-MR-8.5) and +10.3% (projected by MRI-CGCM3-8.5), respectively.

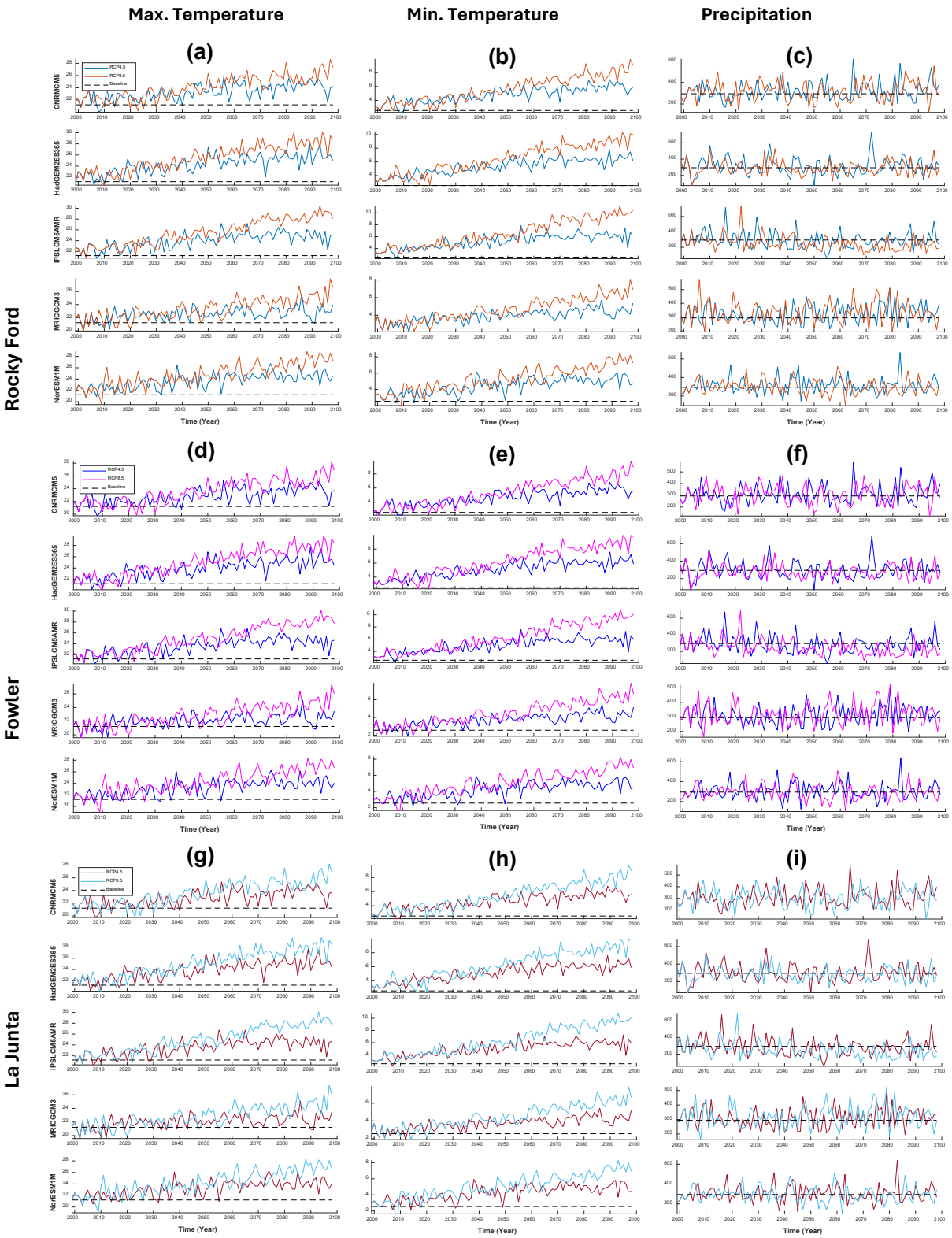


**Figure 3.5.** (a, d & g) and (b, e & h) Projected annual average maximum and minimum temperature (°C); (c, f & i) Projected annual average precipitation (mm) for all climate models under RCP4.5 and RCP8.5 emission scenarios The data is presented for stations Rocky Ford, Fowler, and La Junta within the watershed are shown in Fig. 3.1a. The historical averages from 1999 to 2009 are depicted as dashed lines in each plot for comparison.

The simulated annual average water footprints, encompassing green, blue, and total footprints, along with rainfed, irrigated, and total yields for two major crops, alfalfa and corn, in the Lower Arkansas River Valley (LARV), are presented in Figures A. 1-9 (refer to section A.1 in the provided Appendix as an e-component). These simulations cover the baseline period and account for various climate change scenarios across all five GCM models including CNRM-CM5, HadGEM2-ES365, IPSL-CM5A-MR, MRI-CGCM3, and NorESM1-M and two RCPs (RCP4.5 and RCP8.5), with and without the influence of salinity stress. Additional details on percentage changes in WFs under salinity and climate change scenarios are available in Table 3.4. Figure 3.7 shows the green, blue, and total crop yields as well as green, blue, and total WFs of alfalfa and corn under the combined impact of salinity and IPSL-CM5A-MR-8.5 as the driest climate change scenario.

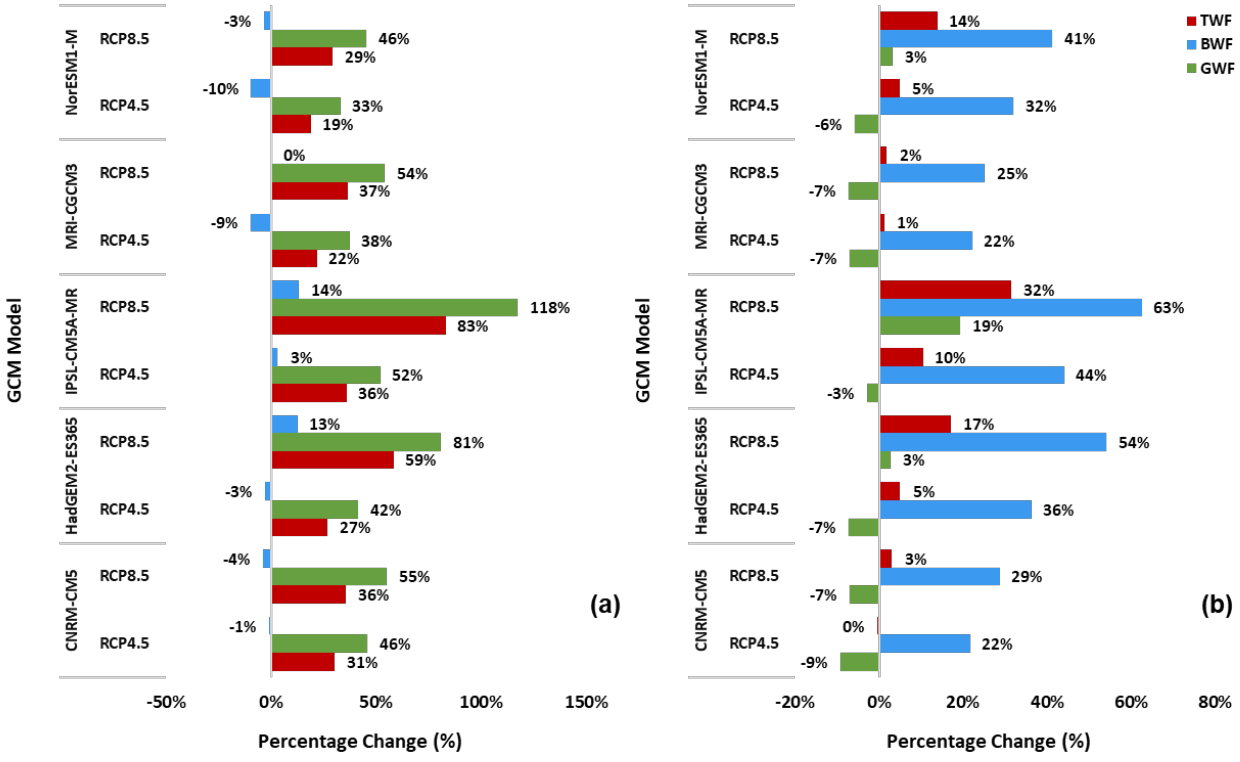


**Figure 3.6.** The percentage changes in green, blue, and total water footprint of (a) alfalfa, (b) corn compared to baseline (1999-2009) and under combined impact of salinity stress and five GCM models in the LARV by 2100.

Projections as shown in Figure 3.6 indicate an increase in alfalfa green, blue, and total WFs under RCP4.5 compared to the baseline, ranging from -9.3% to -2.8%, +21.7% to +44.3%, and -0.5% to +10.5%, respectively. Similarly, the projected changes in green, blue, and total WFs under RCP8.5 range between -7% and +19.4%, +28.8% and +62.8%, and +1.9% and +31.7%, respectively. For corn, the green, blue, and total WFs under RCP4.5 vary between +33.1% and +52.2%, -9.6% and +3.3%, and +19% and +36.1%, respectively. Correspondingly, corn green, blue, and total WFs under RCP8.5 are projected to fluctuate between +45.6% to +117.8%, -3.8% to +13.5%, and +29.4% to +83.3% compared to the baseline WFs.

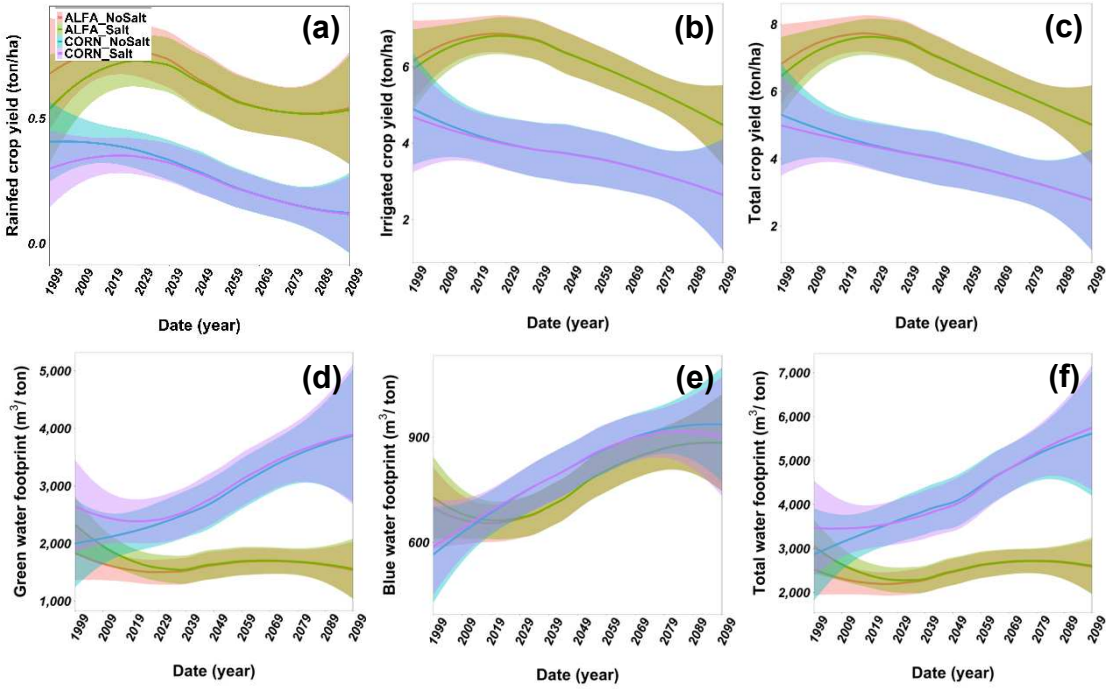


**Figure 3.7.** Area plots above show (a) green crop yield, (b) blue crop yield, (c) total crop yield, (d) green water footprint, (e) blue water footprint, and (f) total water footprint of alfalfa and corn as major crops in the LARV under the mutual impact of IPSL-CM5A-MR-8.5 climate model and salinity stress by 2100.

Across all GCMs, there is a consensus on increased GWF for corn under both RCPs and increased BWF for alfalfa under both RCP scenarios. The most substantial increase in alfalfa's GWF is projected by IPSL-CM5A-MR, reaching +19.4% under RCP8.5, while a similar projection

for corn is +117.8% by the same GCM. The largest increase in alfalfa's BWF is +62.8% under RCP8.5 projected by IPSL-CM5A-MR and for corn, it is +13.5% projected by IPSL-CM5A-MR under RCP8.5. Consequently, IPSL-CM5A-MR projects the most significant increase in alfalfa's total WF, reaching +31.7% under RCP8.5. Similarly, the same GCM model projects an 83.3% increase in corn's total WF under RCP8.5. The results presented in Table 3.4 indicate that the most substantial increase is observed under RCP8.5, as projected by the driest GCM model, owing to the highest $CO_2$ concentration increase when compared to the other GCM models.

**Table 3.4** The baseline and estimated green (WFgreen), blue (WFblue), and total (WFtotal) water footprints under salinity stress condition for five GCM models and two emission scenarios for alfalfa and corn in the study area compared to the baseline water footprints. The number inside the parenthesis under the water footprints represents the percentage change by 2100 compared to the baseline

| Crop | GCM model | Scenario | GWF $\left(m^3 ton^{-1}\right)$ | BWF $\left(m^3 ton^{-1}\right)$ | TWF $\left(m^3 ton^{-1}\right)$ |
|---|---|---|---|---|---|
| Alfalfa | Baseline | - | 1233 | 487 | 1720 |
| | CNRM-CM5 | RCP4.5 | 1119(-9%) | 593(22%) | 1712(-0%) |
| | | RCP8.5 | 1147(-7%) | 627(29%) | 1774(3%) |
| | HadGEM2-ES365 | RCP4.5 | 1143(-7%) | 664(36%) | 1807(5%) |
| | | RCP8.5 | 1266(3%) | 751(54%) | 2017(17%) |
| | IPSL-CM5A-MR | RCP4.5 | 1198(-3%) | 702(44%) | 1900(10%) |
| | | RCP8.5 | 1472(19%) | 792(63%) | 2264(32%) |
| | MRI-CGCM3 | RCP4.5 | 1148(-7%) | 595(22%) | 1743(1%) |
| | | RCP8.5 | 1143(-7%) | 610(25%) | 1753(2%) |
| | NorESM1-M | RCP4.5 | 1163(-6%) | 643(32%) | 1806(5%) |
| | | RCP8.5 | 1272(3%) | 688(41%) | 1960(14%) |
| Corn | Baseline | - | 1497 | 739 | 2236 |
| | CNRM-CM5 | RCP4.5 | 2188(46%) | 732(-1%) | 2920(31%) |
| | | RCP8.5 | 2324(55%) | 711(-4%) | 3035(36%) |
| | HadGEM2-ES365 | RCP4.5 | 2122(42%) | 720(-3%) | 2842(27%) |
| | | RCP8.5 | 2712(81%) | 833(13%) | 3545(59%) |
| | IPSL-CM5A-MR | RCP4.5 | 2278(52%) | 763(3%) | 3041(36%) |
| | | RCP8.5 | 3259(118%) | 839(14%) | 4098(83%) |
| | MRI-CGCM3 | RCP4.5 | 2059(38%) | 669(-9%) | 2728(22%) |
| | | RCP8.5 | 2312(54%) | 741(0%) | 3053(37%) |
| | NorESM1-M | RCP4.5 | 1992(33%) | 668(-10%) | 2660(19%) |
| | | RCP8.5 | 2180(46%) | 714(-3%) | 2894(29%) |

For alfalfa, the projected range of green yield $\left(ton\,ha^{-1}\right)$ is from -5.3% to +14.7% under RCP4.5 and varies between -36.1% to +20.6% under RCP8.5. The blue yield for alfalfa ranges from -3.2% to +6.5% under RCP4.5, and from -9.6% to +4.7% under RCP8.5. Similarly, the total yield for alfalfa ranges from -3.1% to +7.6% under RCP4.5 and varies from -13.1% to +5.2% under RCP8.5. Notably, the most significant reduction in green yield for alfalfa is projected by IPSL-CM5A-MR at -36.1% under RCP8.5. Furthermore, the highest reduction in blue yield for alfalfa is projected by IPSL-CM5A-MR at -9.6% under RCP8.5, and the maximum reduction in total yield for alfalfa is projected by IPSL-CM5A-MR at -13.1% under RCP8.5.

Regarding corn, the reduction in green yield ranges from -43.7% to -32.7% under RCP4.5, with a variation between -69.2% and -40.5% under RCP8.5. The blue yield for corn ranges from +32.1% to +44.7% under RCP4.5, and from +25.8% to +37.7% under RCP8.5. Similarly, the total yield ranges from +15.1% to +26.4% under RCP4.5 and varies from +6.2% to +19.7% under RCP8.5. The most substantial reduction in green yield for corn is projected by IPSL-CM5A-MR at -69.2% under RCP8.5. Additionally, the highest increase in blue yield for corn is projected by NorESM1-M at 44.7% under RCP4.5, and the greatest increase in total yield for corn is projected by NorESM1-M at 26.4% under RCP4.5. The rise in crop yield under emission scenarios (RCP4.5 and RCP8.5) in comparison to the baseline is attributed to elevated $CO_2$ concentrations. This increase in $CO_2$ concentration, known as $CO_2$ fertilization (Sakurai et al., 2014), leads to reduced crop transpiration, ultimately enhancing the yield of crops like soybean and corn (Tijjani et al., 2022).

During the baseline period under salinity stress conditions, there were reductions of 4.6%, 1.6%, and 2.3% in green, blue, and total crop yields, respectively. However, when considering the impact of climate change with five GCM models, the reduction in total crop yield due to salinity

was mitigated, ranging from a 0.44% reduction projected by NorESM1-M to a 0.75% reduction projected by IPSL-CM5A-MR, both under the RCP8.5 scenarios, as outlined in Table 3.5. The highest reduction in green yield (rainfed crop yield) is projected at -1.78% by IPSL-CM5A-MR, the driest GCM model, under RCP8.5 (higher $CO_2$ emission than RCP4.5). IPSL-CM5A-MR also predicts the highest reduction in blue crop yield at 1.87% under RCP8.5. Consequently, the total WF over the baseline period increases by 6.5%, with a 7.6% increase in green WF and a 4.4% increase in blue WF. The green WF is projected to increase by 3.2% according to IPSL-CM5A-MR and HadGEM2-ES365, both under RCP8.5. IPSL-CM5A-MR projects the highest increase in blue WF by 1.9% under RCP8.5, and the total crop production WF is expected to increase by about 3% under RCP8.5 according to IPSL-CM5A-MR.

**Table 3.5** The green, blue, and total yields as well as the green (WFgreen), blue (WFblue), and total (WFtotal) water footprints changes under salinity stress condition and considering five GCM models and two emission scenarios by the end of 21st century compared to the baseline period within the LARV

| GCM Model | Green Yield $\left(ton\,ha^{-1}\right)$ | | Blue Yield $\left(ton\,ha^{-1}\right)$ | | Total Yield $\left(ton\,ha^{-1}\right)$ | |
|---|---|---|---|---|---|---|
| Emission Scenario | RCP4.5 | RCP 8.5 | RCP 4.5 | RCP 8.5 | RCP 4.5 | RCP 8.5 |
| Baseline | -4.62% | | -1.63% | | -2.34% | |
| CNRM_CM5 | -1.18% | -0.66% | -0.37% | -0.40% | -0.53% | -0.45% |
| HadGEM2_ES365 | -1.11% | -1.59% | -0.35% | -0.38% | -0.52% | -0.60% |
| IPSL_CM5A_MR | -1.26% | -1.78% | -0.48% | -0.56% | -0.62% | -0.75% |
| MRI_CGCM3 | -1.03% | -0.80% | -0.48% | -0.40% | -0.60% | -0.48% |
| NorESM1-M | -1.04% | -1.10% | -0.33% | -0.29% | -0.48% | -0.44% |
| GCM Model | GWF $\left(m^3 ton^{-1}\right)$ | | BWF $\left(m^3 ton^{-1}\right)$ | | TWF $\left(m^3 ton^{-1}\right)$ | |
| Emission Scenario | RCP 4.5 | RCP 8.5 | RCP 4.5 | RCP 8.5 | RCP 4.5 | RCP 8.5 |
| Baseline | 7.57% | | 4.44% | | 6.54% | |
| CNRM_CM5 | 2.10% | 1.29% | 1.04% | 0.80% | 1.86% | 1.17% |
| HadGEM2_ES365 | 1.30% | 3.25% | 1.00% | 1.68% | 1.24% | 2.89% |
| IPSL_CM5A_MR | 1.76% | 3.25% | 1.04% | 1.87% | 1.60% | 2.98% |
| MRI_CGCM3 | 2.98% | 1.77% | 0.21% | -0.01% | 2.32% | 1.32% |
| NorESM1-M | 1.62% | 1.75% | 0.50% | 0.90% | 1.37% | 1.57% |

Figure 3.8 a,b,c illustrates the average percentage changes in green, blue, and total crop yields, while Figure 3.8d,e,f shows the percentage changes in WFs under the combined impact of salinity and the driest climate change scenario. Additionally, Figures A. 10-18 (available in Appendix A.2, provided as e-component alongside the manuscript) depict the simulated average percentage changes in green, blue, and total crop yields, along with the corresponding WFs, for the 29 crops in the Lower Arkansas River Valley (LARV) under salinity conditions and four remaining GCMs considering both RCP4.5 and RCP8.5 scenarios.

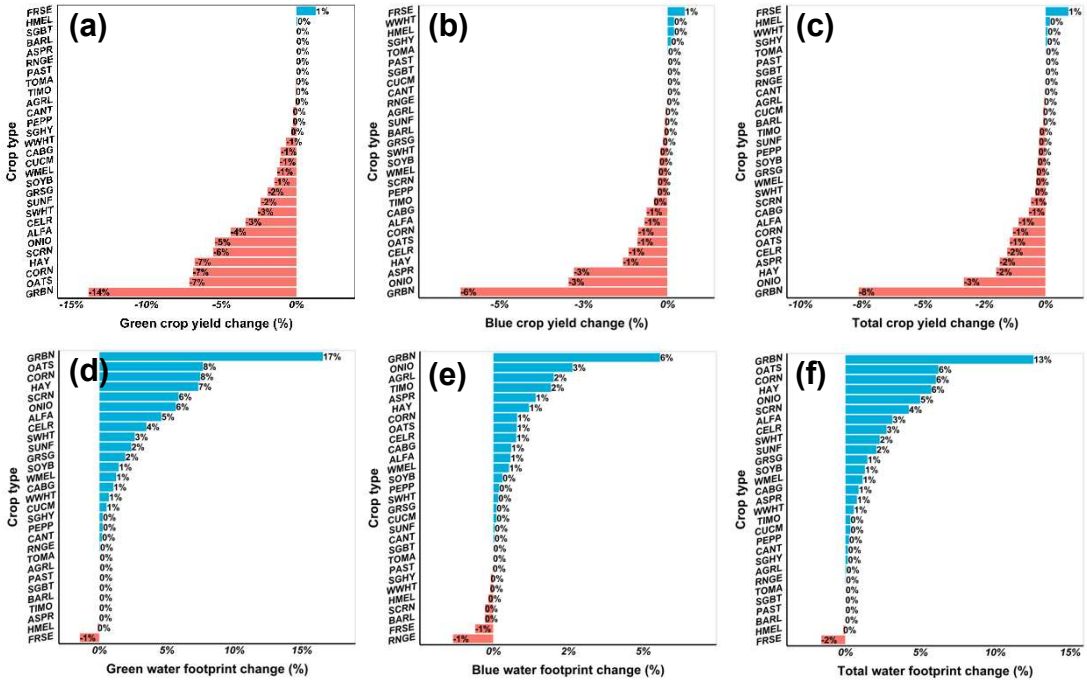


**Figure 3.8.** Average percentage changes in (a) green crop yield, (b) blue crop yield, (c) total crop yield, (d) green water footprint, (e) blue water footprint, and (f) total water footprint of 29 crops in the LARV considering IPSL-CM5A-MR-8.5 climate model and salinity stress by 2100.

Observing the results, it is evident that among the 29 crops in the region, green beans exhibit the most substantial reduction in total crop yield across all models. The highest reduction, reaching 8%, is projected by the IPSL-CM5A-MR-8.5 model. Additionally, when considering the total WF, green beans also experience the greatest increase under all models. The highest rise, reaching 13%, is projected by the driest GCM model, IPSL-CM5A-MR-8.5. Analyzing the percentage changes

in crop yields and WFs relative to the baseline period and under salinity stress, it is noteworthy that the impacts on these values are mitigated when considering the mutual influence of salinity and climate change scenarios. This suggests that, in the long term, the impact of salinity is expected to decrease across all scenarios.

These findings underscore the vulnerability of specific crops such as green beans, oats, corn, alfalfa, hay and onion to the effects of salinity stress, leading to higher reductions in crop yields. The variations observed across GCMs emphasize the significance of accounting for diverse climate scenarios when assessing the impact of salinity on both crop yield and WF. The data presented in these figures provide valuable insights for understanding the potential consequences of salinity stress and climate change on different crops in the LARV.

### 3.3.3 Study Limitations

This study investigates the influence of salinity and climate changes on crop production WFs within a semi-arid agricultural watershed. Certain limitations and recommendations for future research are noteworthy. The calculation of the total WF exclusively considered green and blue WFs, while the grey WF of crop production in the region was assumed to be zero. Future studies could benefit from estimating and including the grey WF in total WF calculations in various regions. In assessing the impact of climate change on salinity fate and transport, and crop production WFs, this study utilized the CMIP5, focusing on climatic outputs from five widely used GCM models and two RCP emission scenarios (RCP4.5 and RCP8.5). Hence, future research could enhance its scope by incorporating additional climate models, diverse climate scenarios, emission scenarios, land-use change scenarios, and employing the model at different scales, including regional or smaller scales.

## 3.4. SUMMARY AND CONCLUSIONS

In this study, the recently developed SWAT-MODFLOW-Salt model was employed to assess the impact of salinity on green, blue, and total WFs of crop production. The model was also utilized to quantify the combined effects of salinity and climate change on crop production WFs in the Lower Arkansas River Valley (LARV), CO, USA by the end of century. Projected and downscaled climate data encompassing temperature, precipitation, solar radiation, wind speed, and relative humidity were derived from MACA dataset including five GCM models input into the calibrated and validated SWAT-MODFLOW-Salt model for the LARV to simulate future crop yields and crop production WFs within the watershed. Key findings of this study indicate that:

- Over the baseline period (1999-2009), there was a 2.3% decrease in the total average annual crop yield and a 6.5% rise in the WF due to salinity stress conditions. Among the primary crops in the area, the annual average crop yield for alfalfa decreased by 3.8%, leading to an 8.3% increase in the total WF. In the case of corn, the annual average crop yield decreased by 4.9%, resulting in a 10.9% rise in the total WF. Among the crops that exhibited the most significant percentage changes, excluding corn and alfalfa, onion experienced a 10.7% decrease in the annual average crop yield, resulting in a 16.4% increase in the total WF. Green beans showed a 14.7% decrease in the annual average crop yield, accompanied by a 16.6% increase in the total WF, and watermelon witnessed a 6.0% decrease in the annual average crop yield, leading to a 7.6% increase in the total WF.
- Among the climate models considered, the IPSL-CM5A-MR-8.5 model exhibited the most significant reduction in total crop yield, with a 0.8% decrease, and an approximately 3% increase in the overall crop production WF associated with the impact of salinity on crop production in the region. When considering all GCMs and the RCP4.5 scenario under average future conditions, the total crop yield decreased by 0.6%, and the total WF increased by 1.7%.

Conversely, under the RCP8.5 scenario, the crop yield declined by 0.5%, and the total WF raised by 2%.

- The findings of this study offer valuable insights into the implementation of effective management practices for reclaiming salt-affected soils in the agricultural sector. Emphasis should be placed on adopting water-efficient irrigation systems, incorporating organic amendments like biochar and diverse composts, utilizing inorganic amendments rich in calcium such as fly ash and gypsum, selecting salt-tolerant crops (genotypes), implementing changes in land-use management through alterations in cropping systems, promoting agroforestry, and integrating fruit crops to enhance soil quality. Additionally, opting for climate-smart conservation agriculture (CSCA) is recommended, particularly to mitigate potential impacts of soil salinity under changing climate conditions (Mukhopadhyay et al., 2021).

    • In decision-making processes, especially within arid and semi-arid regions like LARV with higher water footprints (WFs) compared to the global average, the consideration of crop production WFs is essential. This can provide policymakers with valuable insights to promote optimal management practices, preventing reductions in crop production and ensuring sustainable water resources management. This significance is heightened in the context of climate change, which is expected to further intensify water scarcity in these areas in the future.

# REFERENCES


Abatzoglou, J.T., Brown, T.J., 2012. A comparison of statistical downscaling methods suited for wildfire applications. International Journal of Climatology 32, 772–780. https://doi.org/10.1002/joc.2312

Aliyari, F., Bailey, R.T., Arabi, M., 2021. Appraising climate change impacts on future water resources and agricultural productivity in agro-urban river basins. Science of The Total Environment 788, 147717. https://doi.org/10.1016/j.scitotenv.2021.147717

Aliyari, F., Bailey, R.T., Tasdighi, A., Dozier, A., Arabi, M., Zeiler, K., 2019. Coupled SWAT-MODFLOW model for large-scale mixed agro-urban river basins. Environmental Modelling and Software 115, 200–210. https://doi.org/10.1016/J.ENVSOFT.2019.02.014

Allan, J.A., 1998. Virtual Water: A Strategic Resource Global Solutions to Regional Deficits. Ground Water 1998, 4, 545-546. [WWW Document]. URL (accessed 7.1.22).

Arnold, J.G., Srinivasan, R., Muttiah, R.S., Williams, J.R., 1998. LARGE AREA HYDROLOGIC MODELING AND ASSESSMENT PART I: MODEL DEVELOPMENT1. JAWRA Journal of the American Water Resources Association 34, 73–89. https://doi.org/10.1111/J.1752-1688.1998.TB05961.X

Bailey, R.T., Hosseini, P., 2023. Comprehensive simulation of salinity transport in irrigated watersheds using an updated version of SWAT-MODFLOW. Environmental Modelling & Software 159, 105566. https://doi.org/10.1016/J.ENVSOFT.2022.105566

Bailey, R.T., Tavakoli-Kivi, S., Wei, X., 2019. A salinity module for SWAT to simulate salt ion fate and transport at the watershed scale. Hydrology and Earth System Sciences 23, 3155–3174. https://doi.org/10.5194/hess-23-3155-2019

Bailey, R.T., Wible, T.C., Arabi, M., Records, R.M., Ditty, J., 2016. Assessing regional-scale spatio-temporal patterns of groundwater–surface water interactions using a coupled SWAT-MODFLOW model. Hydrological Processes 30, 4420–4433. https://doi.org/10.1002/HYP.10933

Bocchiola, D., Nana, E., Soncini, A., 2013. Impact of climate change scenarios on crop yield and water footprint of maize in the Po valley of Italy. Agricultural Water Management 116, 50–61. https://doi.org/10.1016/J.AGWAT.2012.10.009

Burkhalter, J.P., Asce, M., Gates, T.K., 2005. Agroecological Impacts from Salinization and Waterlogging in an Irrigated River Valley. Journal of Irrigation and Drainage Engineering 131, 197–209. https://doi.org/10.1061/(ASCE)0733-9437(2005)131:2(197)

Cao, X., Wu, P., Wang, Y., Zhao, X., 2014. Water Footprint of Grain Product in Irrigated Farmland of China. Water Resources Management: An International Journal, Published for the European Water Resources Association (EWRA) 28, 2213–2227. https://doi.org/10.1007/S11269-014-0607-1

Casella, P., De Rosa, L., Salluzzo, A., De Gisi, S., 2019. Combining GIS and FAO's crop water productivity model for the estimation of water footprinting in a temporary river catchment. Sustainable Production and Consumption 17, 254–268. https://doi.org/10.1016/j.spc.2018.11.002

Chapagain, A.K., Hoekstra, A.Y., 2011. The blue, green and grey water footprint of rice from production and consumption perspectives. Ecological Economics 70, 749–758. https://doi.org/10.1016/j.ecolecon.2010.11.012

Chapagain, A.K., Hoekstra, A.Y., 2007. The water footprint of coffee and tea consumption in the Netherlands. Ecological Economics 64, 109–118. https://doi.org/10.1016/j.ecolecon.2007.02.022

Chukalla, A.D., Krol, M.S., Hoekstra, A.Y., 2015. Green and blue water footprint reduction in irrigated agriculture: Effect of irrigation techniques, irrigation strategies and mulching. Hydrology and Earth System Sciences 19, 4877–4891. https://doi.org/10.5194/hess-19-4877-2015

Chunn, D., Faramarzi, M., Smerdon, B., Alessi, D.S., 2019. Application of an Integrated SWAT–MODFLOW Model to Evaluate Potential Impacts of Climate Change and Water Withdrawals on Groundwater–Surface Water Interactions in West-Central Alberta. Water 11, 110. https://doi.org/10.3390/w11010110

Döll, P., Siebert, S., 2002. Global modeling of irrigation water requirements. Water Resources Research 38, 8–1. https://doi.org/10.1029/2001WR000355

Elbeltagi, A., Aslam, M.R., Malik, A., Mehdinejadiani, B., Srivastava, A., Bhatia, A.S., Deng, J., 2020. The impact of climate changes on the water footprint of wheat and maize production in the Nile Delta, Egypt. Science of the Total Environment 743. https://doi.org/10.1016/j.scitotenv.2020.140770

FAO. 2017. The future of food and agriculture – Trends and challenges. Rome., 2017.

Fowler, H.J., Blenkinsop, S., Tebaldi, C., 2007. Linking climate change modelling to impacts studies: recent advances in downscaling techniques for hydrological modelling. International Journal of Climatology 27, 1547–1578. https://doi.org/10.1002/joc.1556

Garofalo, P., Ventrella, D., Kersebaum, K.C., Gobin, A., Trnka, M., Giglio, L., Dubrovský, M., Castellini, M., 2019. Water footprint of winter wheat under climate change: Trends and uncertainties associated to the ensemble of crop models. Science of the Total Environment 658, 1186–1208. https://doi.org/10.1016/j.scitotenv.2018.12.279

Gates, T.K., Asce, M., Burkhalter, ; J Philip, Labadie, J.W., Valliant, J.C., Broner, I., 2002. Monitoring and Modeling Flow and Salt Transport in a Salinity-Threatened Irrigated Valley. Journal of Irrigation and Drainage Engineering 128, 87–99. https://doi.org/10.1061/(ASCE)0733-9437(2002)128:2(87)

Gerbens-Leenes, W., Hoekstra, A.Y., 2012. The water footprint of sweeteners and bio-ethanol. Environment International 40, 202–211. https://doi.org/10.1016/j.envint.2011.06.006

Haj-Amor, Z., Bouri, S., 2020. Use of HYDRUS-1D–GIS tool for evaluating effects of climate changes on soil salinization and irrigation management. Archives of Agronomy and Soil Science 66, 193–207. https://doi.org/10.1080/03650340.2019.1608438

Heidari, H., Arabi, M., Warziniack, T., Kao, S.-C., 2020. Assessing Shifts in Regional Hydroclimatic Conditions of U.S. River Basins in Response to Climate Change over the 21st Century. Earth's Future 8, e2020EF001657. https://doi.org/10.1029/2020EF001657

Hoekstra, A.Y., Chapagain, A.K., 2007. The water footprints of Morocco and the Netherlands: Global water use as a result of domestic consumption of agricultural commodities. Ecological Economics 64, 143–151. https://doi.org/10.1016/j.ecolecon.2007.02.023

Hoekstra, A.Y., Chapagain, A.K., Aldaya, M.M., Mekonnen, M.M., n.d. The water footprint assessment manual 2011. Earthscan Ltd., Dunstan House, 14a St Cross Street, London EC1N 8XA, UK.

Hoekstra, A.Y., Hung, P.Q., n.d. Hoekstra, A.Y. and Hung, P.Q. Virtual Water Trade: A Quantification of Virtual Water Flows between Nations in Relation to Crop Trade. Value of Water Research Report 2002, Series 11.

Holmberg, M.J., 2017. Hydrogeologic characteristics and geospatial analysis of water-table changes in the alluvium of the lower Arkansas River Valley, southeastern Colorado, 2002, 2008, and 2015. Scientific Investigations Map. https://doi.org/10.3133/SIM3378

Hosseini, P., Bailey, R.T., 2022. Investigating the controlling factors on salinity in soil, groundwater, and river water in a semi-arid agricultural watershed using SWAT-Salt. Science of the Total Environment 810. https://doi.org/10.1016/j.scitotenv.2021.152293

Joyce, L.A., Coulson, D., 2020. Climate scenarios and projections: A technical document supporting the USDA Forest Service 2020 RPA Assessment (No. RMRS-GTR-413). U.S. Department of Agriculture, Forest Service, Rocky Mountain Research Station, Fort Collins, CO. https://doi.org/10.2737/RMRS-GTR-413

Luan, X., Wu, P., Sun, S., Wang, Y., Gao, X., 2018. Quantitative study of the crop production water footprint using the SWAT model. Ecological Indicators 89, 1–10. https://doi.org/10.1016/j.ecolind.2018.01.046

Masud, M.B., McAllister, T., Cordeiro, M.R.C., Faramarzi, M., 2018. Modeling future water footprint of barley production in Alberta, Canada: Implications for water use and yields to 2064. Science of the Total Environment 616–617, 208–222. https://doi.org/10.1016/j.scitotenv.2017.11.004

Mekonnen, M.M., Hoekstra, A.Y., 2011. The green, blue and grey water footprint of crops and derived crop products. Hydrology and Earth System Sciences 15, 1577–1600. https://doi.org/10.5194/hess-15-1577-2011

Molina-Navarro, E., Bailey, R.T., Andersen, H.E., Thodsen, H., Nielsen, A., Park, S., Jensen, J.S., Jensen, J.B., Trolle, D., 2019. Comparison of abstraction scenarios simulated by SWAT and SWAT-MODFLOW. https://doi.org/10.1080/02626667.2019.1590583 64, 434–454. https://doi.org/10.1080/02626667.2019.1590583

Morway, E.D., Gates, T.K., 2012. Regional Assessment of Soil Water Salinity across an Intensively Irrigated River Valley. Journal of Irrigation and Drainage Engineering 138, 393–405. https://doi.org/10.1061/(asce)ir.1943-4774.0000411

Morway, E.D., Gates, T.K., Niswonger, R.G., 2013. Appraising options to reduce shallow groundwater tables and enhance flow conditions over regional scales in an irrigated alluvial aquifer system. Journal of Hydrology 495, 216–237. https://doi.org/10.1016/J.JHYDROL.2013.04.047

Mukhopadhyay, R., Sarkar, B., Jat, H.S., Sharma, P.C., Bolan, N.S., 2021. Soil salinity under climate change: Challenges for sustainable agriculture and food security. Journal of Environmental Management 280, 111736. https://doi.org/10.1016/J.JENVMAN.2020.111736

Musa Ahmed, S., Ribbe, L., 2011. ANALYSIS OF WATER FOOTPRINTS OF RAINFED AND IRRIGATED CROPS IN SUDAN. Journal of Natural Resources and Development. https://doi.org/10.5027/jnrd.v1i0.03

Niswonger, R., Panday, S., Survey, M.I.-U.G., 2011, undefined, 2011. MODFLOW-NWT, a Newton formulation for MODFLOW-2005. pubs.usgs.gov.

Sakurai, G., Iizumi, T., Nishimori, M., Yokozawa, M., 2014. How much has the increase in atmospheric CO2 directly affected past soybean production? Sci Rep 4, 4978. https://doi.org/10.1038/srep04978

Shiru, M.S., Hyuck Kim, J., Chung, E.-S., 2022. Water Resources and Hydrologic Engineering Variations in Projections of Precipitations of CMIP6 Global Climate Models under SSP 2-45 and SSP 5-85. KSCE Journal of Civil Engineering 26, 5404–5416. https://doi.org/10.1007/s12205-022-0149-7

Shrestha, S., Chapagain, R., Babel, M.S., 2017. Quantifying the impact of climate change on crop yield and water footprint of rice in the Nam Oon Irrigation Project, Thailand. Science of the Total Environment 599–600, 689–699. https://doi.org/10.1016/j.scitotenv.2017.05.028

Shrestha, S., Pandey, V.P., Chanamai, C., Ghosh, D.K., 2013. Green, Blue and Grey Water Footprints of Primary Crops Production in Nepal. Water Resources Management 27, 5223–5243. https://doi.org/10.1007/s11269-013-0464-3

Skrzypek, G., Dogramaci, S., Grierson, P.F., 2013. Geochemical and hydrological processes controlling groundwater salinity of a large inland wetland of northwest Australia. Chemical Geology 357, 164–177. https://doi.org/10.1016/j.chemgeo.2013.08.035

Song, Y.H., Chung, E.S., Shahid, S., 2022. Differences in extremes and uncertainties in future runoff simulations using SWAT and LSTM for SSP scenarios. Science of The Total Environment 838, 156162. https://doi.org/10.1016/J.SCITOTENV.2022.156162

Sun, S.-K., Wu, P.-T., Wang, Y.-B., Zhao, X.-N., 2013. The virtual water content of major grain crops and virtual water flows between regions in China. Journal of the Science of Food and Agriculture 93, 1427–1437. https://doi.org/10.1002/jsfa.5911

Tavakoli-Kivi, S., Bailey, R.T., Gates, T.K., 2019. A salinity reactive transport and equilibrium chemistry model for regional-scale agricultural groundwater systems. Journal of Hydrology 572, 274–293. https://doi.org/10.1016/j.jhydrol.2019.02.040

Tijjani, S.B., Giri, S., Woznicki, S.A., 2022. Quantifying the potential impacts of climate change on irrigation demand, crop yields, and green water scarcity in the New Jersey Coastal Plain. Science of the Total Environment 838. https://doi.org/10.1016/J.SCITOTENV.2022.156538

Wang, X., Li, X., Fischer, G., Sun, L., Tan, M., Xin, L., Liang, Z., 2015. Impact of the changing area sown to winter wheat on crop water footprint in the North China Plain. Ecological Indicators 57, 100–109. https://doi.org/10.1016/j.ecolind.2015.04.023

Wei, X., Bailey, R.T., 2019. Assessment of system responses in intensively irrigated stream-aquifer systems using SWAT-MODFLOW. Water (Switzerland) 11. https://doi.org/10.3390/W11081576

Wei, X., Bailey, R.T., Tasdighi, A., 2018. Using the SWAT Model in Intensively Managed Irrigated Watersheds: Model Modification and Application. Journal of Hydrologic Engineering 23. https://doi.org/10.1061/(asce)he.1943-5584.0001696

Xiang, Z., Bailey, R.T., Nozari, S., Husain, Z., Kisekka, I., Sharda, V., Gowda, P., 2020. DSSAT-MODFLOW: A new modeling framework for exploring groundwater conservation strategies in irrigated areas. Agricultural Water Management 232. https://doi.org/10.1016/j.agwat.2020.106033

Zheng, J., Wang, W., Ding, Y., Liu, G., Xing, W., Cao, X., Chen, D., 2020. Assessment of climate change impact on the water footprint in rice production: Historical simulation and future projections at two representative rice cropping sites of China. Science of the Total Environment 709. https://doi.org/10.1016/j.scitotenv.2019.136190

Zhuo, L., Hoekstra, A.Y., 2017. The effect of different agricultural management practices on irrigation efficiency, water use efficiency and green and blue water footprint. Frontiers of Agricultural Science and Engineering 4, 185–194. https://doi.org/10.15302/J-FASE-2017149

Zhuo, L., Mekonnen, M.M., Hoekstra, A.Y., 2016a. Benchmark levels for the consumptive water footprint of crop production for different environmental conditions: A case study for winter wheat in China. Hydrology and Earth System Sciences 20, 4547–4559. https://doi.org/10.5194/hess-20-4547-2016

Zhuo, L., Mekonnen, M.M., Hoekstra, A.Y., Wada, Y., 2016b. Inter- and intra-annual variation of water footprint of crops and blue water scarcity in the Yellow River basin (1961-2009). Advances in Water Resources 87, 29–41. https://doi.org/10.1016/j.advwatres.2015.11.002

Zörb, C., Geilfus, C.M., Dietz, K.J., 2019. Salinity and crop yield. Plant Biology 21, 31–38. https://doi.org/10.1111/plb.12884

# Chapter 4. ASSESSMENT OF IRRIGATION MANAGEMENT AND CLIMATE CHANGE ON SALINITY FATE AND TRANSPORT AND CROP PRODUCTION IN A SEMI-ARID INTENSIVELY IRRIGATED WATERSHED

## 4.1. INTRODUCTION

Salinity is a pervasive environmental challenge that adversely impacts agricultural productivity, particularly in arid and semi-arid regions where irrigation is critical for sustaining crop growth. High soil salinity can impact plant physiological processes, such as water uptake and nutrient absorption, leading to osmotic stress, ion toxicity, and nutritional imbalances result in substantial reductions in crop yields (Munns and Tester, 2008). This issue is exacerbated using saline irrigation water, inadequate drainage, and the presence of salt minerals within the soil profile (Bailey et al., 2019; Gates et al., 2002). The detrimental effects of salinity on soil health, crop yield, and environmental ecosystems necessitate comprehensive management strategies in agricultural watersheds. These strategies should not only mitigate the immediate adverse impacts of salinity but also address long-term considerations, particularly in light of projected climatic changes that are likely to exacerbate water availability issues due to increased temperatures and decreased precipitation. This requires the adoption of enhanced irrigation practices and effective salinity management to alleviate these impacts and maintain agricultural productivity in affected regions.

The interplay between various irrigation methods and soil salinity is a critical factor in determining agricultural outcomes and managing salinity effectively. In semi-arid regions like the Lower Arkansas River Valley (LARV), salinity significantly threatens agriculture, worsened by climate change and historical irrigation practices, causing notable declines in crop yields (Burkhalter et al., 2005; Morway and Gates, 2012). In the LARV, flood irrigation is predominantly

used, resulting in significant water losses through runoff and deep percolation due to its relatively low efficiency. However, sprinkler and drip irrigation methods are also employed in certain localized areas (Bailey et al., 2019). Each irrigation method affects salt mobilization and accumulation in the soil in distinct ways. Flood irrigation has been shown to decrease salinity in the root zone by facilitating the leaching of salts deeper into the soil profile. This process helps to move salts away from the root zone, thus reducing salt stress on crops. While flood irrigation can lead to potential drawbacks such as waterlogging and inefficient water use, its ability to promote deep percolation is beneficial for lowering salinity levels in the root zone. This reduction in salinity can improve soil health and enhance crop viability under certain conditions. (Gates et al., 2002; Hosseini and Bailey, 2022).

Sprinkler irrigation provides a more controlled method of water distribution, achieving efficiencies of approximately 75-85%. This method mitigates some of the water losses associated with flood irrigation by reducing evaporation and runoff, thereby offering a more uniform water distribution that helps maintain soil moisture at optimal levels (Chauhdary et al., 2024). However, compared to flood irrigation, sprinkler irrigation is less effective in leaching salts from the root zone. While it optimizes water use efficiency and prevents surface salt accumulation, it does not provide the same degree of salt leaching, potentially leaving higher salinity levels in the root zone over time.

Drip irrigation is recognized as the most efficient irrigation method, with efficiencies reaching up to 90-95%. This system delivers water directly to the root zone, minimizing losses due to evaporation and reducing the leaching of essential nutrients. It offers substantial advantages in salinity management by preventing the surface accumulation of salts and ensuring that water and nutrients are delivered directly to the plant roots. This targeted delivery enhances water use

efficiency and can potentially increase crop yields under saline conditions. Additionally, drip irrigation maintains a consistently moist soil environment, which inhibits the upward movement of salts through capillary action. By reducing the risk of salt stress on crops, drip irrigation keeps the salinity levels in the root zone low and stable. The precision in water application inherent in drip systems allows for more accurate salinity management, minimizing the risk of salt buildup. This contributes to improved soil health and crop viability. Moreover, the continuous and localized delivery of water in drip irrigation systems supports optimal soil moisture conditions, which are crucial for plant growth and productivity. This method's ability to control the soil salinity more effectively than other irrigation practices makes it a critical tool for sustainable agricultural practices in areas prone to salinity. By mitigating the adverse effects of salinity, drip irrigation not only maximizes resource use efficiency but also promotes long-term agricultural sustainability in saline-affected regions. (Machado and Serralheiro, 2017).

Climate change complicates salinity management by altering hydrological patterns and worsening water scarcity. Increased temperatures and changes in precipitation can degrade irrigation water quality and limit the natural flushing of salts from the root zone (Haj-Amor and Bouri, 2020; Mukhopadhyay et al., 2021). These changes are expected to intensify in the coming decades, with significant implications for salinity management. Higher temperatures can increase evapotranspiration rates, leading to greater salt accumulation in soils. Additionally, changes in precipitation patterns, including more intense and less frequent rainfall events, can reduce the effectiveness of natural leaching processes that help flush salts from the soil profile (Masson-Delmotte et al., 2021). These climatic shifts necessitate a reevaluation of existing irrigation practices to adapt to increased water demands and altered hydrological conditions. Integrating

efficient irrigation technologies with advanced water management strategies becomes crucial to ensure sustainable water use and maintain agricultural productivity in the face of climate change.

This study aims to investigate the combined effects of salinity, climate change, and various irrigation practices on crop production in an irrigated semi-arid watershed. Specifically, it focuses on understanding the interplay between irrigation efficiency and water loss in terms of runoff ratio, climate change, and salinity transport in the LARV. The goal is to provide insights into the most effective management practices for sustaining agricultural productivity amid increasing salinity and changing climatic conditions. This has been achieved by applying the SWAT-MODFLOW-Salt model, which integrates hydrological and salt transport processes to offer a comprehensive assessment of salinity dynamics in irrigated agricultural systems (Bailey and Hosseini, 2023). This model simulates the fate and transport of major salt ions ($SO_4^{2-}$, $Cl^-$, $CO_3^{2-}$, $HCO_3^-$, $Ca^{2+}$, $Na^+$, $Mg^{2+}$, $K^+$) in watershed systems, accounting for water and salt mass storage in soils, aquifers, and streams, and the movement of water and salt mass in surface runoff, soil lateral flow, percolation and recharge, groundwater flow, and groundwater-surface water exchange. The findings inform policymakers and stakeholders about effective strategies to enhance irrigation efficiency and mitigate the water loss, alleviate the adverse effects of salinity, and ensure the sustainability of agricultural systems under changing environmental conditions.

## 4.2. MATERIALS AND METHODS

### 4.2.1 Study area

The study area is located in the Lower Arkansas River Valley (LARV) in southeastern Colorado, covering an area of approximately 732 km² (see Fig. 4.1). This region is characterized by a semi-arid climate, with average monthly temperatures ranging from -12.6°C in January to 35.9°C in July, and an annual mean temperature of approximately 13.6°C. The average annual

precipitation is about 376 mm, which is insufficient to meet the water demands of the region's agriculture (Holmberg, 2017). Consequently, irrigation is essential for sustaining agricultural productivity in the LARV.

The primary crops cultivated in this area include alfalfa, melons, corn, beans, sorghum, wheat, onion, and pepper (as shown in Fig.1b). Alfalfa, corn, and pasture/grass collectively account for approximately 80% of the total crop yield during the 1999-2009 period, while the remaining crops contribute around 20% of the overall crop yield (Bailey and Hosseini, 2023). The significance of these crops to the region's agricultural economy necessitates effective water management strategies to mitigate salinity issues.

Due to the semi-arid nature of the region, high evapotranspiration rates, and insufficient average annual precipitation, the LARV agriculture relies heavily on irrigation. Irrigation water is primarily sourced from the Arkansas River through six major irrigation canals and is supplemented by groundwater from an alluvial aquifer (as shown in Fig.1a &c). This aquifer, composed mainly of sand and gravel, has a thickness ranging from 4 to 34 meters and is situated along the Arkansas River corridor (Morway et al., 2013). The irrigation season typically spans from March 15th to November 15th each year. Approximately 500 pumping wells are utilized to support surface water irrigation with groundwater (Hosseini and Bailey, 2022).

Soil salinity in the LARV is a significant concern, driven by several factors including the dissolution of existing salt minerals in the soil profile, irrigation with saline water from the Arkansas River and the aquifer, and hyper-concentration of salinity brought to the shallow subsurface by groundwater. Shallow groundwater levels, resulting from excessive irrigation, seepage from canals, and inadequate drainage, have led to elevated soil salinity levels, reducing crop yields by 11% to 19% over the past few decades (Burkhalter et al., 2005; Gates et al., 2002;

Morway and Gates, 2012). Field measurements over the past twenty years indicate that average soil water salinity, measured by electrical conductivity, is approximately 4.11 dS/m, with groundwater salinity concentrations ranging between 2,700 and 3,000 mg/L (Bailey and Hosseini, 2023).

The Arkansas River, a critical water source for irrigation in the LARV, has been subject to significant salinity issues. Salinity levels in the river and its tributaries have been found to range from 1,145 mg/L to 560 mg/L for Total Dissolved Solids (TDS) and sulfate ($SO_4$) concentrations, respectively (Morway and Gates, 2012). These elevated salinity levels are primarily attributed to natural salt deposits and human activities, including irrigation practices and return flows from agricultural fields.

The region's topography and geology further contribute to the salinity challenges. The LARV is characterized by relatively flat terrain with low gradients, which limits the natural drainage of saline water. The presence of highly permeable soils and an extensive network of irrigation canals and ditches exacerbate the issue by facilitating the movement of saline water into the root zone (Hosseini and Bailey, 2022). This combination of factors creates a complex hydrological system where salinity dynamics are influenced by both natural processes and agricultural practices.

Groundwater monitoring has been an essential component of understanding salinity trends in the LARV. Comprehensive data collection efforts have included the sampling of groundwater from 75 monitoring wells between 2006 and 2010. The findings revealed that the mean concentration of groundwater salinity within the watershed ranged from 2,700 to 3,000 mg/L. The prevalent presence of gypsum ($CaSO_4$) in the region led to elevated levels of sulfate ($SO_4$), with minimum, maximum, and average concentrations of 147 mg/L, 29,457 mg/L, and 1,878 mg/L, respectively, which constitute 56% of the total salinity. This data underscores the significant impact of soil and

groundwater salinity on the region's agriculture necessitates the implementation of effective salinity management practices to sustain agricultural productivity (Morway and Gates, 2012).

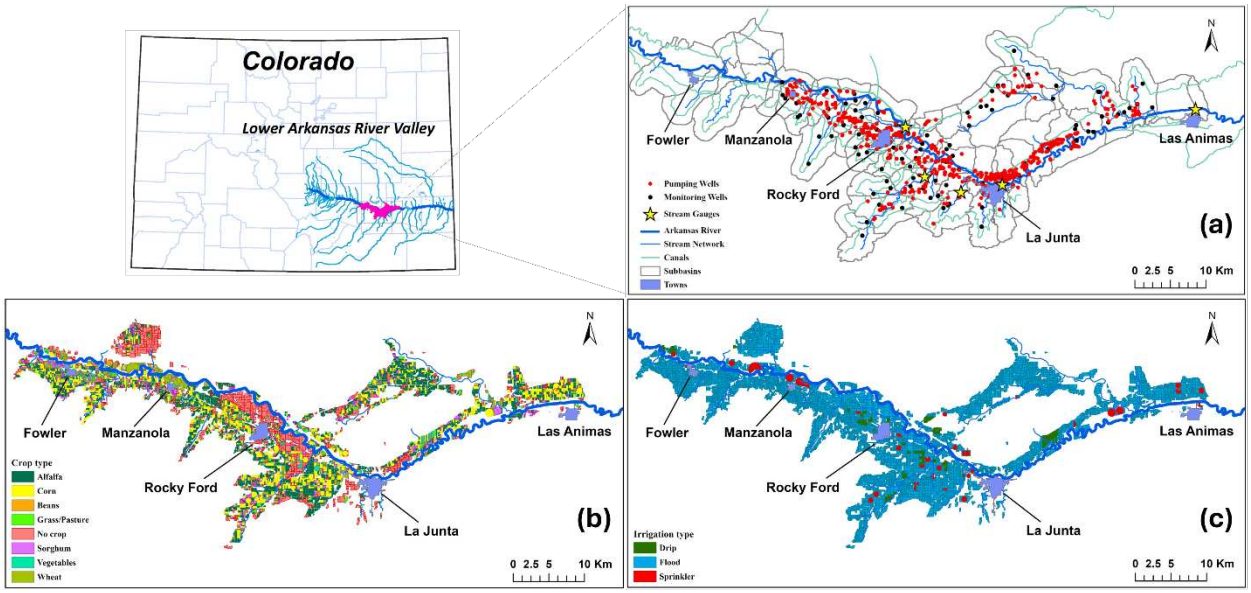


**Figure 4.1**. Study area in the Lower Arkansas River Valley (LARV). (a) Map of the location of stream gauges, monitoring wells, pumping wells, canals, and stream networks within the watershed. (b) Map of crop type distribution in the study area, and (c) Map of the irrigation type within the LARV.

## 4.2.2 SWAT-MODFLOW-Salt model overview

The SWAT-MODFLOW-Salt model, developed by Bailey and Hosseini in 2023, is an integration of the existing SWAT-MODFLOW model, which incorporates RT3D capabilities for nutrient transport within the groundwater system (Wei and Bailey, 2019) and the SWAT-Salt code (Bailey et al., 2019), simulates the transport and fate of eight major salt ions ($SO_4^{2-}$, $Cl^-$, $CO_3^{2-}$, $HCO_3^-$, $Ca^{2+}$, $Na^+$, $Mg^{2+}$, $K^+$) within the soil, groundwater, and stream system. This integrated model simulates salt transport across all key hydrological pathways, including surface runoff, streamflow, soil lateral flow, soil percolation, groundwater recharge, groundwater pumping, applied irrigation, canal diversions, groundwater flows within the aquifer system, and the exchanges between groundwater and streams, tailored for each hydrologic response unit (HRU),

grid cell, and stream channel. Additionally, the model calculates the mass balance of water and salts in the soil profile, accounting for processes such as infiltration, percolation, and lateral flow. It simulates salt ion concentrations in each soil layer, influenced by irrigation practices and natural precipitation. The original SWAT-MODFLOW model (Bailey et al., 2016) combines the capabilities of the Soil and Water Assessment Tool (SWAT) (originally developed by Arnold et al. in 1998 (Arnold et al., 1998)) and the Modular Finite-Difference Groundwater Flow Model (MODFLOW) (developed by Niswonger et al. in 2011 (Niswonger et al., 2011)), enhanced with a salinity transport module. This integrated modeling framework allows SWAT to simulate a variety of land surface and soil profile processes, such as surface runoff, evapotranspiration, crop growth, percolation, soil lateral flow, recharge, and stream discharge. In parallel, MODFLOW manages the groundwater head, storage, flow, and interactions between groundwater and surface water within a heterogeneous, multi-layer aquifer system. SWAT supplies recharge data from hydrologic response units (HRUs) to the MODFLOW grid cells, which then calculate groundwater-stream exchange rates for each subbasin stream. These dynamic exchanges are simulated with daily resolution over the modeling period.

The SWAT-Salt model, introduced by Bailey et al. (2019), outlines the processes of salt transport across the land surface, particularly through hydrologic response units (HRUs), soil layers, and stream channels. This model adeptly handles the fate and transport of eight main ions—Sulfate ($SO_4^{2-}$), Calcium ($Ca^{2+}$), Magnesium ($Mg^{2+}$), Sodium ($Na^{+}$), Chloride ($Cl^{-}$), Potassium ($K^{+}$), Carbonate ($CO_3^{2-}$), and Bicarbonate ($HCO_3^{-}$) across the entire watershed. It addresses various salinity transport mechanisms, including surface runoff, groundwater flow, streamflow, soil percolation and leaching, upward groundwater flux into the soil, and soil lateral flow. The model quantifies salt ion concentrations across three main compartments: soil water in each HRU,

groundwater in each HRU aquifer, and surface water in each subbasin stream. These concentrations are determined by salinity fluxes coupled with chemical reactions like precipitation-dissolution, complexation, and cation exchange, computed on a daily basis. Furthermore, the model incorporates features that simulate how irrigation practices contribute to the mass loading of salt ions within the soil profile, adjusting for the removal of salt ions from aquifer units during groundwater irrigation and from subbasin streams during surface water irrigation. In addition to the SWAT-Salt capabilities, the salinity module adapted from Tavakoli-Kivi et al. (2019) (Tavakoli-Kivi et al., 2019) for RT3D (termed RT3D-Salt) focuses on solute transport in groundwater systems, specifically under irrigation. This module conducts mass balance and equilibrium chemistry calculations for salt mineral precipitation-dissolution among the eight salt ions within each aquifer grid cell.

The SWAT-MODFLOW-Salt framework integrates the Fortran codes of SWAT-MODFLOW, SWAT-Salt, and RT3D-Salt into a cohesive code. Within this integrated model, SWAT-Salt manages salt mass balance and chemistry across land surfaces, soils, and channels, while RT3D-Salt handles these processes within the groundwater system. It efficiently links salt mass from soil leaching to the RT3D grid cells and facilitates the exchange of salt ion loads between groundwater and streams, aligning flow rates from MODFLOW with concentrations from RT3D-Salt. This comprehensive approach ensures that salt ion dynamics within stream flows are accurately routed downstream, adhering to SWAT's routing algorithms, and integrates groundwater head simulations from MODFLOW to adjust water and associated salt transfers within the HRU soil profiles (Bailey and Hosseini, 2023).

In this study, the SWAT-MODFLOW-Salt model is applied to the Lower Arkansas River Valley (LARV) in southeastern Colorado. This region has experienced elevated salinity levels in soils,

groundwater, and streams due to long-term irrigation practices and inadequate drainage. The model setup for the LARV involves detailed parameterization based on extensive field data and previous modeling efforts (Wei and Bailey, 2019). The model configuration includes HRUs defined by unique combinations of soil, land use, and topographic features, with each HRU representing a distinct agricultural field within the watershed. The groundwater model uses a grid with specified aquifer properties, including hydraulic conductivity and storage coefficients, and incorporates groundwater pumping rates and well locations into the model. Initial concentrations of salt ions in soil water and groundwater are specified based on field measurements. The model includes solubility products for key salt minerals ($CaSO_4$, $CaCO_3$, $MgCO_3$, NaCl, $MgSO_4$) and parameters for equilibrium chemistry reactions (Bailey et al., 2019). Additionally, the model simulates the impact of salinity stress on crop yield by applying the relative yield equation developed by Maas (1993), which incorporates specific threshold and slope parameters relevant to different crop types. For a deeper understanding of the theoretical basis and the mass balance equations utilized in the SWAT-MODFLOW-Salt model, refer to the detailed exposition provided by Bailey and Hosseini (2023).

The SWAT-MODFLOW-Salt model employed in this research is the same version initially introduced by Bailey and Hosseini (2023). The SWAT-MODFLOW model for the study area, as described by Wei and Bailey (2019), combines the SWAT model (Wei et al., 2018) and the MODFLOW model (Morway et al., 2013). The original SWAT model for the region (Wei et al., 2018) was created using data on soil, land use, topography, weather, and canal diversions (Table 4.1). This model uses automatic irrigation and calculates crop potential evapotranspiration (PET) with the Penman-Monteith method. It includes various management practices, such as planting, harvesting, and tillage, for both rainfed and irrigated conditions (Wei et al., 2018). The model

covers 72 subbasins (refer to Fig. 4.1a for boundaries) and contains 5270 HRUs, with each cultivated field assigned as a unique HRU.

The MODFLOW model incorporates data on aquifer properties, pumping rates, and groundwater head (Table 4.1). Bailey et al. (2019) developed the SWAT-Salt model to include the transport and fate of eight major salt ions in soil, groundwater, and streams. Later, Bailey and Hosseini (2023) merged the SWAT-MODFLOW and SWAT-Salt models to create the SWAT-MODFLOW-Salt model for the region. This model integrates salt mineral fractions, soil water salt ion concentrations, and groundwater salt ion concentrations from SSURGO and field data (Table 4.1). The SWAT-MODFLOW-Salt model is run from 1999 to 2100 to simulate hydrological and salinity dynamics under varying climatic conditions and irrigation efficiencies. The model performance is validated against observed data for stream discharge, soil salinity, groundwater salt ion concentrations, in-stream salt ion loads, and crop yields (Bailey and Hosseini, 2023; Wei and Bailey, 2019).

**Table 4.1** Datasets used in the construction of the SWAT-MODFLOW-Salt model.

| Data type | Data Sources | Scale/Date |
|---|---|---|
| **Soil data** | US Digital General Soil Map (STATSGO) from National Resources Conservation Service | 1:250,000 |
| **Land use** | National Agricultural Statistics Service (NASS) | 30 m ×30 m |
| **Meteorological data** | Colorado Agricultural Meteorological Network (CoAgMet) | 1999-2010 |
| **Canal diversion** | Colorado's Decision Support Systems (CDSS) | 1999-2010 |
| **Streamflow** | Colorado Division of Water Resources | 1999-2010 |
| **Topography (DEM)** | The National Map System, US Geological Survey | 30 m ×30 m |
| **Stream network** | National Hydrography Data Set, US Geological Survey | 30 m ×30 m |
| **Aquifer properties** | (Morway et al., 2013) | 250 m ×250 m |
| **Pumping rates** | Colorado Division of Water Resources | Monthly |
| **Groundwater head** | US Geological Survey (NWIS) | 1999-2010 |
| **CaCO3 + CaSO4** | SSURGO | 1:250,000 |
| **Groundwater salt ion concentrations** | Field data (Gates et al., 2016, 2009) | 1999-2010 |
| **In-stream salt ion concentrations** | Field data (Gates et al., 2016, 2009) | 1999-2010 |

### 4.2.3 Climate change projections

In this study, the calibrated and validated SWAT-MODFLOW-Salt model was utilized along with projected climate data from 2010 to 2100 to explore the impact of climate change on salinity fate and transport, as well as to assess crop production under the combined stresses of salinity, climate change, and various irrigation practices throughout the 21st century. Five climate models

and two Representative Concentration Pathway (RCP) emission scenarios, 4.5 and 8.5, were considered.

Due to the coarse spatial resolution of Global Climate Models (GCMs), their outputs often need to be downscaled using either dynamic or statistical methods. For this study, we employed the Multivariate Adaptive Constructed Analogs (MACA) statistical method to downscale climate model outputs for the contiguous United States (Abatzoglou and Brown, 2012). This involved downscaling data from twenty GCMs from the Coupled Model Inter-Comparison Project Phase 5 (CMIP5), which offers higher meteorological data resolution compared to earlier CMIPs (Shiru et al., 2022; Song et al., 2022). The data were transformed from their initial resolutions to either 4 or 6 kilometers, for RCP4.5 and RCP8.5 scenarios, spanning the period from 2010 to 2100. RCPs represent potential future scenarios of greenhouse gas and $CO_2$ emissions, classified by their projected radiative forcing levels by 2100 (Aliyari et al., 2019). In a moderate scenario, RCP4.5, the radiative forcing change by 2100 is 4.5 watts per square meter ($Wm^{-2}$) and 550 ppm $CO_2$. In a more extreme scenario, RCP8.5, this change is 8.5 $Wm^{-2}$ and 1000 ppm $CO_2$ by 2100.

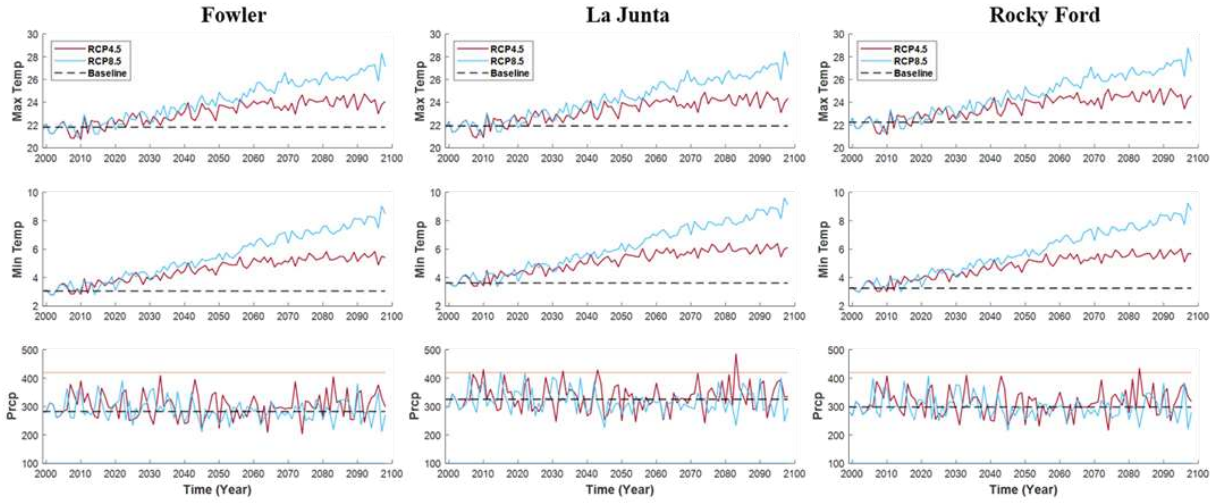


**Figure 4.2**. Projected mean annual average precipitation (mm); Projected mean annual average maximum and minimum temperature (°C) across all climate models. These projections are depicted for the RCP4.5 (red lines) and the RCP8.5 scenarios (blue lines) for the stations at Fowler, La Junta, and Rocky Ford within the watershed highlighted in Fig.1. For comparative purposes, the historical averages from the period 1999 to 2009 are shown as dashed lines in each plot.

The changes in mean annual average minimum and maximum temperatures and precipitation compared to the baseline in Fowler range between +48.2% (projected by RCP4.5) and 80.5% (projected by RCP8.5), between +5.9% (projected by RCP4.5) and 10.7% (projected by RCP8.5), between +7.1% (projected by RCP4.5) and 2.1% (projected by RCP8.5), respectively. In Rocky Ford, the changes in mean annual average minimum and maximum temperatures and precipitation compared to the baseline range between +45.6% (projected by RCP4.5) and 76.3% (projected by RCP8.5), +5.8% (projected by RCP4.5) and +24.6% (projected by RCP8.5), and +5.1% (projected by RCP8.5) and +0.1% (projected by RCP4.5), respectively. Similarly, in La Junta, the changes in mean annual average minimum and maximum temperatures and precipitation compared to the baseline range between +41.4% (projected by RCP4.5) and 69.2% (projected by RCP8.5), +6.1% (projected by RCP4.5) and +10.9% (projected by RCP8.5), and -1.9% (projected by RCP8.5) and +2.7% (projected by RCP4.5), respectively.

To thoroughly evaluate the impact of projected climate change on salinity fate and transport, and the mutual impact of salinity, climate change, and various irrigation practices on crop production in the LARV, we used a combination of five distinct MACA climate models under the RCP4.5 and RCP8.5 emission scenarios. The selected climate models (Table 4.2) include widely used GCMs representing the least warm (Warm), hottest (Hot), driest (Dry), wettest (Wet), and a moderate projection (Mild), which represents the midpoint in terms of temperature and precipitation variability among all the other models at a regional scale (Heidari et al., 2020; Joyce and Coulson, 2020). In this study, the SWAT-MODFLOW-Salt model outputs constructed in the chapter three of current dissertation for the period from 1999 to 2100, which consider the mutual impact of salinity and climate change on salinity transport and crop production in the LARV, are referred to as the "baseline." This baseline is used for comparison with future scenarios that

incorporate the mutual effects of salinity, climate change and various irrigation efficiencies on salt transport and crop production by the end of 2100. The projected downscaled MACA climate dataset from five GCM models was inserted into the SWAT climatic input file, and each individual GCM was separately simulated in the calibrated and validated SWAT-MODFLOW-Salt model, considering both the baseline climate scenarios defined by the two RCPs (RCP4.5 and RCP8.5) and various irrigation practices.

**Table 4.2** Climate models used in scenarios.

| GCM model | Climatic projection | Emission scenarios | Agency | Country |
|---|---|---|---|---|
| HadGEM2-ES365 | Hot | RCP4.5, RCP8.5 | Met Office Hadley Center | UK |
| MRI-CGCM3 | Warm | RCP4.5, RCP8.5 | Meteorological Research Institute | Japan |
| IPSL-CM5A-MR | Dry | RCP4.5, RCP8.5 | Institute Pierre Simon Laplace | France |
| NorESM1-M | Mild | RCP4.5, RCP8.5 | Norwegian Climate Center | Norway |
| CNRM-CM5 | Wet | RCP4.5, RCP8.5 | National Centre of Meteorological Research | France |

### 4.2.4 Irrigation management and crop production

Effective irrigation management is crucial for optimizing water use efficiency, enhancing crop yields, and sustaining agricultural productivity, especially in arid and semi-arid regions where water scarcity is a significant challenge. With the growing global population and the impacts of climate change, efficient water management practices are essential to ensure food security and sustainable agricultural practices. Irrigation management involves the strategic application of water to crops at the right time and in the right amounts, reducing water wastage and maximizing crop productivity (Arbat and Masseroni, 2024). In salinity-affected agricultural regions, effective irrigation management plays a crucial role in optimizing crop productivity and ensuring

sustainable water use. This management involves not only the selection of an appropriate irrigation method but also the application of adequate water to leach salts below the root zone, especially in soils with poor drainage. The frequency and amount of irrigation must be carefully managed to avoid the buildup of salts within the root zone, which can be detrimental to crop health and yield. In areas with significant rainfall, the natural leaching effect of rain can aid in this process, but in arid regions, artificial leaching through additional irrigation is often necessary. The choice of irrigation strategy and its proper management are vital for sustainable agriculture in saline environments, as they directly affect the distribution and concentration of salts in the soil profile, soil health, and crop productivity (Machado and Serralheiro, 2017).

Surface irrigation methods, including flood and furrow irrigation, are cost-effective and widely used; however, they generally exhibit low water use efficiency (WUE), typically ranging from 40% to 50%. This inefficiency is primarily due to significant water losses through evaporation, surface runoff, and deep percolation, as well as the tendency to create uneven water distribution, which can exacerbate salt accumulation. Despite these drawbacks, flood irrigation has a higher potential for controlling soil salinity compared to other methods. It promotes the leaching of salts deeper into the soil profile, away from the root zone, thereby reducing salt stress on crops and improving soil health over time. While flood irrigation is not typically the optimal method for non-saline soils, it can be effectively utilized for salinity management with careful planning and management (Ahmadzadeh et al., 2016; Eckhoff et al., 2005).

Sprinkler irrigation provides a more controlled method of water distribution, achieving efficiencies of approximately 75-85%. This method mitigates water losses associated with flood irrigation by reducing evaporation and runoff, thereby offering a more uniform water distribution that helps maintain soil moisture at optimal levels. In non-saline soils, sprinkler irrigation is

particularly beneficial as it enhances water use efficiency and prevents uneven water distribution, promoting healthier crop growth and higher yields. In saline soils, however, sprinkler irrigation has limitations in managing soil salinity. While it prevents surface salt accumulation, it does not facilitate the leaching of salts as effectively as flood irrigation. This can lead to the retention of salts in the root zone over time, potentially increasing salinity stress on crops. Therefore, while sprinkler irrigation is highly efficient and beneficial for non-saline soils, its effectiveness in saline soil conditions requires careful management to avoid salt buildup and ensure sustainable crop productivity (Ahmadzadeh et al., 2016).

Drip irrigation is renowned for its high efficiency, often ranging between 90% to 95%. By delivering water directly to the root zone, this method significantly reduces evaporation and prevents the surface accumulation of salts, making it an ideal choice for salinity management. The precision in water and nutrient delivery directly to the plant roots also helps in maintaining optimal soil moisture levels, thus ensuring that salts do not adversely affect plant growth (Wu et al., 2019). On the other hand, Subsurface Drip Irrigation (SDI) builds on the benefits of drip irrigation by placing the water delivery system below the soil surface, which minimizes evaporation further and effectively manages salt distribution in the soil profile. This method is particularly suitable for areas with severe salinity issues, as it helps keep salts away from the plant roots and reduces the impact on crop yield and health.

The decision on the right irrigation method involves assessing the specific conditions of the field, including water availability, soil type, crop type and requirements, prevailing salinity levels, and economic considerations. While sprinkler and drip irrigation systems offer higher efficiency and better salinity management, their initial cost and maintenance requirements are higher compared to surface irrigation systems. The decision must balance economic considerations with

environmental benefits, particularly in terms of managing soil salinity which can severely impact crop yields.

Irrigation efficiency (IE) serves as a comprehensive indicator that encapsulates the effectiveness of irrigation projects, water management, and irrigation technology at multiple levels. It plays a crucial role in accurately assessing the utilization of irrigation water and the success of water conservation efforts in irrigation (Wu et al., 2019). As shown in Fig. 4.1c, flood irrigation is the dominant irrigation method in the LARV followed by sprinkler and drip irrigation. In this study we investigate the combined effects of salinity, climate change, and irrigation practices on crop production by shifting from flood to sprinkler irrigation, leveraging improvements in irrigation efficiency and water loss considering two different scenarios. In scenario (1), the amount of irrigation water is kept constant while irrigation efficiency is improved by 5% and water loss due to runoff is reduced by 5% in each subscenario, resulting in four distinct irrigation subscenarios compared to the baseline flood irrigation in the LARV. In scenario (2), the irrigation water amount is reduced to half of the baseline flood irrigation gradually, with a 5% enhancement in irrigation efficiency and a 5% reduction in water loss due to runoff in each subscenario. Understanding how these factors interact is vital for developing sustainable management strategies that can cope with the challenges posed by climate variability and soil salinity.

## 4.3. RESULTS AND DISCUSSION

In this section, we present the findings illustrating the combined effects of salinity, climate change, and two distinct irrigation management scenarios on crop yields for two dominant crops in the LARV, corn and alfalfa, by the end of century.

### 4.3.1 Mutual impact of climate change, salinity, and irrigation practices on crop production

Figure 4.3 shows the combined impact of salinity, climate change, and scenario (1) irrigation practices on the yields of alfalfa and corn, in comparison to the baseline scenario using flood irrigation by the year 2100. This analysis specifically addresses the differential responses of corn and alfalfa to the impact of incremental increases in irrigation efficiency (5%, 10%, 15%, and 20%) and reductions in water loss through surface runoff (5%, 10%, 15%, and 20%) while maintaining a constant amount of irrigation water, on corn and alfalfa yields dynamics under conditions of salinity stress, utilizing projections from five global climate models under two distinct Representative Concentration Pathway (RCP) scenarios, RCP4.5 and RCP8.5.

The combined impact of salinity, climate change, and irrigation practices in scenario (1) on corn shows a clear sensitivity to salinity stress, demonstrates significant yield reductions under salinity stress across all climate models and scenarios. This sensitivity is pronounced, given corn's critical demand for water during key growth stages such as flowering and grain filling. The introduction of improved irrigation efficiencies with the irrigation water amount remaining constant, reveals a trend of yield recovery, where each increment in efficiency and water loss contributes to a reduction in yield gaps between salinity stressed and unstressed conditions. Notably, as irrigation efficiency increases from 5% to 20% and runoff ratio decreases from 5% to 20%, the adverse effects of salinity are progressively mitigated, highlighting the critical role of efficient water management in sustaining corn production in saline environments.

Under the moderate scenario (RCP4.5), there is a noticeable trend where increased irrigation efficiency and reduced runoff ratio (from 5% to 20%) consistently mitigates yield losses across all models. The MRI-CGCM3 and IPSL-CM5A-MR models, in particular, show a robust improvement in yield as irrigation efficiency increases, suggesting that these models predict a less

severe climate impact, allowing for more effective mitigation through improved water management. In the more severe RCP8.5 scenario, the gap between salinity stressed and non-stressed yields widens, yet the benefits of higher irrigation efficiencies become even more crucial. GCM models such as HadGEM2-ES365 exhibit greater yield recoveries with increased irrigation efficiencies, indicating that in more extreme climate conditions, precise water management is even more critical for sustaining corn production.

Alfalfa, known for its higher tolerance to saline conditions, exhibits a less dramatic decrease in yields under similar stress. This resilience is attributed to alfalfa's deeper root system, which can access subsurface water, mitigating the impact of surface-level salinity. However, the enhancement of irrigation efficiency still plays a beneficial role, particularly at higher levels of efficiency improvement. Even modest increases in efficiency (5% to 10%) begin to show benefits, with more notable improvements as efficiency reaches 15% and 20% and water loss decreases by 15% to 20%. While the yield improvements in alfalfa are not as marked as in corn, the trend indicates that even salt-tolerant crops can benefit from optimized irrigation practices. This is particularly evident under the RCP8.5 scenario, where the more severe predicted climate conditions amplify the benefits of higher irrigation efficiencies. Under a moderate scenario, alfalfa benefits from increases in irrigation efficiency, with all models showing some level of yield improvement. However, the yield increase is not as substantial as seen in corn, reflecting alfalfa's inherent drought and salinity tolerance. Under the severe scenario, despite the harsher conditions projected by models like NorESM1-M and CNRM-CM5, alfalfa shows a commendable adaptability, with yield improvements becoming more noticeable as irrigation efficiency increases to 15% and 20%. These improvements suggest that while alfalfa is less sensitive to salinity than corn, it still gains yield advantages from enhanced water management, which can optimize its

growth and productivity even under suboptimal conditions. The results also show that alfalfa can maintain productivity even under heightened climatic stresses, provided that water management is optimized.

The comparative analysis between the RCP4.5 and RCP8.5 scenarios suggests that future emission pathways significantly influence crop yield responses to salinity stress. Under RCP8.5, the yield disparities induced by salinity are more pronounced, yet they are also more effectively alleviated by increased irrigation efficiency. This underscores the potential of advanced irrigation strategies to serve as a countermeasure to the compounded stresses of higher salinity and more extreme climate conditions projected in the future. The variability in yield responses to salinity stress under different GCMs and RCPs highlights the importance of selecting and tailoring irrigation strategies based on specific crop sensitivities and projected climatic conditions. For corn, prioritizing high-efficiency irrigation systems is crucial, especially under scenarios predicting more extreme temperature and precipitation changes. In contrast, alfalfa's resilience suggests that while it benefits from improved irrigation, the focus might also include optimizing frequency and timing to maximize efficiency and sustainability. These underscore the importance of integrating efficient irrigation technologies and practices into salinity management strategies to enhance crop resilience. For regions facing similar environmental challenges, adopting such measures could be crucial in maintaining agricultural productivity in the face of escalating salinity pressures and changing climatic conditions. This analysis not only highlights the variable sensitivity of different crops to salinity but also demonstrates the potential of targeted agricultural interventions to mitigate these impacts.

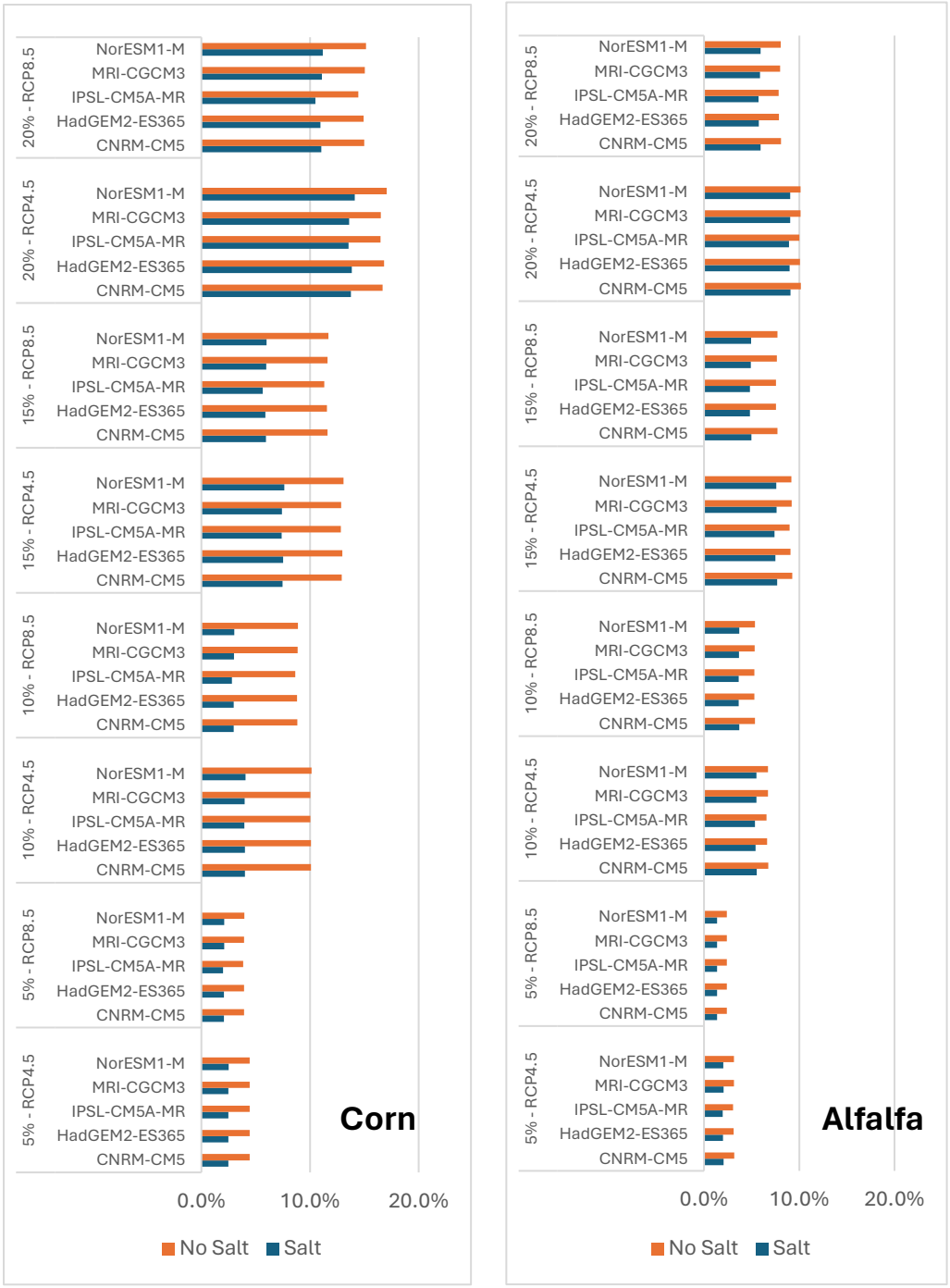


**Figure 4.3.** Average percentage changes in crop yields of corn and alfalfa under salinity stress conditions, as projected by five GCM models. The data is presented for two emission scenarios and four irrigation scenarios and irrigation scenario (1), where irrigation efficiency is increased by 5%, 10%, 15%, and 20% and the water loss via surface runoff reduced by 5%, 10%, 15%, and 20% relative to baseline yields in the LARV.

Figure 4.4 illustrates the trends in alfalfa and corn yields by 2100, under salinity stress condition, five GCM models, the RCP4.5 scenario, and the irrigation practice scenario (1) with

20% increase in irrigation efficiency and 20% reduction in irrigation water loss relative to baseline. The shaded area in the plots represents the confidence intervals, which illustrate the range within which the true yield values are expected to fall. The upper and lower bounds of these intervals account for the variation and uncertainty in the annual average yield values. These confidence intervals provide a visual representation of the reliability and precision of the data, indicating the extent of potential fluctuation in yield estimates due to inherent variability and uncertainty. This allows for a more robust interpretation of the data by highlighting the degree of confidence in the reported yields. The results for incremental increases and reductions of 5%, 10%, and 15% in irrigation efficiency and irrigation water loss under the RCP4.5 and RCP8.5 scenarios for both corn and alfalfa are detailed in Appendix. The projection for alfalfa yields shows a general upward trend with increased irrigation efficiency. This trend is consistent across all five GCMs evaluated—NorESM1-M, MRI-CGCM3, IPSL-CM5A-MR, HadGEM2-ES365, and CNRM-CM5—indicating a positive response of alfalfa to improved water availability. The consistency of this trend suggests that alfalfa, known for its resilience, can benefit significantly from strategic irrigation enhancements. With a 20% increase in irrigation efficiency and 20% reduction in irrigation water loss, alfalfa yields demonstrate notable improvements. The enhancements range from moderate to substantial, depending on the specific climate model. For instance, the IPSL-CM5A-MR and MRI-CGCM3 models show higher relative increases in yield, which may be attributed to their particular sensitivity to changes in irrigation practices under the RCP4.5 scenario. These results underscore the potential of efficient irrigation to mitigate the adverse impacts of climatic variability on crop productivity. The RCP4.5 scenario represents a moderate climate change trajectory, and the observed yield improvements suggest that alfalfa could maintain or even increase productivity under such conditions. This resilience is particularly significant given

the potential for more extreme climate conditions under higher emission scenarios like RCP8.5. The findings from this analysis have important implications for agricultural management in semi-arid and arid regions. The demonstrated benefits of increased irrigation efficiency highlight the need for investments in advanced irrigation technologies. By optimizing water use, farmers can enhance alfalfa productivity, ensuring more stable yields despite the uncertainties of future climate conditions. Furthermore, these results support the broader adoption of precision agriculture practices, which can tailor water application to specific crop needs, thereby maximizing efficiency and reducing waste. Such practices not only improve crop resilience but also contribute to sustainable water resource management.

The analysis of corn yield projections, derived from multiple global climate models, demonstrates a clear trend of yield improvement associated with a 20% increase in irrigation efficiency and 20% reduction in irrigation water loss under the RCP4.5 scenario. Across all models, the enhancement of irrigation efficiency correlates with an upward trend in corn yields. This improvement is consistent, albeit with varying magnitudes across the different models, reflecting the diversity in how these models simulate climate impacts on agricultural systems. Notably, the MRI-CGCM3 and IPSL-CM5A-MR models exhibit particularly robust responses to increased irrigation efficiency, suggesting that these models may capture more effectively the soil moisture and crop growth dynamics that are critical in a semi-arid climate under moderated climate change conditions. These yield improvements are particularly significant given the context of the RCP4.5 scenario, which assumes a moderate trajectory of greenhouse gas emissions and associated climatic changes. Under this scenario, the results indicate that strategic water management can effectively compensate for potential adverse climate impacts. The yield gains observed suggest that corn, a crop with substantial water requirements, can benefit significantly from the precise

application and efficient use of water resources. The findings suggest that investment in advanced irrigation technologies, capable of delivering water more efficiently to the root zones of crops, could be a key adaptive strategy to sustain and possibly enhance corn production in the face of global climate change. This strategy is not only beneficial for maintaining yield levels but also for conserving water—a critical consideration in regions facing potential water scarcity.

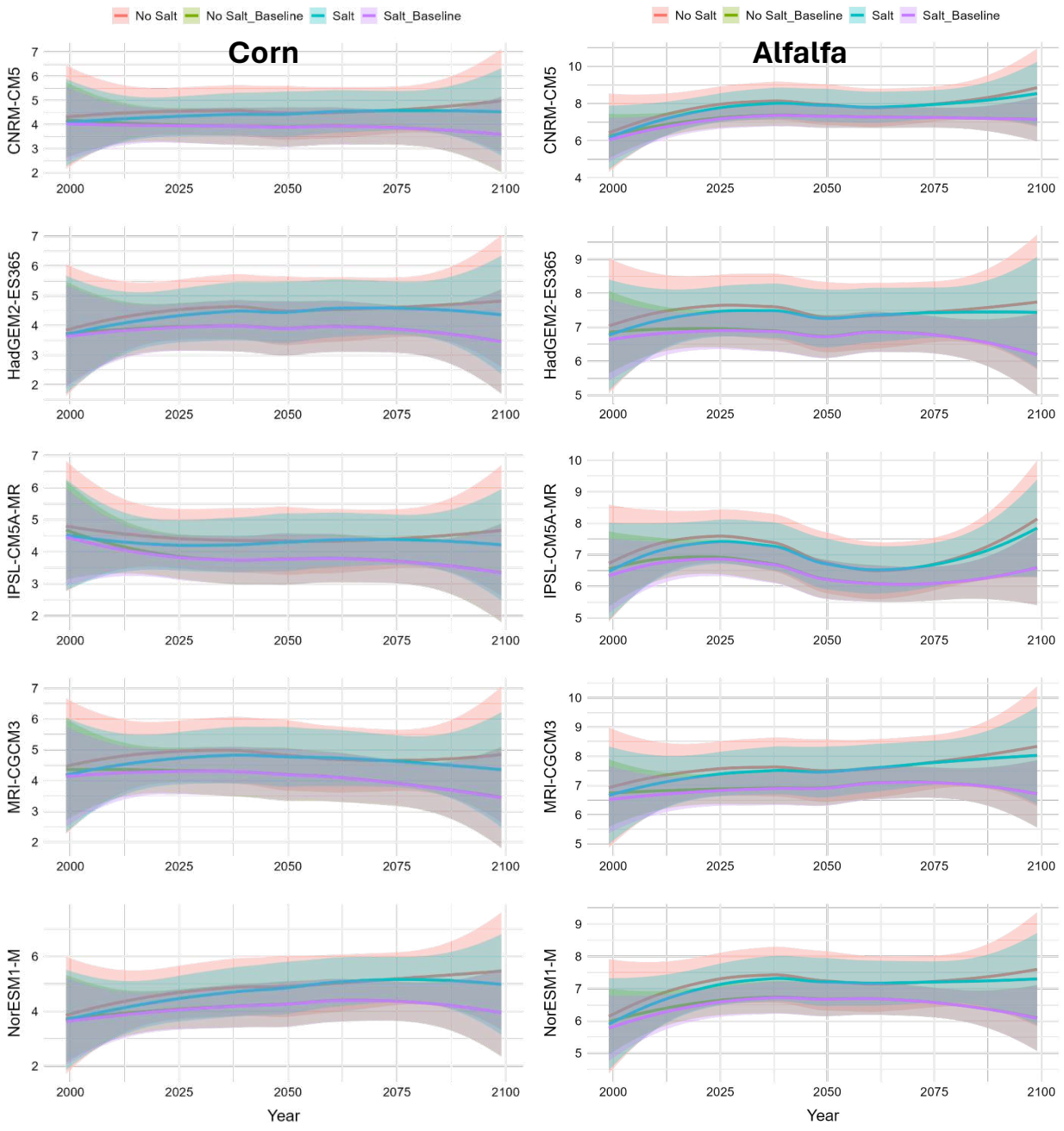


**Figure 4.4.** Area plots above show corn and alfalfa yields, under the salinity stress, five GCM climate model, RCP4.5, and the irrigation practice scenario (1) 20% increase in irrigation efficiency and 20% reduction in irrigation water loss relative to baseline by the year 2100.

Table 4.3 presents the yields of alfalfa and corn both under salinity stress conditions and without, across five GCM climate models and two emission scenarios, RCP4.5 and RCP8.5, and irrigation practice scenario (1). It details the effects of incremental 5% increases and reductions in irrigation

efficiency and irrigation water loss from the baseline, up to a total of 20%, respectively. Corn yields exhibited a trend of gradual increase across all GCMs and scenarios as irrigation efficiency improved, regardless of salinity presence. Notably, under the CNRM-CM5 model with RCP4.5, in salinity stress conditions, corn yields improved from 3.91 ton/ha at baseline to 4.45 ton/ha at 20% increased irrigation efficiency and 20% irrigation water loss reduction, marking an increase of approximately 13.8%. Without salt, the yields progressed from 3.94 ton/ha to 4.59 ton/ha, showing an increase of around 16.5%. The HadGEM2-ES365 model under RCP8.5 with salt stress presented a yield increase from 3.63 ton/ha to 4.03 ton/ha, translating to a growth of about 11.0%, which was among the lowest increments observed, reflecting the sensitivity of corn to higher salinity under more severe climate conditions. Alfalfa yields under similar conditions showed resilience, with consistent yield improvements as irrigation efficiency increased. In the MRI-CGCM3 model under RCP4.5 with salt, alfalfa yields rose from 6.92 ton/ha to 7.55 ton/ha as irrigation efficiency increased by 20% and irrigation water loss decreased by 20%, reflecting an increase of 9.1%. In no salt conditions, the increase was from 6.97 ton/ha to 7.76 ton/ha, indicating a gain of 10.0%. Under the NorESM1-M model with RCP8.5 and salt, the yield increment was less pronounced, moving from 6.35 ton/ha to 6.73 ton/ha, 5.9% increase, which still highlights crop resilience in higher salinity and emission conditions. The analysis shows that both corn and alfalfa benefit from increased irrigation efficiency and irrigation water loss reduction, particularly in mitigating the effects of salinity stress. However, the extent of benefit varies by crop and environmental scenario.

**Table 4.3** The baseline and estimated crop yields under salinity stress conditions, five GCM models, two emission scenarios, and scenario (1) irrigation management four irrigation scenarios for alfalfa and corn in the study area. The percentages listed under the yield column indicate the change in irrigation efficiency and irrigation water loss.

| Crop | GCM model | Emission scenario | Salinity | Yield ($tonha^{-1}$) | | | | |
|---|---|---|---|---|---|---|---|---|
| | | | | Baseline | 5% | 10% | 15% | 20% |
| Alfalfa | CNRM-CM5 | RCP4.5 | Salt | 7.1 | 7.2 | 7.5 | 7.6 | 7.7 |
| | | | No Salt | 7.2 | 7.3 | 7.6 | 7.8 | 7.8 |
| | | RCP8.5 | Salt | 6.9 | 7.0 | 7.2 | 7.3 | 7.3 |
| | | | No Salt | 7.0 | 7.1 | 7.3 | 7.5 | 7.5 |
| | HadGEM2-ES365 | RCP4.5 | Salt | 6.8 | 6.9 | 7.1 | 7.3 | 7.4 |
| | | | No Salt | 6.8 | 7.0 | 7.2 | 7.4 | 7.5 |
| | | RCP8.5 | Salt | 6.3 | 6.4 | 6.5 | 6.6 | 6.7 |
| | | | No Salt | 6.4 | 6.5 | 6.7 | 6.8 | 6.8 |
| | IPSL-CM5A-MR | RCP4.5 | Salt | 6.4 | 6.6 | 6.8 | 6.9 | 7.0 |
| | | | No Salt | 6.5 | 6.7 | 6.9 | 7.1 | 7.1 |
| | | RCP8.5 | Salt | 6.0 | 6.1 | 6.2 | 6.3 | 6.4 |
| | | | No Salt | 6.1 | 6.2 | 6.4 | 6.5 | 6.5 |
| | MRI-CGCM3 | RCP4.5 | Salt | 6.9 | 7.0 | 7.3 | 7.4 | 7.5 |
| | | | No Salt | 7.0 | 7.1 | 7.4 | 7.6 | 7.6 |
| | | RCP8.5 | Salt | 6.7 | 6.8 | 7.0 | 7.1 | 7.1 |
| | | | No Salt | 6.8 | 6.9 | 7.1 | 7.3 | 7.3 |
| | NorESM1-M | RCP4.5 | Salt | 6.5 | 6.6 | 6.8 | 7.0 | 7.1 |
| | | | No Salt | 6.5 | 6.7 | 6.9 | 7.1 | 7.2 |
| | | RCP8.5 | Salt | 6.3 | 6.4 | 6.5 | 6.6 | 6.7 |
| | | | No Salt | 6.4 | 6.5 | 6.7 | 6.8 | 6.9 |
| Corn | CNRM-CM5 | RCP4.5 | Salt | 3.9 | 4.0 | 4.0 | 4.2 | 4.4 |
| | | | No Salt | 3.9 | 4.1 | 4.3 | 4.4 | 4.6 |
| | | RCP8.5 | Salt | 3.9 | 4.0 | 4.0 | 4.2 | 4.4 |
| | | | No Salt | 4.0 | 4.1 | 4.3 | 4.4 | 4.6 |
| | HadGEM2-ES365 | RCP4.5 | Salt | 3.8 | 3.9 | 4.0 | 4.1 | 4.4 |
| | | | No Salt | 3.9 | 4.0 | 4.2 | 4.4 | 4.5 |
| | | RCP8.5 | Salt | 3.6 | 3.7 | 3.7 | 3.8 | 4.0 |
| | | | No Salt | 3.6 | 3.8 | 3.9 | 4.0 | 4.2 |
| | IPSL-CM5A-MR | RCP4.5 | Salt | 3.7 | 3.9 | 3.9 | 4.0 | 4.3 |
| | | | No Salt | 3.8 | 4.0 | 4.2 | 4.3 | 4.4 |
| | | RCP8.5 | Salt | 3.7 | 3.7 | 3.7 | 3.8 | 4.0 |
| | | | No Salt | 3.7 | 3.8 | 4.0 | 4.1 | 4.2 |
| | MRI-CGCM3 | RCP4.5 | Salt | 4.1 | 4.2 | 4.2 | 4.4 | 4.6 |
| | | | No Salt | 4.1 | 4.3 | 4.5 | 4.6 | 4.7 |
| | | RCP8.5 | Salt | 3.7 | 3.8 | 3.9 | 4.0 | 4.2 |
| | | | No Salt | 3.8 | 3.9 | 4.1 | 4.2 | 4.3 |
| | NorESM1-M | RCP4.5 | Salt | 4.1 | 4.2 | 4.3 | 4.4 | 4.7 |
| | | | No Salt | 4.2 | 4.3 | 4.6 | 4.7 | 4.8 |
| | | RCP8.5 | Salt | 3.9 | 4.0 | 4.1 | 4.2 | 4.4 |
| | | | No Salt | 4.0 | 4.1 | 4.3 | 4.4 | 4.6 |

Corn demonstrated a significant yield improvement, particularly under less severe emission scenarios (RCP4.5), but its performance was relatively constrained under the more stringent

conditions of RCP8.5, illustrating its higher vulnerability to increased salinity. Conversely, alfalfa displayed remarkable resilience, with consistently greater yield increases across both scenarios, indicating its suitability for regions increasingly affected by salinity as a result of climate change. These outcomes underline the critical need for adopting adaptive irrigation strategies tailored to the distinct sensitivities of various crops to the anticipated future climatic conditions. Such a strategic approach is essential for maintaining and possibly enhancing agricultural productivity amid escalating challenges posed by salinity and climate change.

Figure 4.5 illustrates the combined effects of salinity, climate change, and irrigation practices on crop yields, specifically for alfalfa and corn, under scenario (2). This scenario entails incremental increases in irrigation efficiency (5%, 10%, 15%, and 20%) and reductions in water loss via surface runoff (5%, 10%, 15%, and 20%), with the total amount of irrigation water reduced to half of the baseline flood irrigation scenario gradually. Yield projections are derived from multiple global climate models (GCMs) under two Representative Concentration Pathway (RCP) scenarios, RCP4.5 and RCP8.5.

Corn yields exhibit significant sensitivity to salinity stress in scenario (2), with marked reductions observed under saline conditions across all climate models and scenarios. Corn, which requires substantial water during critical growth stages, experiences pronounced yield decreases due to the combined effects of reduced water availability and increased salinity stress. Under salinity stress, a 5% increase in irrigation efficiency and simultaneous 5% reduction in water loss through runoff resulted in a 2.7% decrease in yields. Increasing the irrigation efficiency and decreasing the runoff ratio by 10%, 15%, and 20% resulted in yield decreases of 4.6%, 7.3%, and 9.8%, respectively.

Under non-saline conditions, a 5% increase and decrease in irrigation efficiency and water loss via surface runoff led to a 1.9% decrease in yields. Similarly, 10%, 15%, and 20% increases and reductions in irrigation efficiency and water loss resulted in yield decreases of 4.6%, 6.7%, and 9.3%, respectively. Incremental increases in irrigation efficiency and reductions in runoff ratios help mitigate yield losses, although overall yields still decrease. Enhanced irrigation efficiency and reduced water loss alleviate some of the adverse effects of salinity but yield gaps between salinity-stressed and non-stressed conditions remain significant. Under the moderate RCP4.5 scenario, incremental improvements in irrigation efficiency and reductions in runoff help to lessen yield losses across all models. The MRI-CGCM3 and IPSL-CM5A-MR models, in particular, demonstrate some recovery in yield with increased irrigation efficiency, suggesting that these models predict less severe climate impacts and allow for more effective mitigation through improved water management.

In the more severe RCP8.5 scenario, the disparity between salinity-stressed and non-stressed yields widens further, emphasizing the critical importance of achieving higher irrigation efficiencies. Models such as HadGEM2-ES365 show some yield recovery with increased irrigation efficiencies, underscoring the necessity of precise water management to sustain corn production under extreme climate conditions.

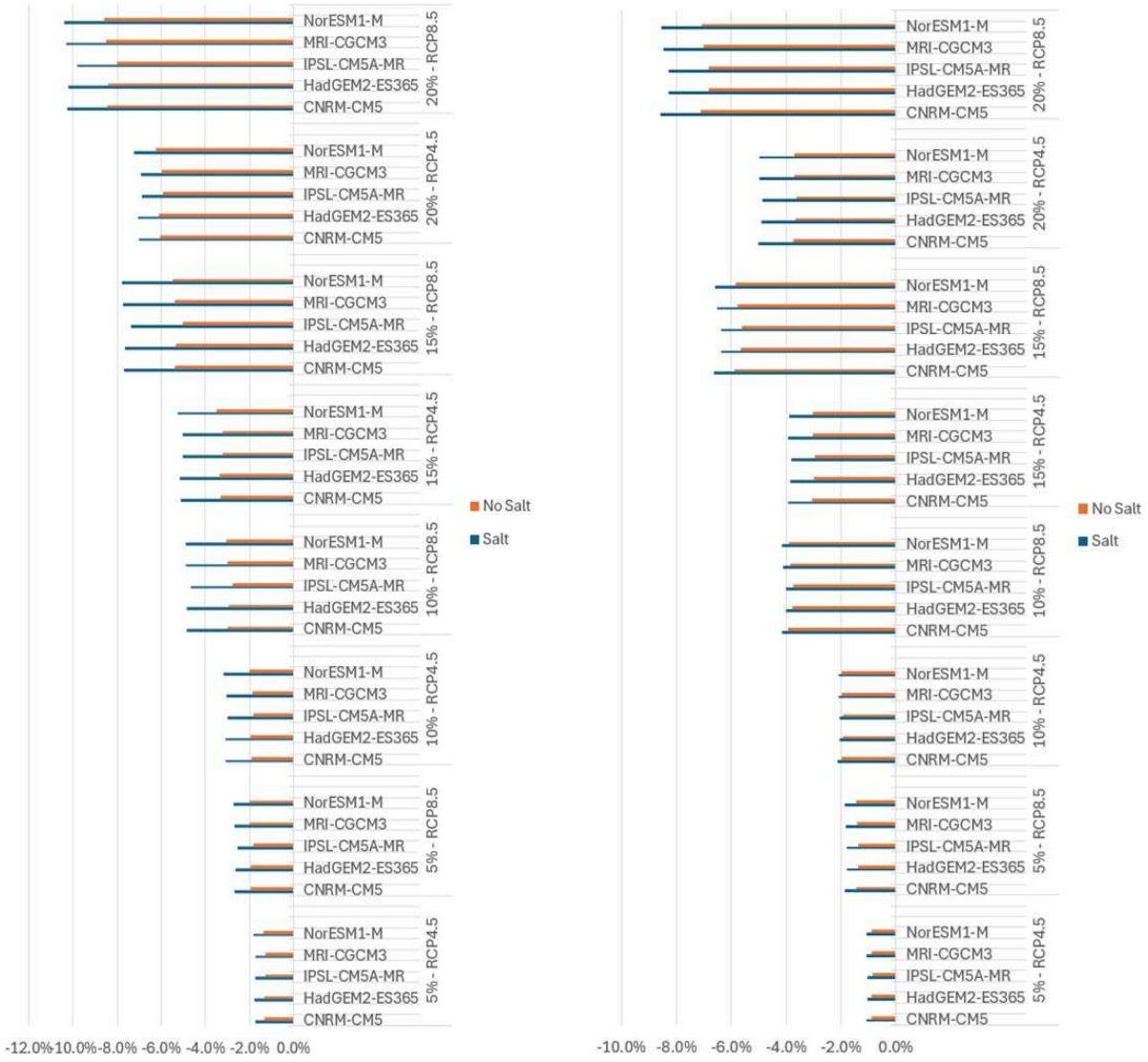


**Figure 4.5.** Average percentage changes in crop yields of corn and alfalfa under salinity stress conditions, as projected by five GCM models. The data is presented for two emission scenarios and irrigation scenario (2), where irrigation efficiency is increased by 5%, 10%, 15%, and 20% and the water loss via surface runoff reduced by 5%, 10%, 15%, and 20% relative to baseline yields in the LARV.

Table 4.4 displays the yields of alfalfa and corn under both salinity stress conditions and non-stress conditions, as projected by five GCM climate models under two emission scenarios, RCP4.5 and RCP8.5, within the context of irrigation practice scenario (2). It highlights the impact

of reduction in irrigation water amount, incremental increases of 5% in irrigation efficiency and reductions in irrigation water loss, progressing up to a total of 20% from the baseline.

Alfalfa, as mentioned prior, known for its higher tolerance to saline conditions, shows less dramatic yield decreases under similar stress. This resilience is attributed to alfalfa's deeper root system, which can access subsurface water and mitigate the impact of surface-level salinity. Nonetheless, improvements in irrigation efficiency provide benefits, although overall yields still decline. Under salinity stress, a 5% increase and 5% reduction in irrigation efficiency and water loss via surface runoff led to a 1.8% decrease in yields. Increasing and declining the irrigation efficiency and surface runoff by 10%, 15%, and 20% resulted in yield decreases of 3.9%, 6.8%, and 8.9%, respectively.

Under non-saline conditions, a 5% increase in irrigation efficiency led to a 1.3% decrease in yields. Similarly, 10%, 15%, and 20% increases and reductions in irrigation efficiency and surface runoff resulted in yield decreases of 3.9%, 5.6%, and 8.3%, respectively. Even modest increases in efficiency help reduce yield losses, with more significant mitigation observed as efficiency reaches higher levels. While yield reductions in alfalfa are less pronounced than in corn, the trend indicates that optimized irrigation practices can still benefit even salt-tolerant crops. This is particularly evident under the RCP8.5 scenario, where severe predicted climate conditions magnify the importance of higher irrigation efficiencies.

Under the moderate RCP4.5 scenario, alfalfa yields benefit from increased irrigation efficiency, with all models showing some mitigation of yield losses. The reduction in yield is not as severe as seen in corn, reflecting alfalfa's inherent drought and salinity tolerance. Despite harsher conditions projected by models like NorESM1-M and CNRM-CM5 under the severe scenario, alfalfa demonstrates commendable adaptability, with yield reductions being lessened as

irrigation efficiency increases. These findings suggest that while alfalfa is less sensitive to salinity than corn, it still benefits from enhanced water management practices.

**Table 4.4** The baseline and estimated crop yields under salinity stress conditions, five GCM models, two emission scenarios, and scenario (2) irrigation management for alfalfa and corn in the study area. The percentages listed under the yield column indicate the change in irrigation efficiency and irrigation water loss.

| Crop | GCM model | Scenario | Salinity | Yield | | | | |
|---|---|---|---|---|---|---|---|---|
| | | | | Baseline | 5% | 10% | 15% | 20% |
| Alfalfa | CNRM-CM5 | RCP4.5 | Salt | 7.12 | 7.05 | 6.97 | 6.84 | 6.77 |
| | | | No Salt | 7.16 | 7.10 | 7.02 | 6.95 | 6.90 |
| | | RCP8.5 | Salt | 6.98 | 6.85 | 6.69 | 6.52 | 6.38 |
| | | | No Salt | 7.02 | 6.91 | 6.74 | 6.60 | 6.52 |
| | HadGEM2-ES365 | RCP4.5 | Salt | 6.80 | 6.73 | 6.66 | 6.54 | 6.46 |
| | | | No Salt | 6.84 | 6.78 | 6.71 | 6.64 | 6.59 |
| | | RCP8.5 | Salt | 6.34 | 6.23 | 6.09 | 5.94 | 5.82 |
| | | | No Salt | 6.38 | 6.30 | 6.14 | 6.02 | 5.95 |
| | IPSL-CM5A-MR | RCP4.5 | Salt | 6.48 | 6.42 | 6.35 | 6.24 | 6.17 |
| | | | No Salt | 6.53 | 6.47 | 6.40 | 6.33 | 6.29 |
| | | RCP8.5 | Salt | 6.04 | 5.93 | 5.80 | 5.66 | 5.54 |
| | | | No Salt | 6.08 | 6.00 | 5.85 | 5.74 | 5.67 |
| | MRI-CGCM3 | RCP4.5 | Salt | 6.92 | 6.85 | 6.78 | 6.65 | 6.58 |
| | | | No Salt | 6.97 | 6.90 | 6.83 | 6.76 | 6.71 |
| | | RCP8.5 | Salt | 6.76 | 6.64 | 6.49 | 6.32 | 6.19 |
| | | | No Salt | 6.80 | 6.70 | 6.54 | 6.41 | 6.32 |
| | NorESM1-M | RCP4.5 | Salt | 6.50 | 6.43 | 6.36 | 6.24 | 6.17 |
| | | | No Salt | 6.54 | 6.48 | 6.41 | 6.34 | 6.30 |
| | | RCP8.5 | Salt | 6.35 | 6.24 | 6.09 | 5.94 | 5.81 |
| | | | No Salt | 6.39 | 6.30 | 6.14 | 6.02 | 5.94 |
| Corn | CNRM-CM5 | RCP4.5 | Salt | 3.91 | 3.84 | 3.79 | 3.71 | 3.64 |
| | | | No Salt | 3.94 | 3.88 | 3.86 | 3.81 | 3.70 |
| | | RCP8.5 | Salt | 3.97 | 3.86 | 3.78 | 3.67 | 3.56 |
| | | | No Salt | 4.00 | 3.92 | 3.88 | 3.78 | 3.66 |
| | HadGEM2-ES365 | RCP4.5 | Salt | 3.87 | 3.81 | 3.75 | 3.68 | 3.60 |
| | | | No Salt | 3.89 | 3.84 | 3.82 | 3.76 | 3.65 |
| | | RCP8.5 | Salt | 3.63 | 3.54 | 3.46 | 3.36 | 3.26 |
| | | | No Salt | 3.65 | 358% | 3.55 | 3.46 | 3.35 |
| | IPSL-CM5A-MR | RCP4.5 | Salt | 3.79 | 3.73 | 3.68 | 3.60 | 3.53 |
| | | | No Salt | 3.82 | 3.77 | 3.75 | 3.70 | 3.59 |
| | | RCP8.5 | Salt | 3.68 | 3.58 | 3.51 | 3.41 | 3.32 |
| | | | No Salt | 3.71 | 3.64 | 3.60 | 3.52 | 3.41 |
| | MRI-CGCM3 | RCP4.5 | Salt | 4.08 | 4.01 | 3.96 | 3.87 | 3.80 |
| | | | No Salt | 4.11 | 4.06 | 4.03 | 3.98 | 3.86 |
| | | RCP8.5 | Salt | 3.77 | 3.67 | 3.59 | 3.48 | 3.38 |
| | | | No Salt | 3.80 | 3.72 | 3.68 | 3.59 | 3.47 |
| | NorESM1-M | RCP4.5 | Salt | 4.16 | 4.08 | 4.03 | 3.94 | 3.86 |
| | | | No Salt | 4.18 | 4.12 | 4.09 | 4.03 | 3.92 |
| | | RCP8.5 | Salt | 3.97 | 3.86 | 3.78 | 3.66 | 3.56 |
| | | | No Salt | 3.99 | 3.91 | 3.87 | 3.77 | 3.65 |

Figure 4.6 shows the projected trends in alfalfa and corn yields by 2100 under salinity stress conditions, using five Global Climate Models (GCMs) under the RCP4.5 scenario, and irrigation practice scenario (2), which involves a 20% increase in irrigation efficiency and a 20% reduction in irrigation water loss relative to the baseline. The results for incremental increases and reductions of 5%, 10%, and 15% in irrigation efficiency and irrigation water loss under the RCP4.5 and RCP8.5 scenarios for both corn and alfalfa are presented in Appendix. As can be seen, for corn, all models predict a declining trend in corn yields throughout the study period, with more pronounced declines under salinity stress conditions. Despite the improvements in irrigation efficiency and reduced water loss, yields continue to decline, highlighting the severe impact of salinity stress on corn production. The CNRM-CM5 model shows the steepest decline in yields under salinity stress, and the MRI-CGCM3 model predicts relatively higher yields compared to other models, though the overall downward trend remains consistent. The enhancements in irrigation efficiency and reductions in water loss mitigate some yield losses but are insufficient to fully counteract the adverse effects of salinity stress. Yield gaps between salinity-stressed and non-stressed conditions widen over time, highlighting the increasing impact of salinity under future climate scenarios. Alfalfa yields decline over time under salinity stress conditions, though the rate of decline is less steep compared to corn. These yield reductions are more pronounced despite the 20% increase in irrigation efficiency and 20% reduction in irrigation water loss. The CNRM-CM5 model predicts more significant yield declines for alfalfa under salinity stress compared to other models. The NorESM1-M model shows relatively stable yields, indicating better resilience under projected climate conditions. Incremental increases in irrigation efficiency and reductions in water loss help reduce yield losses, although overall yields still decline under salinity stress. These improvements in irrigation efficiency and reduced water loss partially offset the negative impacts

of reduced water availability and salinity stress. The RCP4.5 scenario shows declining trends in yields for both corn and alfalfa, with more severe declines observed under salinity stress conditions.

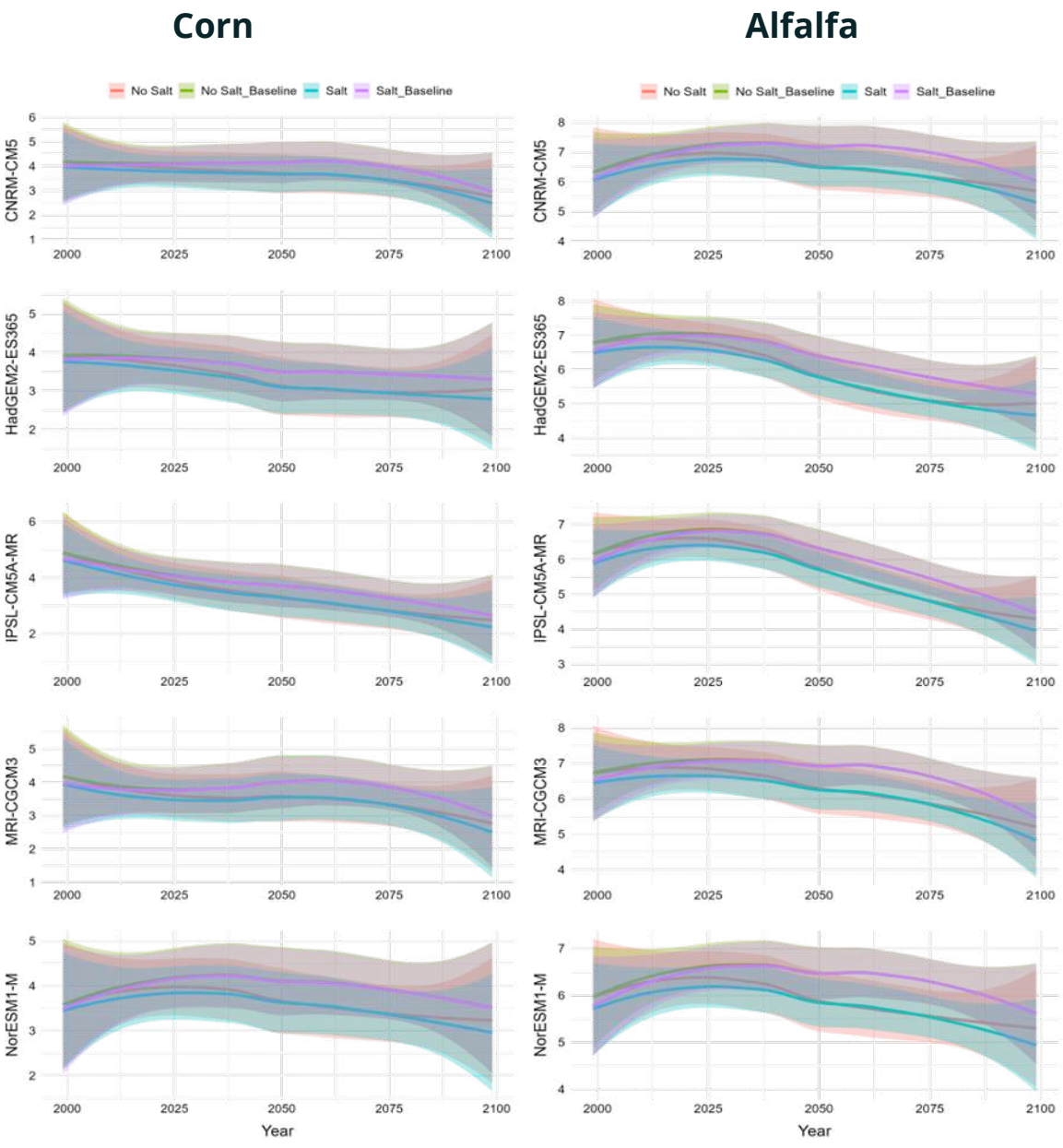


**Figure 4.6.** Plots above show corn and alfalfa yields, under the salinity stress, five GCM climate model, RCP4.5, and the irrigation practice scenario (2) with 20% increase in irrigation efficiency and 20% reduction in irrigation water loss relative to baseline by the year 2100.

The comparative analysis between the RCP4.5 and RCP8.5 scenarios demonstrate declining trends in yields for corn and alfalfa, with more severe declines observed under RCP8.5 indicating that future emission pathways significantly influence crop yield responses to salinity stress. Corn, being more sensitive to salinity stress, shows more pronounced yield declines compared to alfalfa. Under RCP8.5, yield disparities caused by salinity are more pronounced but can be somewhat mitigated by increased irrigation efficiency. The benefits of increased irrigation efficiency and reduced water loss are critical under both scenarios but are less effective under the more extreme conditions of RCP8.5. This underscores the potential of advanced irrigation strategies and integrated water management practices to counteract the compounded stresses of higher salinity and more extreme climate conditions projected in the future on agricultural productivity.

The variability in yield responses to salinity stress across different GCMs and RCPs highlights the importance of selecting and tailoring irrigation strategies based on specific crop sensitivities and projected climatic conditions. In terms of salinity control, scenario (1) proves to be more effective in maintaining lower salinity levels in the root zone. By keeping a constant irrigation water amount while improving efficiency and reducing runoff, this scenario ensures better management of salinity. The consistent water supply facilitates the leaching of salts deeper into the soil profile, thereby reducing salt stress on crops. In contrast, scenario (2), which involves reducing the total amount of irrigation water while enhancing efficiency and reducing runoff, results in higher salinity levels in the root zone. The reduced water volume is less effective in leaching salts, leading to greater salt accumulation and increased salinity stress on crops. Regarding the prevention of crop yield reductions, scenario (1) yields better outcomes. The constant water supply, combined with increased efficiency, helps sustain crop yields more effectively under salinity stress compared

to scenario (2). Although scenario (2) includes improvements in irrigation efficiency and reductions in runoff, the overall reduction in irrigation water exacerbates the negative impacts of salinity stress, leading to greater yield reductions. This comparative analysis highlights the critical importance of maintaining adequate irrigation water volumes alongside efficiency improvements to manage salinity and sustain crop yields. In conclusion, integrating efficient irrigation technologies and practices into salinity management strategies is essential for enhancing crop resilience. Adopting such measures is vital for maintaining agricultural productivity in regions facing increasing salinity pressures and changing climatic conditions.

### 4.3.2 Study Limitations

This study investigates the combined influence of salinity, climate changes, and various irrigation practices on crop production within a semi-arid agricultural watershed. Notably, several limitations and areas for future research are identified. Throughout the scenarios in this study, it was assumed that irrigation water was readily available without limitations and that the crops did not suffer from water stress due to deficit irrigation. We also assumed that the irrigation water depth remains constant across the various irrigation scenarios. Future research could explore the effects of implementing deficit irrigation under similar conditions. In assessing the mutual impact of climate change, salinity stress, and irrigation practices on crop production, this study made use of the CMIP5, focusing on climatic data from five commonly used GCM models and two RCP emission scenarios (RCP4.5 and RCP8.5). Future investigations could broaden their scope by including additional climate models, diverse climate and emission scenarios, changes in land use, and applying the model across various scales, from regional to more localized scale. Given that flood irrigation is the primary method employed in the study area, our scenarios were developed based on transitioning from this method, although future research might investigate the impacts of

more efficient irrigation techniques such as sprinkler and drip irrigation on crop production in fields affected by salinity. Additionally, while this study only considered dominant local crops, corn and alfalfa, subsequent studies might evaluate the effects on a wider range of crop types, including those more sensitive or more tolerant to salinity stress.

## 4.4. SUMMARY AND CONCLUSIONS

In this study, the newly developed SWAT-MODFLOW-Salt model was utilized to evaluate the combined impact of salinity, climate change, and irrigation management on the dynamics of salinity and the production of two primary crops, corn and alfalfa, in the Lower Arkansas River Valley (LARV), Colorado, USA, through the end of the century. Projected and downscaled climate data, covering temperature, precipitation, solar radiation, wind speed, and relative humidity, were obtained from the MACA dataset. This dataset included outputs from five GCM models, which were integrated into the calibrated and validated SWAT-MODFLOW-Salt model for the LARV. This integration was used to simulate future crop yields across the watershed under five climate models, two emission scenarios, and four irrigation scenarios. The findings from this extensive study underscore the critical importance of advanced irrigation management strategies in sustaining crop yields amid the dual challenges of salinity and climate change. The detailed analysis revealed that corn, a crop highly sensitive to salinity, can achieve yield improvements of up to 13.8% when irrigation efficiency is increased by 20% and irrigation water loss is decreased by 20% under less severe climate conditions (RCP4.5). Similarly, under non-salinity conditions, corn yields improved by 16.5%, highlighting the significant benefits of enhanced irrigation practices. Alfalfa, which demonstrates greater salinity tolerance, showed similar benefits with yield improvements. In the RCP4.5 scenario with salinity stress, alfalfa yields increased by 9.1% under the MRI-CGCM3 model with a 20% increase in irrigation efficiency, showcasing its strong

response to optimized water management. Under non-salinity conditions, this improvement was even more substantial, confirming alfalfa's resilience and efficiency under improved irrigation settings. These significant enhancements in crop yields highlight the effectiveness of tailored irrigation practices in mitigating the impact of environmental stresses.

The comparative analysis between the RCP4.5 and RCP8.5 scenarios indicates that while both scenarios benefit from increased irrigation efficiency, the benefits are more pronounced under the more extreme conditions of RCP8.5. This underscores the critical role of precision agriculture technologies that can dynamically adjust irrigation practices based on real-time soil and meteorological data. By optimizing water usage and mitigating salinity stress, these technologies not only enhance agricultural productivity but also conserve water resources in semi-arid regions such as the LARV, which face increasing threats from salinity and climatic variability. Moreover, considering long-term irrigation via sprinklers and the assumptions in this study regarding improved irrigation efficiency and reduced water loss through surface runoff compared to flood irrigation, overall crop yield exhibited an increase under climate change scenarios relative to flood irrigation. Flood irrigation, due to prolonged over-irrigation with saline water, can lead to waterlogging and elevated groundwater levels. This process facilitates the return flow of groundwater to the root zone, reintroducing salts into the root zone over time and adversely impacting crop yield.

In conclusion, this research elucidates the essential role of irrigation efficiency in addressing salinity and adapting to climate change, providing a robust foundation for policy and practice reforms in agricultural management. The insights gained are crucial for policymakers and stakeholders in developing strategies to enhance the sustainability and resilience of agricultural systems in semi-arid environments.

# REFERENCES


Abatzoglou, J.T., Brown, T.J., 2012. A comparison of statistical downscaling methods suited for wildfire applications. International Journal of Climatology 32, 772–780. https://doi.org/10.1002/joc.2312

Ahmadzadeh, H., Morid, S., Delavar, M., Srinivasan, R., 2016. Using the SWAT model to assess the impacts of changing irrigation from surface to pressurized systems on water productivity and water saving in the Zarrineh Rud catchment. Agricultural Water Management 175, 15–28. https://doi.org/10.1016/j.agwat.2015.10.026

Aliyari, F., Bailey, R.T., Tasdighi, A., Dozier, A., Arabi, M., Zeiler, K., 2019. Coupled SWAT-MODFLOW model for large-scale mixed agro-urban river basins. Environmental Modelling and Software 115, 200–210. https://doi.org/10.1016/J.ENVSOFT.2019.02.014

Arbat, G., Masseroni, D., 2024. The Use and Management of Agricultural Irrigation Systems and Technologies. Agriculture 14, 236. https://doi.org/10.3390/agriculture14020236

Arnold, J.G., Srinivasan, R., Muttiah, R.S., Williams, J.R., 1998. LARGE AREA HYDROLOGIC MODELING AND ASSESSMENT PART I: MODEL DEVELOPMENT1. JAWRA Journal of the American Water Resources Association 34, 73–89. https://doi.org/10.1111/J.1752-1688.1998.TB05961.X

Bailey, R.T., Hosseini, P., 2023. Comprehensive simulation of salinity transport in irrigated watersheds using an updated version of SWAT-MODFLOW. Environmental Modelling & Software 159, 105566. https://doi.org/10.1016/J.ENVSOFT.2022.105566

Bailey, R.T., Tavakoli-Kivi, S., Wei, X., 2019. A salinity module for SWAT to simulate salt ion fate and transport at the watershed scale. Hydrology and Earth System Sciences 23, 3155–3174. https://doi.org/10.5194/HESS-23-3155-2019

Bailey, R.T., Wible, T.C., Arabi, M., Records, R.M., Ditty, J., 2016. Assessing regional-scale spatio-temporal patterns of groundwater–surface water interactions using a coupled SWAT-MODFLOW model. Hydrological Processes 30, 4420–4433. https://doi.org/10.1002/HYP.10933

Burkhalter, J.P., Asce, M., Gates, T.K., 2005. Agroecological Impacts from Salinization and Waterlogging in an Irrigated River Valley. Journal of Irrigation and Drainage Engineering 131, 197–209. https://doi.org/10.1061/(ASCE)0733-9437(2005)131:2(197)

Eckhoff, J.L.A., Bergman, J.W., Flynn, C.R., 2005. Sprinkler and Flood Irrigation Effects on Sugarbeet Yield and Quality. JSBR 42, 19–30. https://doi.org/10.5274/jsbr.42.1.19

Gates, T.K., Asce, M., Burkhalter, ; J Philip, Labadie, J.W., Valliant, J.C., Broner, I., 2002. Monitoring and Modeling Flow and Salt Transport in a Salinity-Threatened Irrigated Valley. Journal of Irrigation and Drainage Engineering 128, 87–99. https://doi.org/10.1061/(ASCE)0733-9437(2002)128:2(87)

Gates, T.K., Cody, B.M., Donnelly, J.P., Herting Kimley-Horn, A.W., Ryan Bailey, A.T., Mueller Price, J., 2009. Assessing Selenium Contamination in the Irrigated Stream–Aquifer System of the Arkansas River, Colorado. Journal of Environmental Quality 38, 2344–2356. https://doi.org/10.2134/JEQ2008.0499

Gates, T.K., Steed, G.H., Niemann, J.D., Labadie, J.W., 2016. Data for Improved Water Management in Colorado's Arkansas River Basin Hydrological and Water Quality Studies.

Haj-Amor, Z., Bouri, S., 2020. Use of HYDRUS-1D–GIS tool for evaluating effects of climate changes on soil salinization and irrigation management. Archives of Agronomy and Soil Science 66, 193–207. https://doi.org/10.1080/03650340.2019.1608438

Heidari, H., Arabi, M., Warziniack, T., Kao, S.-C., 2020. Assessing Shifts in Regional Hydroclimatic Conditions of U.S. River Basins in Response to Climate Change over the 21st Century. Earth's Future 8, e2020EF001657. https://doi.org/10.1029/2020EF001657

Holmberg, M.J., 2017. Hydrogeologic characteristics and geospatial analysis of water-table changes in the alluvium of the lower Arkansas River Valley, southeastern Colorado, 2002, 2008, and 2015. Scientific Investigations Map. https://doi.org/10.3133/SIM3378

Hosseini, P., Bailey, R.T., 2022. Investigating the controlling factors on salinity in soil, groundwater, and river water in a semi-arid agricultural watershed using SWAT-Salt. Science of the Total Environment 810. https://doi.org/10.1016/j.scitotenv.2021.152293

Joyce, L.A., Coulson, D., 2020. Climate scenarios and projections: A technical document supporting the USDA Forest Service 2020 RPA Assessment (No. RMRS-GTR-413). U.S. Department of Agriculture, Forest Service, Rocky Mountain Research Station, Fort Collins, CO. https://doi.org/10.2737/RMRS-GTR-413

Machado, R.M.A., Serralheiro, R.P., 2017. Soil salinity: Effect on vegetable crop growth. Management practices to prevent and mitigate soil salinization. Horticulturae 3. https://doi.org/10.3390/horticulturae3020030

Masson-Delmotte, V., Zhai, P., Pirani, A., Connors, S.L., Péan, C., Berger, S., Caud, N., Chen, Y., Goldfarb, L., Gomis, M.I., Huang, M., Leitzell, K., Lonnoy, E., Matthews, J.B.R., Maycock, T.K., Waterfield, T., Yelekçi, Ö., Yu, R., Zhou, B. (Eds.), 2021. Climate Change 2021: The Physical Science Basis. Contribution of Working Group I to the Sixth Assessment Report of the Intergovernmental Panel on Climate Change. Cambridge University Press, Cambridge, United Kingdom and New York, NY, USA. https://doi.org/10.1017/9781009157896

Morway, E.D., Gates, T.K., 2012. Regional Assessment of Soil Water Salinity across an Intensively Irrigated River Valley. Journal of Irrigation and Drainage Engineering 138, 393–405. https://doi.org/10.1061/(asce)ir.1943-4774.0000411

Morway, E.D., Gates, T.K., Niswonger, R.G., 2013. Appraising options to reduce shallow groundwater tables and enhance flow conditions over regional scales in an irrigated alluvial aquifer system. Journal of Hydrology 495, 216–237. https://doi.org/10.1016/J.JHYDROL.2013.04.047

Mukhopadhyay, R., Sarkar, B., Jat, H.S., Sharma, P.C., Bolan, N.S., 2021. Soil salinity under climate change: Challenges for sustainable agriculture and food security. Journal of Environmental Management 280, 111736. https://doi.org/10.1016/J.JENVMAN.2020.111736

Munns, R., Tester, M., 2008. Mechanisms of Salinity Tolerance. Annual Review of Plant Biology 59, 651–681. https://doi.org/10.1146/annurev.arplant.59.032607.092911

Niswonger, R., Panday, S., Survey, M.I.-U.G., 2011, undefined, 2011. MODFLOW-NWT, a Newton formulation for MODFLOW-2005. pubs.usgs.gov.

Shiru, M.S., Hyuck Kim, J., Chung, E.-S., 2022. Water Resources and Hydrologic Engineering Variations in Projections of Precipitations of CMIP6 Global Climate Models under SSP 2-45 and SSP 5-85. KSCE Journal of Civil Engineering 26, 5404–5416. https://doi.org/10.1007/s12205-022-0149-7

Song, Y.H., Chung, E.S., Shahid, S., 2022. Differences in extremes and uncertainties in future runoff simulations using SWAT and LSTM for SSP scenarios. Science of The Total Environment 838, 156162. https://doi.org/10.1016/J.SCITOTENV.2022.156162

Tavakoli-Kivi, S., Bailey, R.T., Gates, T.K., 2019. A salinity reactive transport and equilibrium chemistry model for regional-scale agricultural groundwater systems. Journal of Hydrology 572, 274–293. https://doi.org/10.1016/j.jhydrol.2019.02.040

Wei, X., Bailey, R.T., 2019. Assessment of system responses in intensively irrigated stream-aquifer systems using SWAT-MODFLOW. Water (Switzerland) 11. https://doi.org/10.3390/W11081576

Wei, X., Bailey, R.T., Tasdighi, A., 2018. Using the SWAT Model in Intensively Managed Irrigated Watersheds: Model Modification and Application. Journal of Hydrologic Engineering 23. https://doi.org/10.1061/(asce)he.1943-5584.0001696

Wu, D., Cui, Y., Luo, Y., 2019. Irrigation efficiency and water-saving potential considering reuse of return flow. Agricultural Water Management 221, 519–527. https://doi.org/10.1016/j.agwat.2019.05.021

# Chapter 5. SUMMARY AND CONCLUSION

## 5.1. SUMMARY

In this study, Morris and Sobol's sensitivity analysis (SA) methods were used to investigate controlling factors on salt ion fate and transport in soil water, groundwater, and stream water of an irrigated stream-aquifer system located in the Lower Arkansas River Valley, Colorado, USA using the SWAT-Salt model.

The recently developed SWAT-MODFLOW-Salt model was employed to assess the impact of salinity on green, blue, and total WFs of crop production. The model was also utilized to quantify the combined effects of salinity and climate change on crop production WFs in the Lower Arkansas River Valley (LARV), CO, USA by the end of century. Projected and downscaled climate data encompassing temperature, precipitation, solar radiation, wind speed, and relative humidity were derived from MACA dataset including five GCM models input into the calibrated and validated SWAT-MODFLOW-Salt model for the LARV to simulate future crop yields and crop production WFs within the watershed.

Lastly, the newly developed SWAT-MODFLOW-Salt model was utilized to evaluate the combined impact of salinity, climate change, and irrigation management on the dynamics of salinity and the production of two primary crops, corn and alfalfa, in the Lower Arkansas River Valley (LARV), Colorado, USA, through the end of the century. Projected and downscaled climate data, covering temperature, precipitation, solar radiation, wind speed, and relative humidity, were obtained from the MACA dataset. This dataset included outputs from five GCM models, which were integrated into the calibrated and validated SWAT-MODFLOW-Salt model for the LARV. This integration was used to simulate future crop yields across the watershed under five climate models, two emission scenarios, and four irrigation scenarios.

## 5.2. MAJOR FINDINGS

The major findings of this dissertation are summarized below:

To determine the most influential system parameters on soil salinity, groundwater salinity, and streamwater salinity in a semi-arid irrigated watershed system, global sensitivity analysis was applied to the newly developed SWAT-Salt watershed model for the Lower Arkansas river Valley (LARV), CO, USA, which simulates the fate and transport of 8 major salt ions ($SO_4$, Ca, Mg, Na, K, Cl, $CO_3$, and $HCO_3$) in soils, aquifers, and streams subject to equilibrium chemistry reactions of precipitation-dissolution, complexation, and cation exchange.

i) Salt ion concentration in soils and groundwater are controlled principally by hydrologic factors (evaporation, groundwater discharge and upflux, and surface runoff factors) and the initial amounts of salt minerals in soils.

ii) Salt concentration in the Arkansas River is governed by similar factors, likely due to salt ion mass in the streams controlled by surface runoff and groundwater discharge from the aquifer.

iii) Results can be used in decision making regarding the most impactful land and water management strategies for controlling salinity transport and build-up in soils, both for this watershed and other semi-arid salinity-impacted watersheds.

To investigate the long-term influence of salinity and climate change on crop production from 1999 to 2100 in irrigated semi-arid regions, we apply the water footprint (WF) concept using the hydro-chemical watershed model SWAT-MODFLOW-Salt, driven by five General Circulation Models (GCMs) and two climate scenarios (RCP4.5 and RCP8.5), to a 732 $km^2$ irrigated stream-aquifer system within the Lower Arkansas River Valley (LARV), Colorado, USA, focusing on

calculating the green ($WF_{green}$), blue ($WF_{blue}$), and total ($WF_{total}$) crop production WFs for 29 crops in the region, with and without including salinity effect on crop yield.

i) Under the salinity stress and during the baseline period (1999-2009), the total annual average $WF_{green}$, $WF_{blue}$, and $WF_{total}$ increased by 7.6%, 4.4%, and 6.5%, respectively.

ii) Under the salinity stress and during the baseline period (1999-2009), crops experienced reductions of up to 4.6%, 1.6%, and 2.3% in green, blue, and total crop yield.

iii) The mutual impact of salinity and the worst-case climate model (IPSL_CM5A_MR) under the higher emission scenario (RCP8.5) led to a 3.3%, 1.9%, and 3% increase in green, blue, and total crop production WFs.

iv) Among the primary crops in the area, the annual average crop yield for alfalfa decreased by 3.8%, leading to an 8.3% increase in the total WF.

v) The annual average crop yield for corn decreased by 4.9%, resulting in a 10.9% rise in the total WF.

vi) The findings of this study offer valuable insights into the implementation of effective management practices for reclaiming salt-affected soils in the agricultural sector.

Finally, this dissertation explores the interaction between salinity, climate change, and irrigation management on crop yields within the Lower Arkansas River Valley (LARV), focusing on corn and alfalfa. Utilizing the SWAT-MODFLOW-Salt model, this research evaluates how incremental increases and reductions in irrigation efficiency and irrigation water loss (5%, 10%, 15%, and

20%), considering two distinct irrigation scenarios under conditions of salinity stress influence crop production under various scenarios projected through 2100.

i) Under irrigation scenario (1), increasing irrigation efficiency and reducing irrigation water loss by 20% under RCP4.5 can boost corn yields by up to 16.5% and alfalfa yields by up to 10.0%.

ii) Under the RCP4.5 scenario with salinity stress, alfalfa yields increased by 9.1% under the MRI-CGCM3 model with a 20% increase in irrigation efficiency and 20% reduction in irrigation water loss.

iii) Corn can achieve yield improvements of up to 13.8% when irrigation efficiency and irrigation water loss increased and decreased by 20%, respectively, under less severe climate conditions (RCP4.5).

iv) Under irrigation scenario (2) and the more severe emission scenario of RCP8.5, corn yield reductions ranged from -9.8% under salinity stress with a 20% increase and reduction in irrigation efficiency and water loss via surface runoff to -9.3% under non-salinity conditions.

v) Yield reductions for alfalfa under RCP8.5 and salinity stress ranged from -8.9% with a 20% increase and decline in irrigation efficiency and surface runoff loss to -8.3% under non-salinity conditions.

vi) Provides valuable insights for policymakers and agricultural managers on strategic water resource management to sustain crop yields in salinity-affected and water-limited agricultural systems.

## 5.3. FUTURE RESEARCH

This study investigated the influence of salinity and climate changes on crop production WFs within a semi-arid agricultural watershed. Certain limitations and recommendations for future research are noteworthy. The calculation of the total WF exclusively considered green and blue WFs, while the grey WF of crop production in the region was assumed to be zero. Future studies could benefit from estimating and including the grey WF in total WF calculations in various regions. In assessing the impact of climate change on salinity fate and transport, and crop production WFs, this study utilized the CMIP5, focusing on climatic outputs from five widely used GCM models and two RCP emission scenarios (RCP4.5 and RCP8.5). Hence, future research could enhance its scope by incorporating additional climate models, diverse climate scenarios, emission scenarios, land-use change scenarios, and employing the model at different scales, including regional or smaller scales. Furthermore, the combined influence of salinity, climate changes, and various irrigation practices on crop production within a semi-arid agricultural watershed were evaluated in this research. Notably, several limitations and areas for future research are identified. Throughout the scenarios in this study, it was assumed that irrigation water was readily available without limitations and that the crops did not suffer from water stress due to deficit irrigation. Future research could explore the effects of implementing deficit irrigation under similar conditions. In assessing the mutual impact of climate change and irrigation practices on salinity fate and transport, and crop production, this study made use of the CMIP5, focusing on climatic data from five commonly used GCM models and two RCP emission scenarios (RCP4.5 and RCP8.5). Future investigations could broaden their scope by including additional climate models, diverse climate and emission scenarios, changes in land use, and applying the model across various scales, from regional to more localized scale. Given that flood irrigation is the primary method employed in the study area, our scenarios were developed based on transitioning

from this method, although future research might investigate the impacts of more efficient irrigation techniques such as sprinkler and drip irrigation on crop production in fields affected by salinity. Additionally, while this study only considered dominant local crops, corn and alfalfa, subsequent studies might evaluate the effects on a wider range of crop types, including those more sensitive or more tolerant to salinity stress.

# Appendix

## **A.1** Area plots of green, blue, and total crop yields and water footprints of alfalfa and corn under the mutual impact of salinity and various climate change scenarios

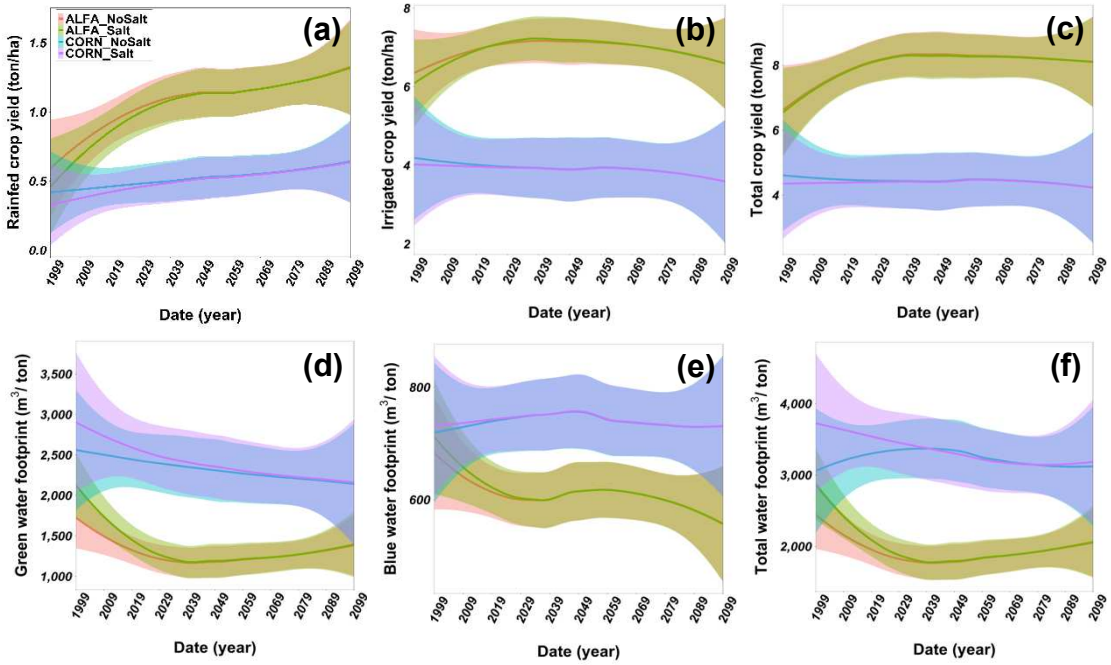


**Figure A.1.1** Area plots above show (a) green crop yield, (b) blue crop yield, (c) total crop yield, (d) green water footprint, (e) blue water footprint, and (f) total water footprint of alfalfa and corn as major crops in the LARV under the mutual impact of CNRM-CM5-4.5 climate model and salinity stress by 2100.

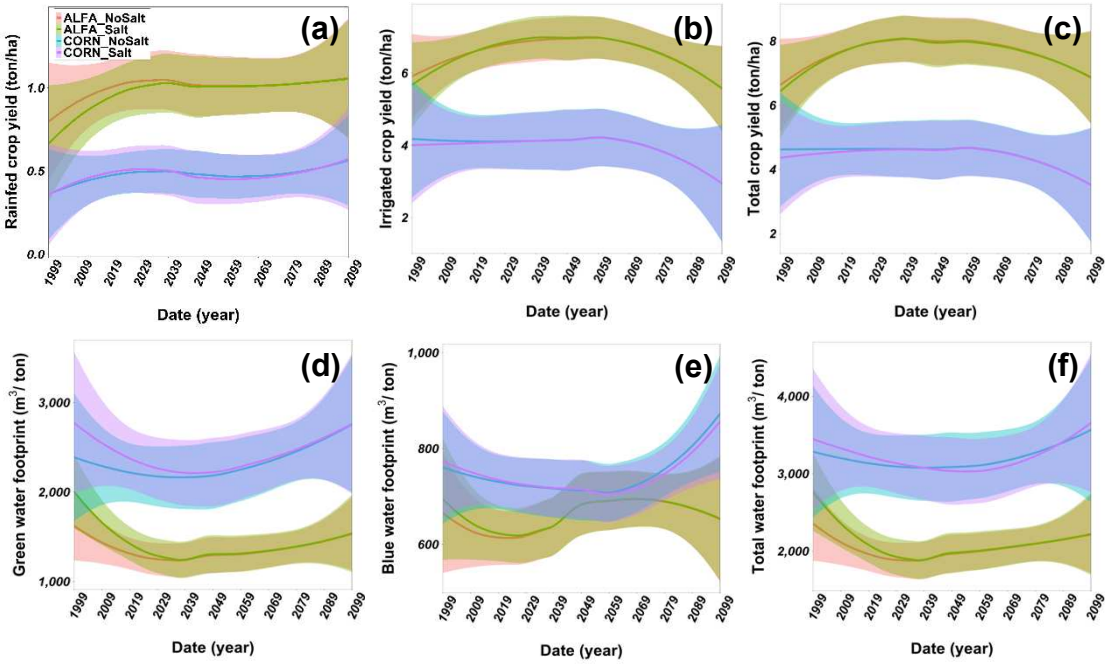


**Figure A.1.2.** Area plots above show (a) green crop yield, (b) blue crop yield, (c) total crop yield, (d) green water footprint, (e) blue water footprint, and (f) total water footprint of alfalfa and corn as major crops in the LARV under the mutual impact of CNRM-CM5-8.5 climate model and salinity stress by 2100.

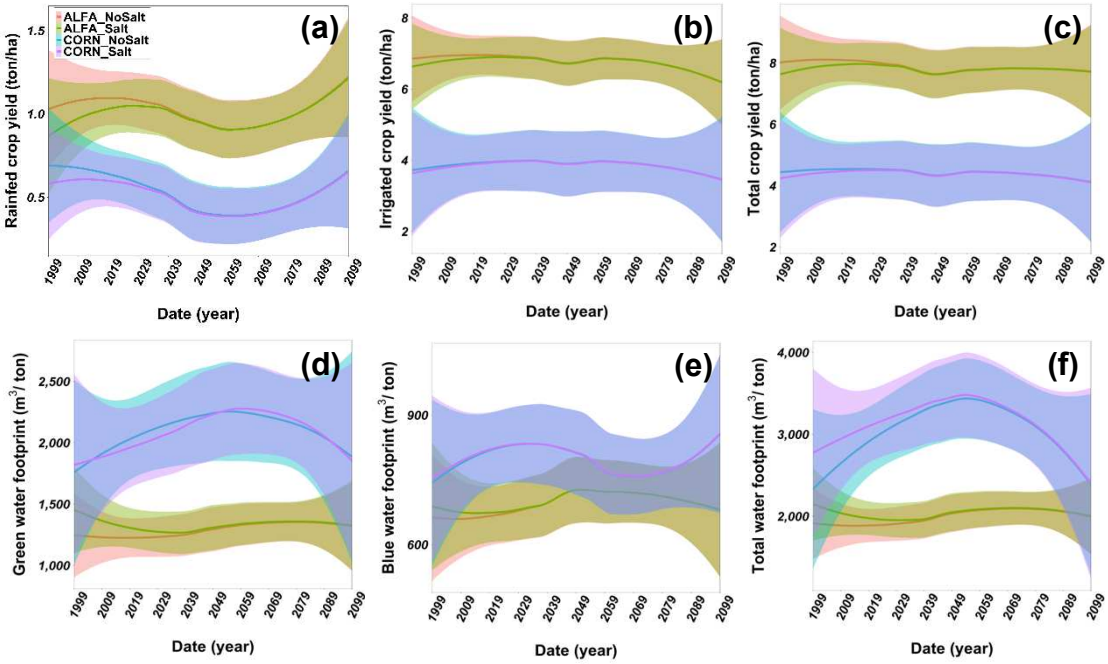


**Figure A.1.3.** Area plots above show (a) green crop yield, (b) blue crop yield, (c) total crop yield, (d) green water footprint, (e) blue water footprint, and (f) total water footprint of alfalfa and corn as major crops in the LARV under the mutual impact of HadGEM2-ES365-4.5 climate model and salinity stress by 2100.

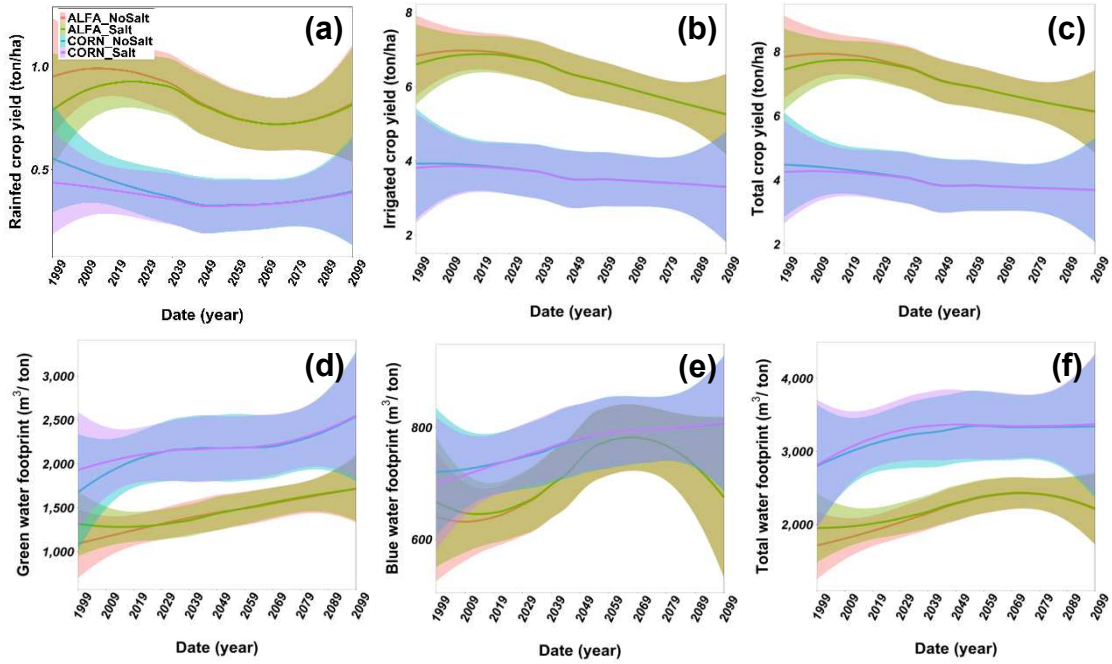


**Figure A.1.4.** Area plots above show (a) green crop yield, (b) blue crop yield, (c) total crop yield, (d) green water footprint, (e) blue water footprint, and (f) total water footprint of alfalfa and corn as major crops in the LARV under the mutual impact of HadGEM2-ES365-8.5 climate model and salinity stress by 2100.

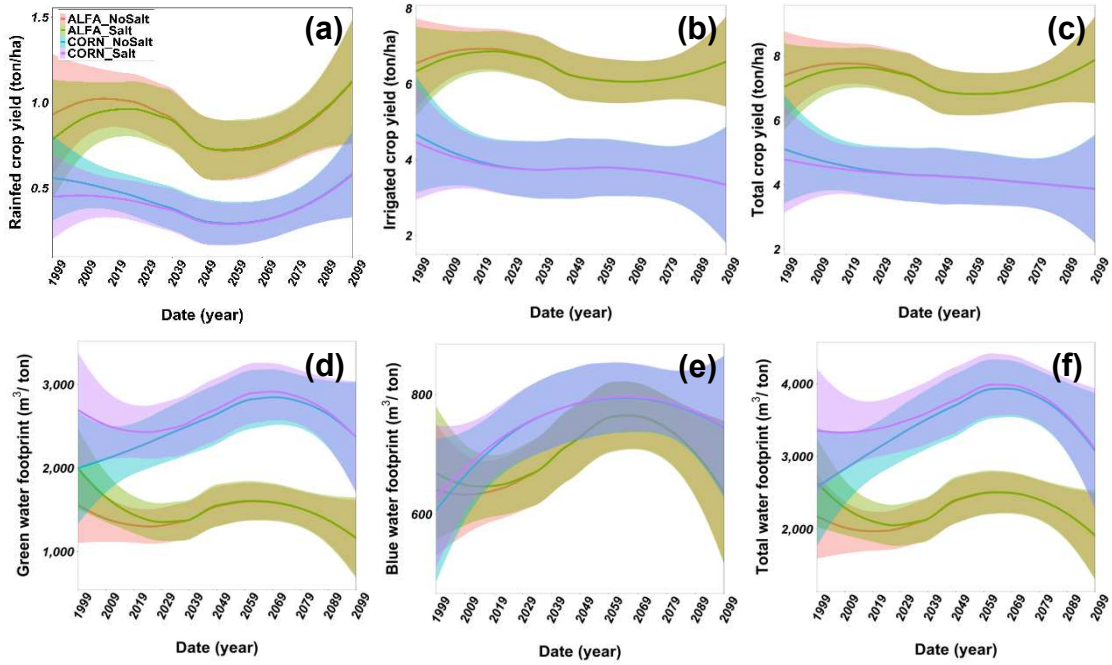


**Figure A.1.5.** Area plots above show (a) green crop yield, (b) blue crop yield, (c) total crop yield, (d) green water footprint, (e) blue water footprint, and (f) total water footprint of alfalfa and corn as major crops in the LARV under the mutual impact of IPSL-CM5A-MR-4.5 climate model and salinity stress by 2100.

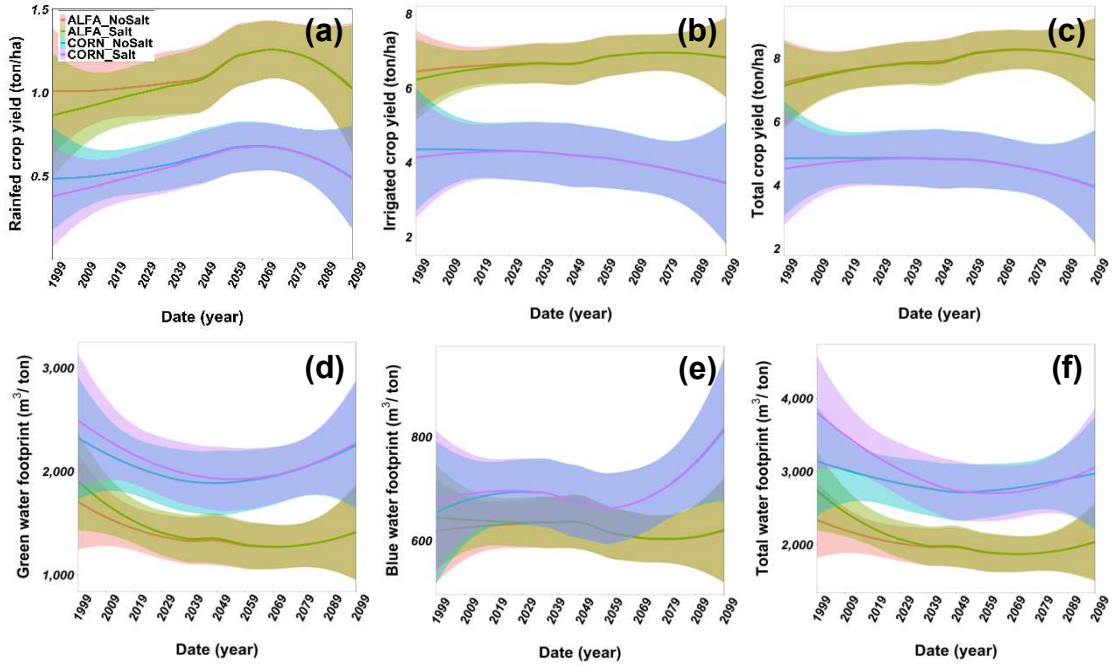


**Figure A.1.6.** Area plots above show (a) green crop yield, (b) blue crop yield, (c) total crop yield, (d) green water footprint, (e) blue water footprint, and (f) total water footprint of alfalfa and corn as major crops in the LARV under the mutual impact of MRI-CGCM3-4.5 climate model and salinity stress by 2100.

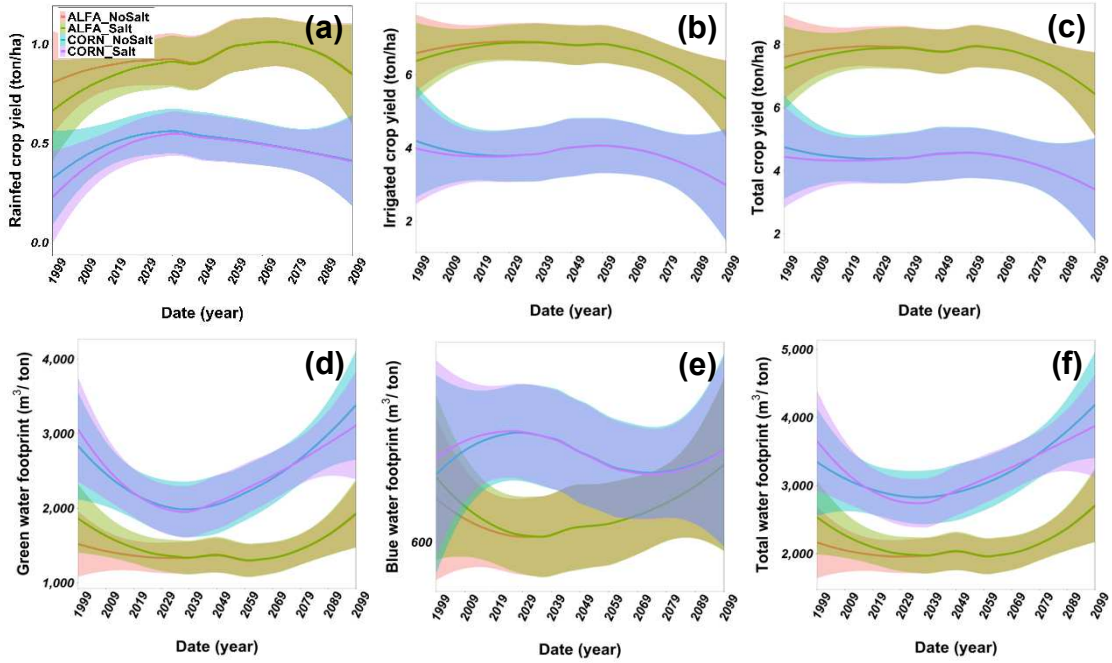


**Figure A.1.7.** Area plots above show (a) green crop yield, (b) blue crop yield, (c) total crop yield, (d) green water footprint, (e) blue water footprint, and (f) total water footprint of alfalfa and corn as major crops in the LARV under the mutual impact of MRI-CGCM3-8.5 climate model and salinity stress by 2100.

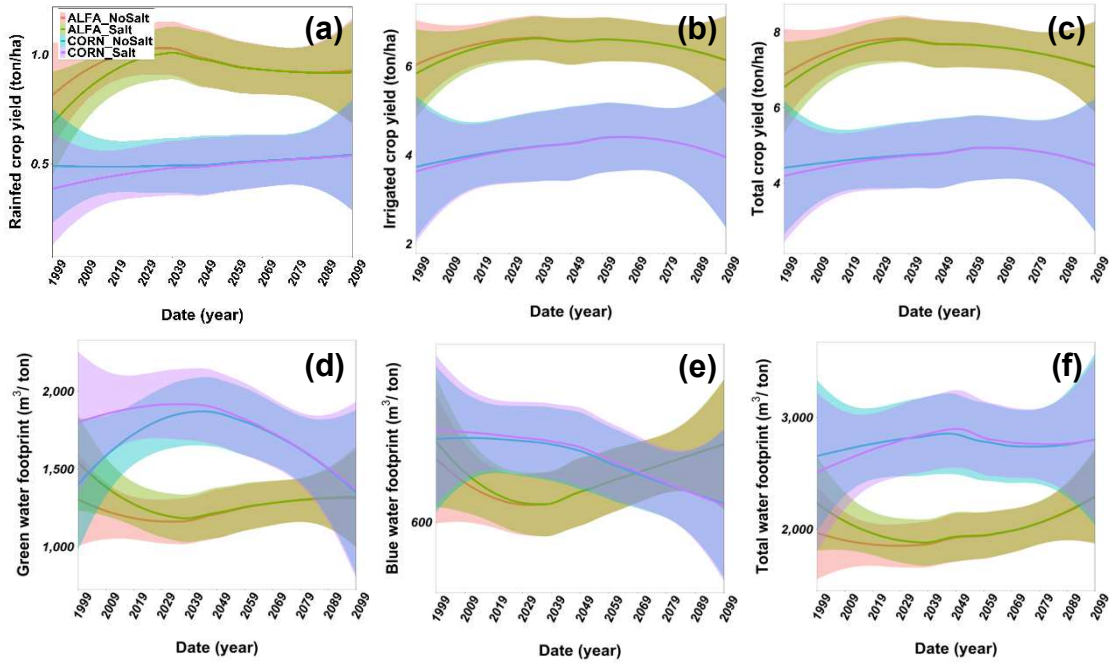


**Figure A.1.8.** Area plots above show (a) green crop yield, (b) blue crop yield, (c) total crop yield, (d) green water footprint, (e) blue water footprint, and (f) total water footprint of alfalfa and corn as major crops in the LARV under the mutual impact of NorESM1-M-4.5 climate model and salinity stress by 2100.

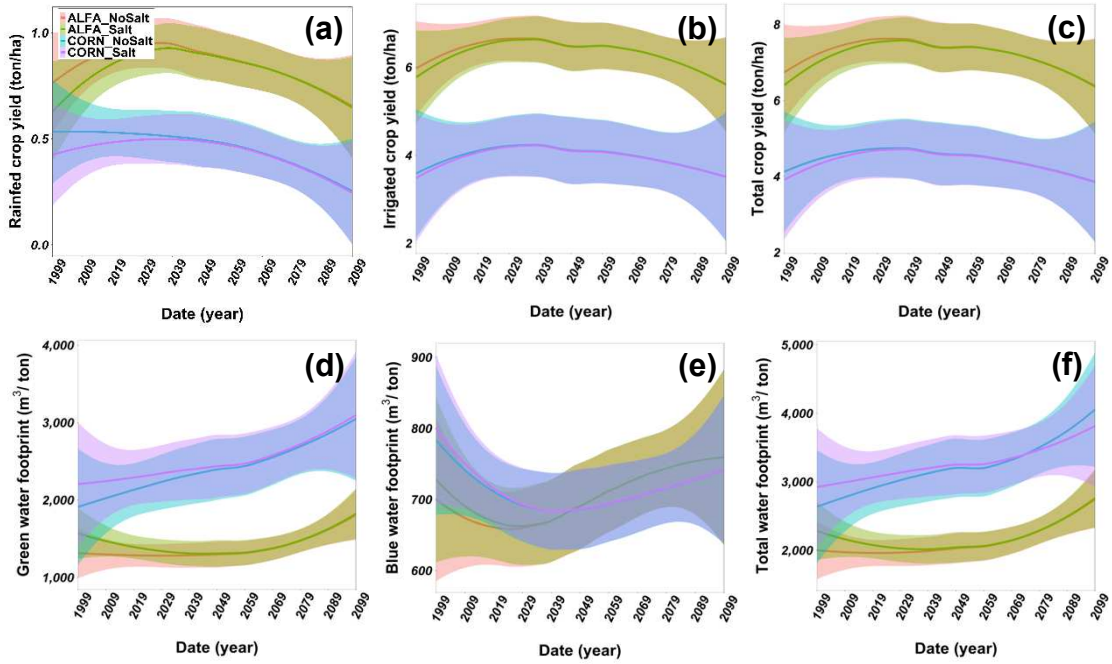


**Figure A.1.9.** Area plots above show (a) green crop yield, (b) blue crop yield, (c) total crop yield, (d) green water footprint, (e) blue water footprint, and (f) total water footprint of alfalfa and corn as major crops in the LARV under the mutual impact of NorESM1-M-8.5 climate model and salinity stress by 2100.

**A.2.** Average percentage changes in green, blue, and total crop yields and water footprints of 29 crops under the mutual impact of salinity and various climate change scenarios.

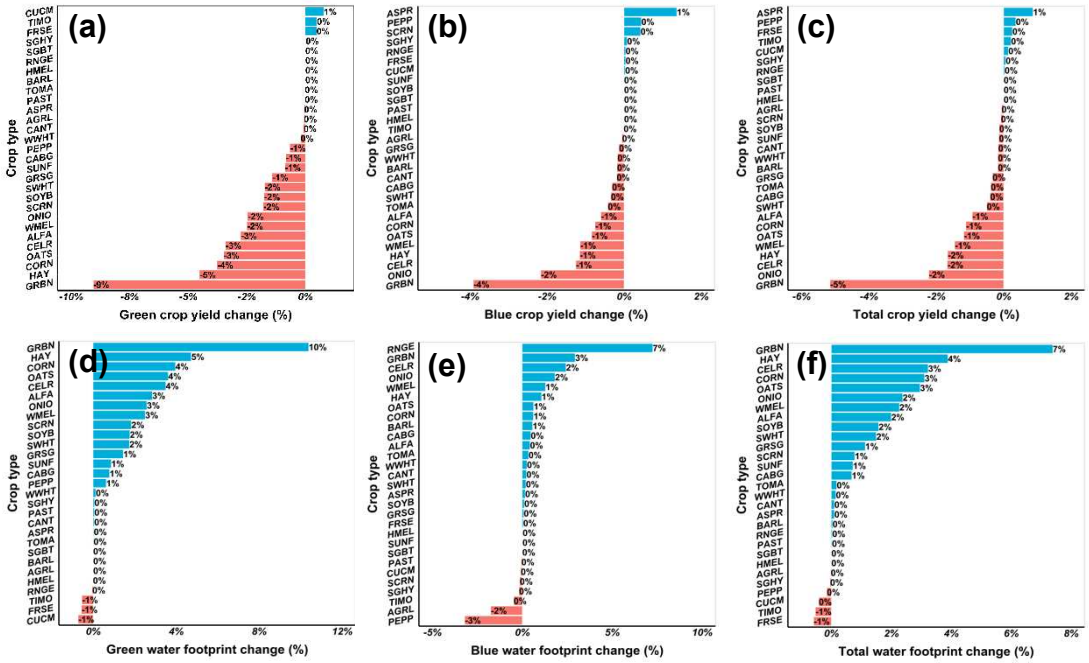


**Figure A.2.1.** Average percentage changes in (a) green crop yield, (b) blue crop yield, (c) total crop yield, (d) green water footprint, (e) blue water footprint, and (f) total water footprint of 29 crops in the LARV considering CNRM-CM5-4.5 climate model and salinity stress by 2100.

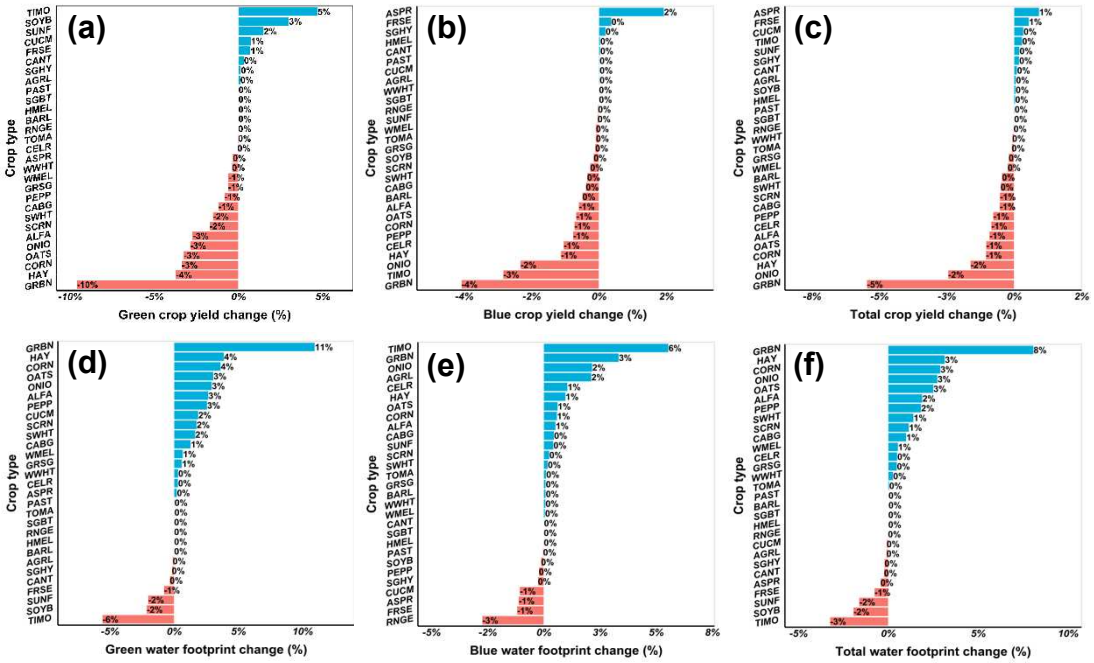


**Figure A.2.2.** Average percentage changes in (a) green crop yield, (b) blue crop yield, (c) total crop yield, (d) green water footprint, (e) blue water footprint, and (f) total water footprint of 29 crops in the LARV considering CNRM-CM5-8.5 climate model and salinity stress by 2100.

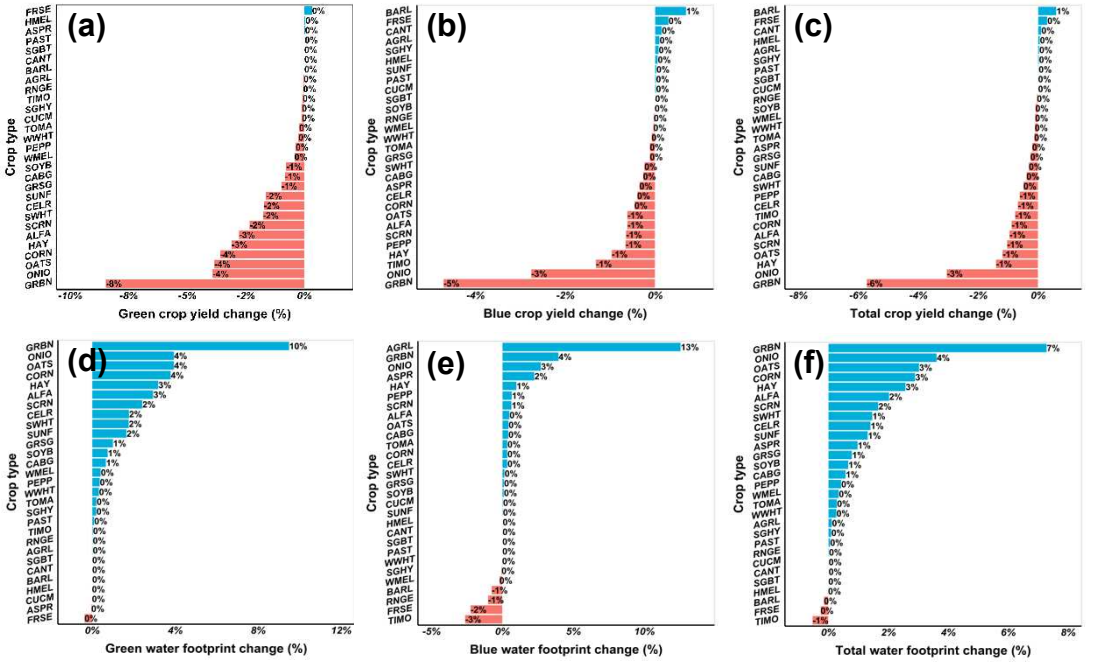


**Figure A.2.3.** Average percentage changes in (a) green crop yield, (b) blue crop yield, (c) total crop yield, (d) green water footprint, (e) blue water footprint, and (f) total water footprint of 29 crops in the LARV considering HadGEM2-ES365-4.5 climate model and salinity stress by 2100.

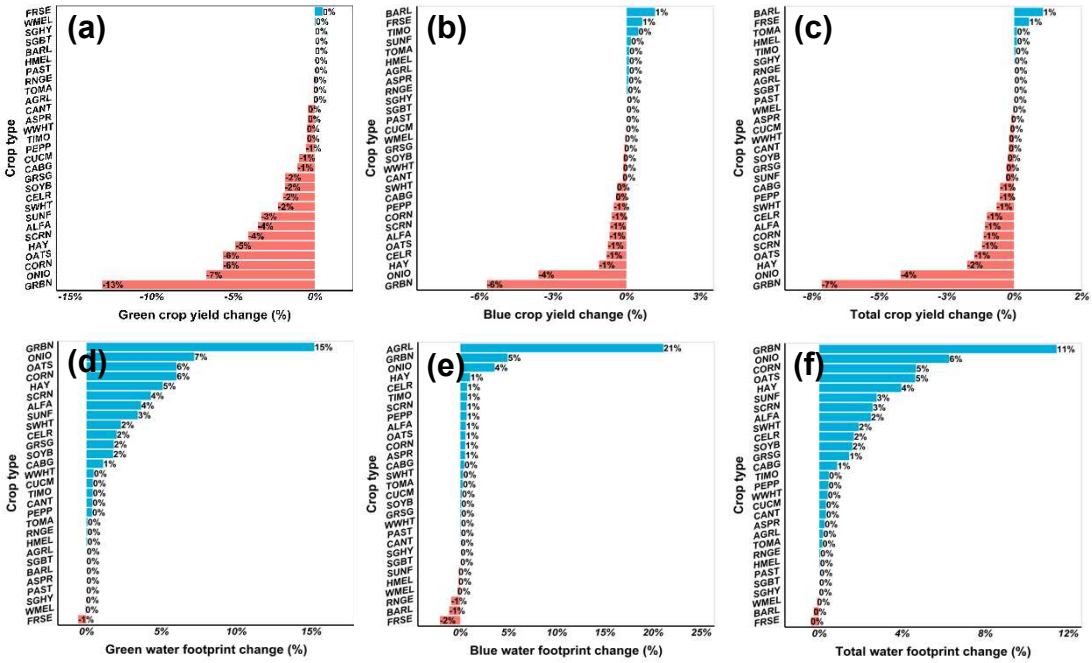


**Figure A.2.4.** Average percentage changes in (a) green crop yield, (b) blue crop yield, (c) total crop yield, (d) green water footprint, (e) blue water footprint, and (f) total water footprint of 29 crops in the LARV considering HadGEM2-ES365-8.5 climate model and salinity stress by 2100.

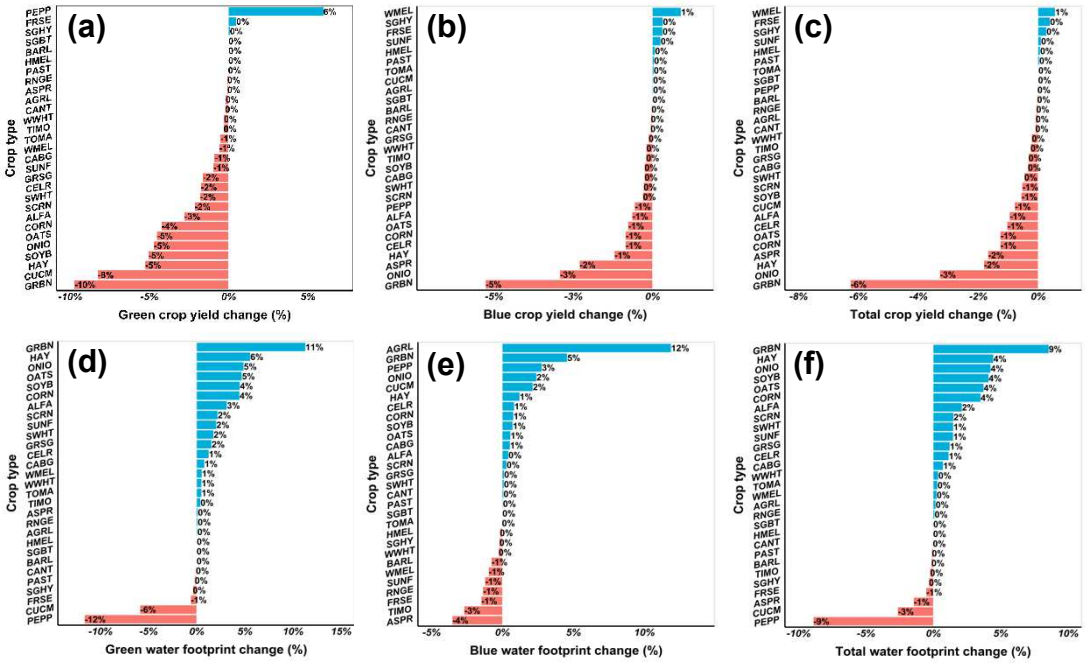


**Figure A.2.5.** Average percentage changes in (a) green crop yield, (b) blue crop yield, (c) total crop yield, (d) green water footprint, (e) blue water footprint, and (f) total water footprint of 29 crops in the LARV considering IPSL-CM5A-MR-4.5 climate model and salinity stress by 2100.

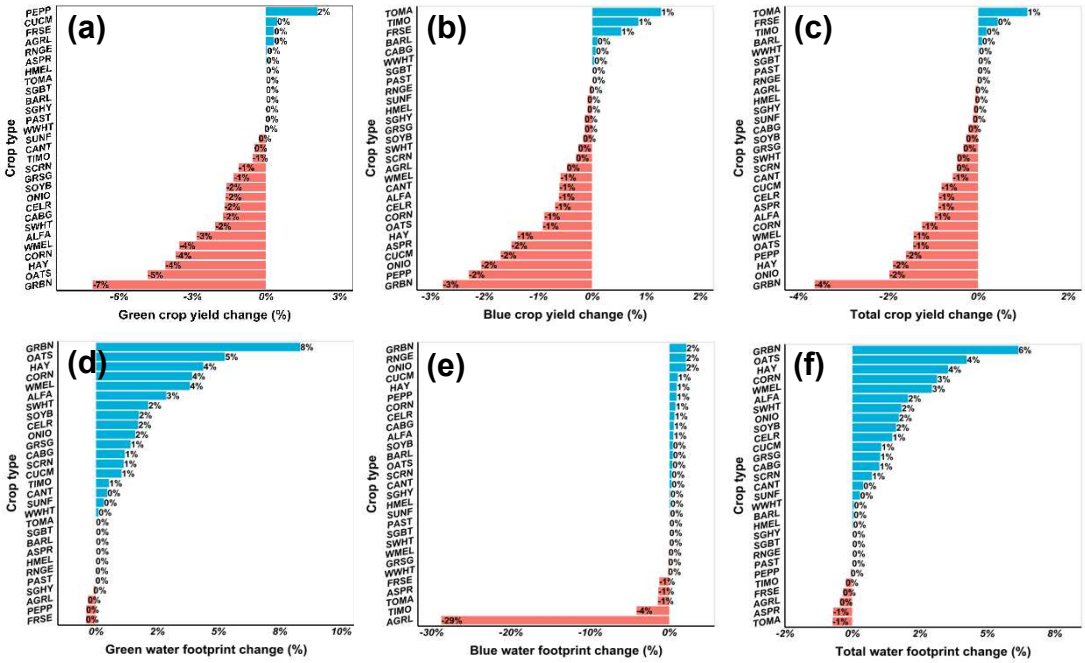


**Figure A.2.6.** Average percentage changes in (a) green crop yield, (b) blue crop yield, (c) total crop yield, (d) green water footprint, (e) blue water footprint, and (f) total water footprint of 29 crops in the LARV considering MRI-CGCM3-4.5 climate model and salinity stress by 2100.

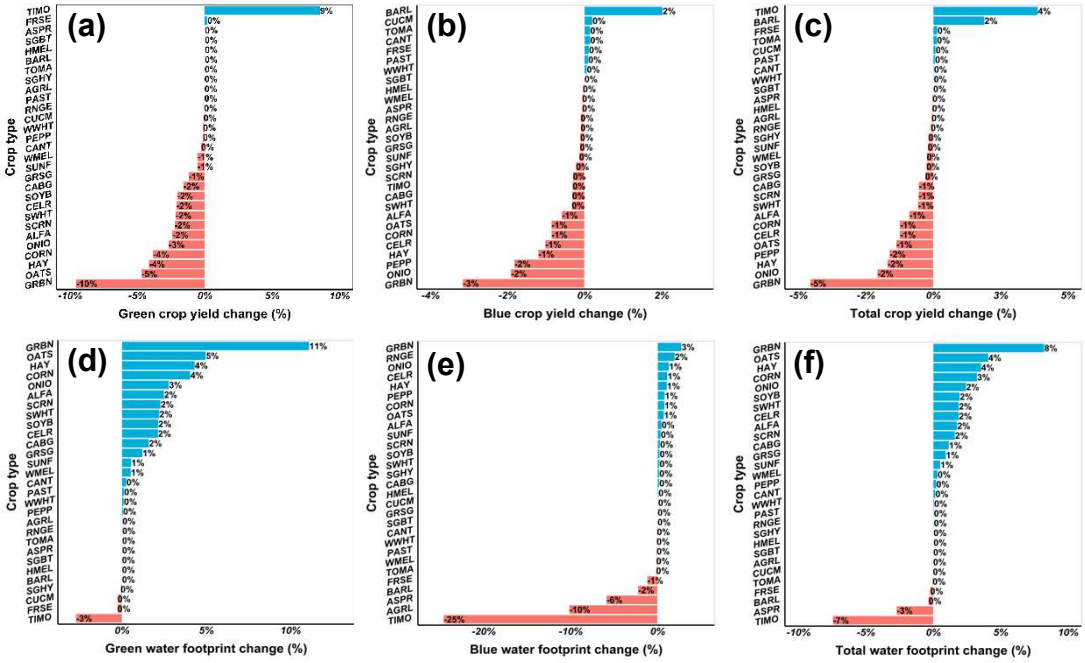


**Figure A.2.7.** Average percentage changes in (a) green crop yield, (b) blue crop yield, (c) total crop yield, (d) green water footprint, (e) blue water footprint, and (f) total water footprint of 29 crops in the LARV considering MRI-CGCM3-8.5 climate model and salinity stress by 2100.

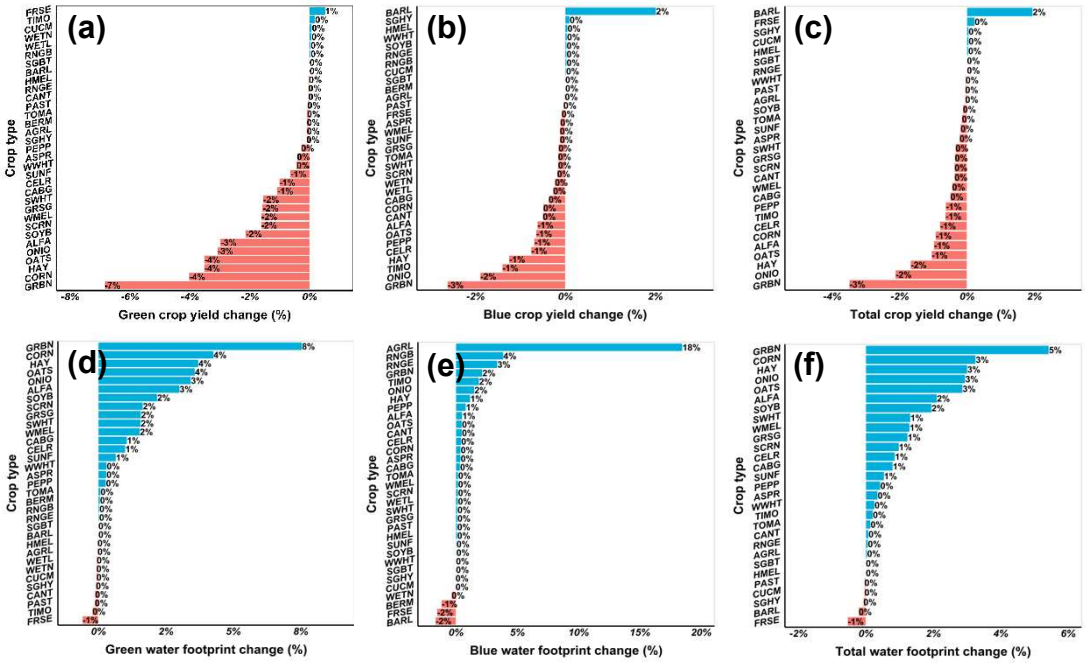


**Figure A.2.8.** Average percentage changes in (a) green crop yield, (b) blue crop yield, (c) total crop yield, (d) green water footprint, (e) blue water footprint, and (f) total water footprint of 29 crops in the LARV considering NorESM1-M-4.5 climate model and salinity stress by 2100.

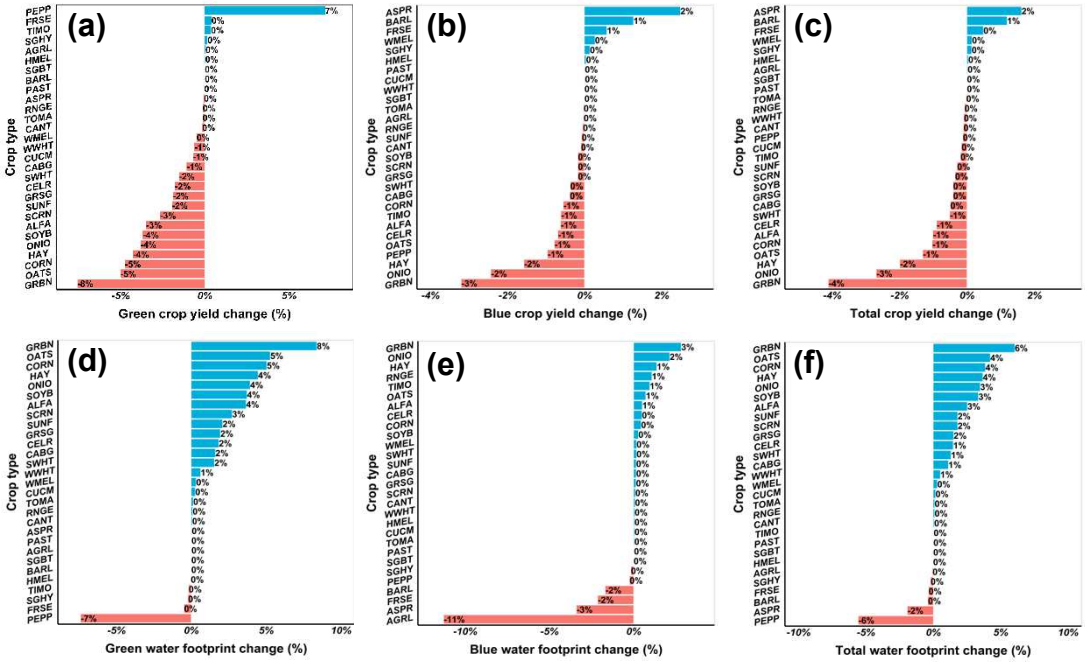


**Figure A.2.9.** Average percentage changes in (a) green crop yield, (b) blue crop yield, (c) total crop yield, (d) green water footprint, (e) blue water footprint, and (f) total water footprint of 29 crops in the LARV considering NorESM1-M-8.5 climate model and salinity stress by 2100.

**A.3**. Plots show corn and alfalfa yields, under the salinity stress, five GCM climate model, and 5-20% increase in irrigation efficiency and 5-20% reduction in irrigation water loss relative to baseline by the year 2100.

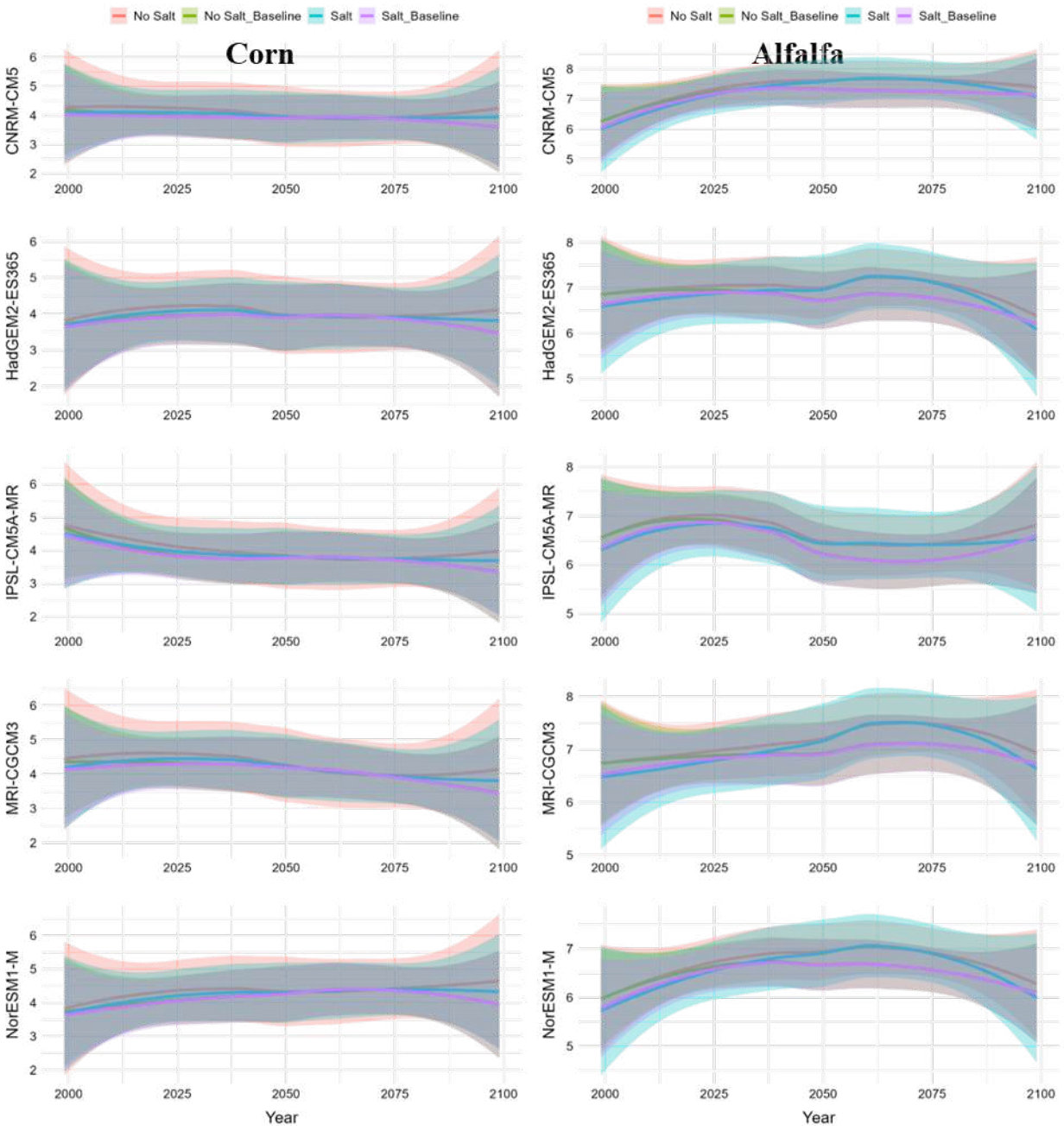


**Figure A.3.1** Plots above show corn and alfalfa yields, under the salinity stress, five GCM climate model, RCP4.5, and the irrigation practice scenario (1) 5% increase in irrigation efficiency and 5% reduction in irrigation water loss relative to baseline by the year 2100.

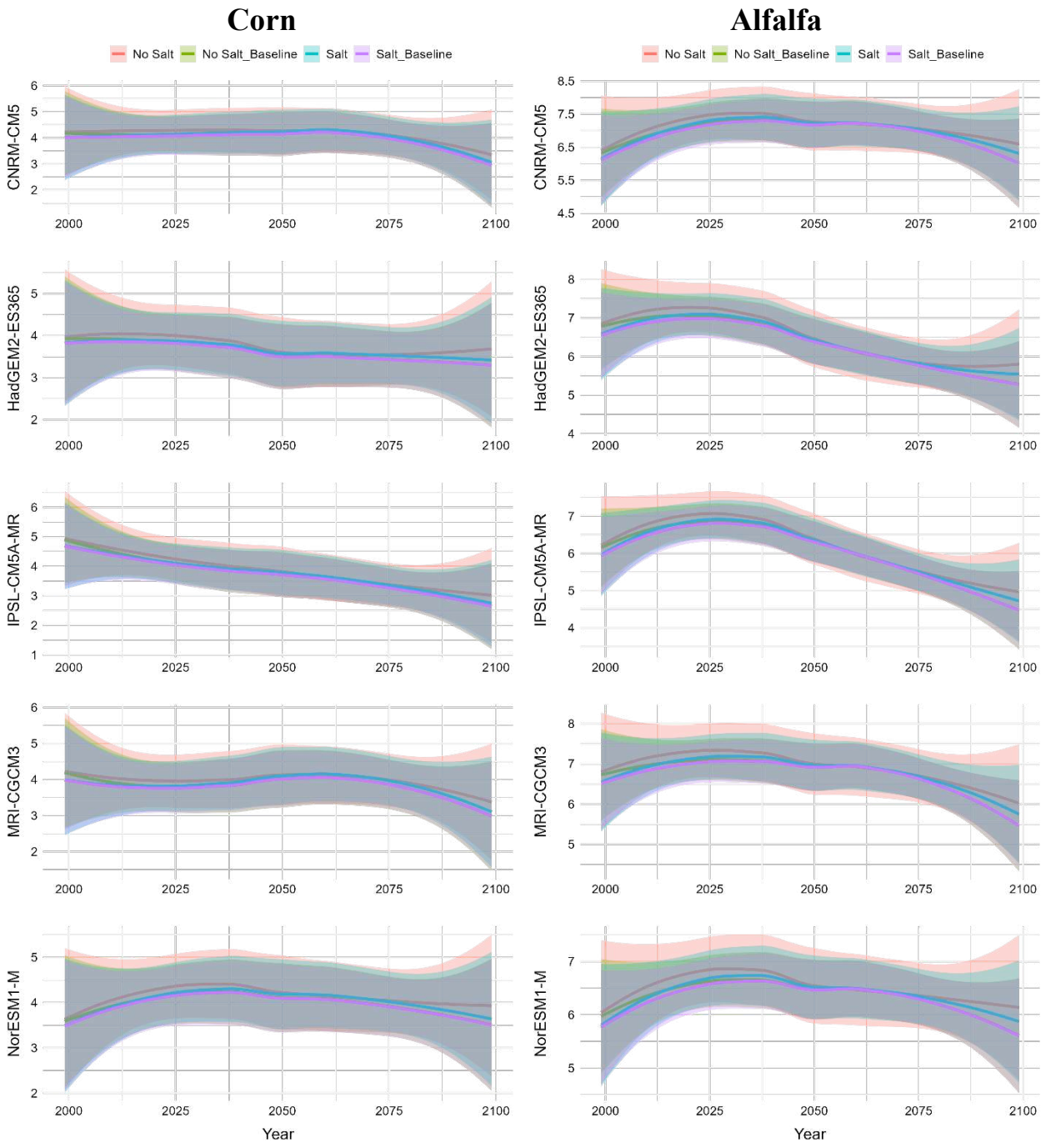


**Figure A.3.2** Plots above show corn and alfalfa yields, under the salinity stress, five GCM climate model, RCP8.5, and the irrigation practice scenario (1) 5% increase in irrigation efficiency and 5% reduction in irrigation water loss relative to baseline by the year 2100.

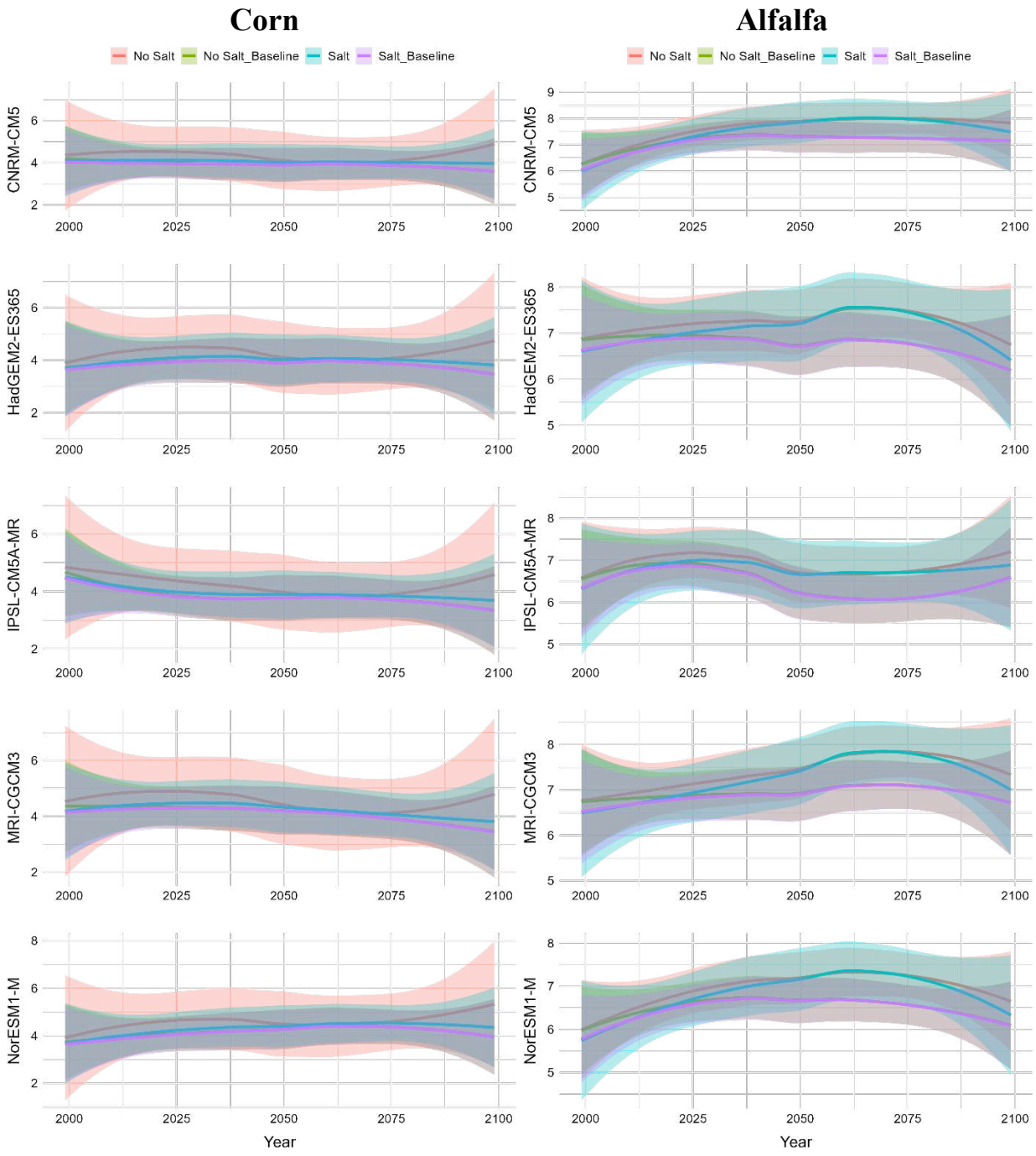


**Figure A.3.3** Plots above show corn and alfalfa yields, under the salinity stress, five GCM climate model, RCP4.5, and the irrigation practice scenario (1) 10% increase in irrigation efficiency and 10% reduction in irrigation water loss relative to baseline by the year 2100.

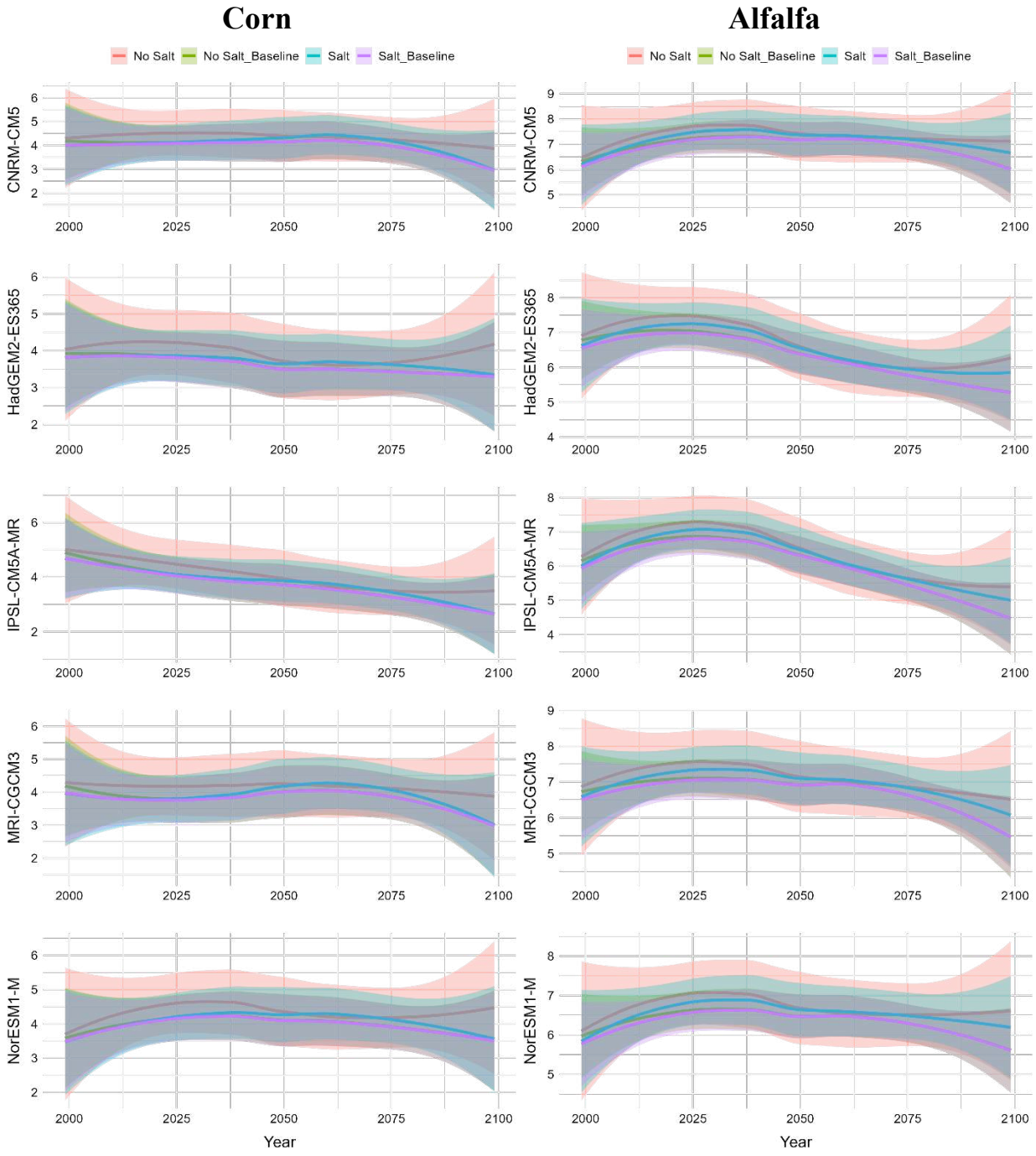


**Figure A.3.4** Plots above show corn and alfalfa yields, under the salinity stress, five GCM climate model, RCP8.5, and the irrigation practice scenario (1) 10% increase in irrigation efficiency and 10% reduction in irrigation water loss relative to baseline by the year 2100.

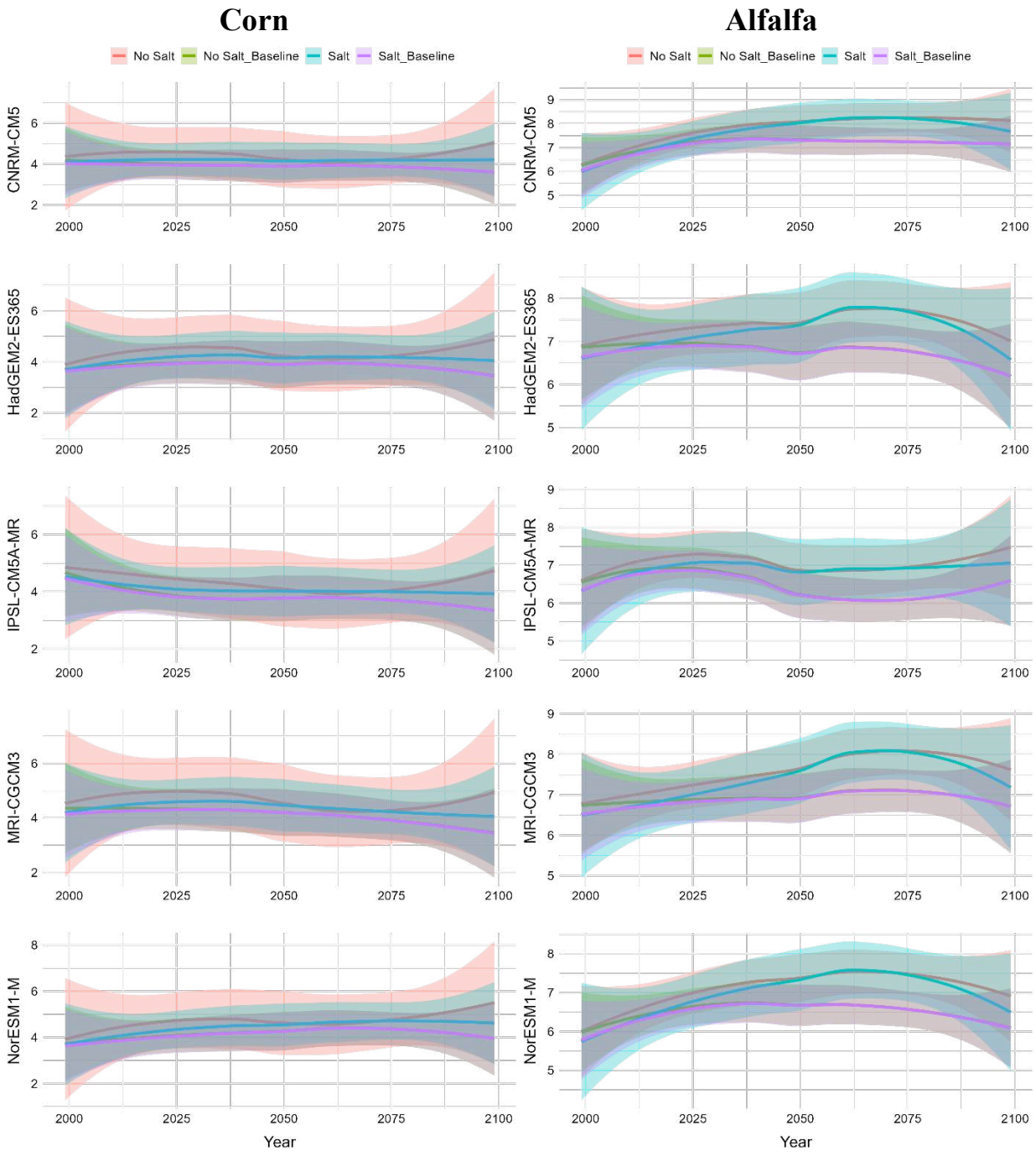


**Figure A.3.5** Plots above show corn and alfalfa yields, under the salinity stress, five GCM climate model, RCP4.5, and the irrigation practice scenario (1) 15% increase in irrigation efficiency and 15% reduction in irrigation water loss relative to baseline by the year 2100.

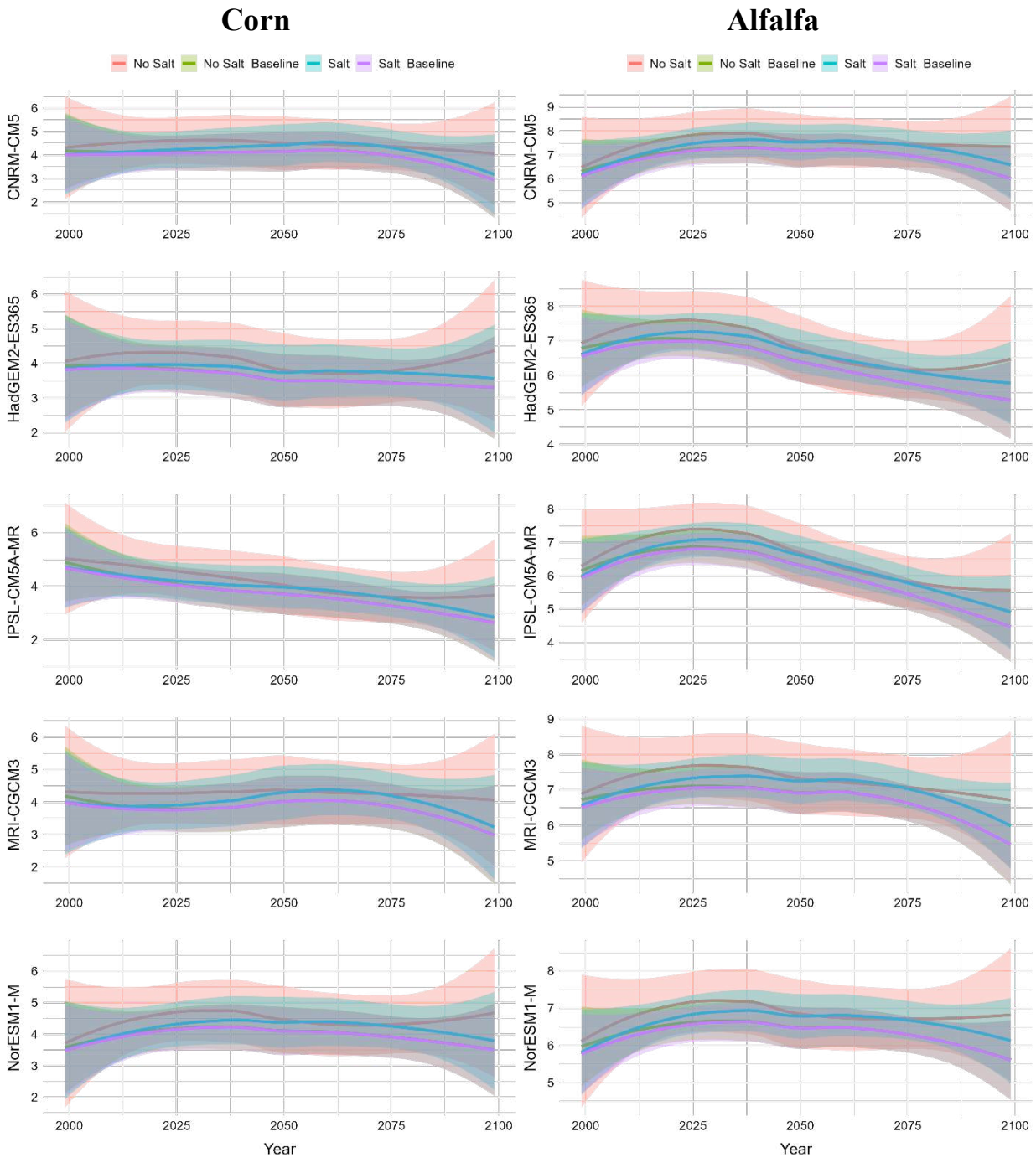


**Figure A.3.6** Plots above show corn and alfalfa yields, under the salinity stress, five GCM climate model, RCP8.5, and the irrigation practice scenario (1) 15% increase in irrigation efficiency and 15% reduction in irrigation water loss relative to baseline by the year 2100.

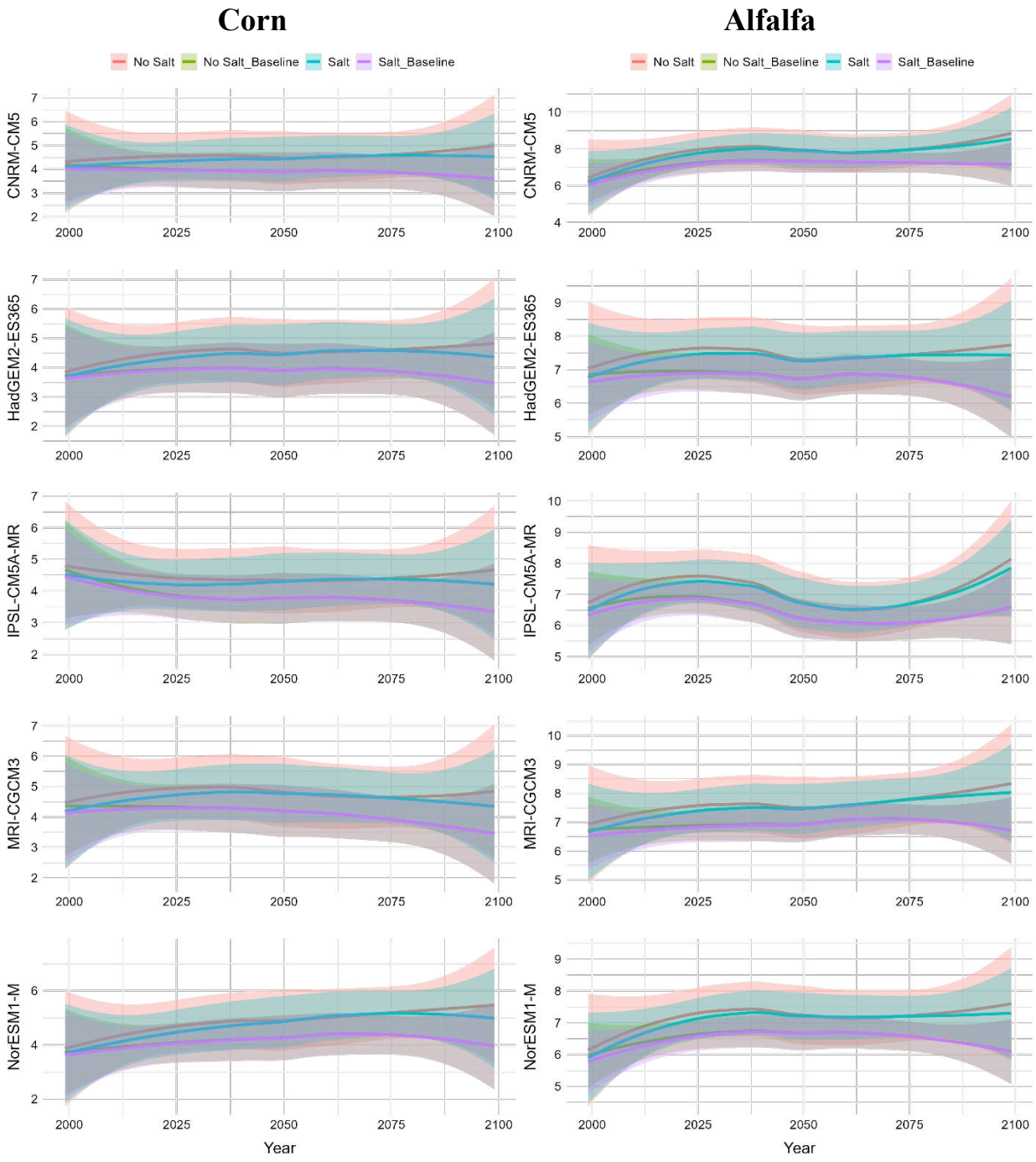


**Figure A.3.7** Plots above show corn and alfalfa yields, under the salinity stress, five GCM climate model, RCP4.5, and the irrigation practice scenario (1) 20% increase in irrigation efficiency and 20% reduction in irrigation water loss relative to baseline by the year 2100.

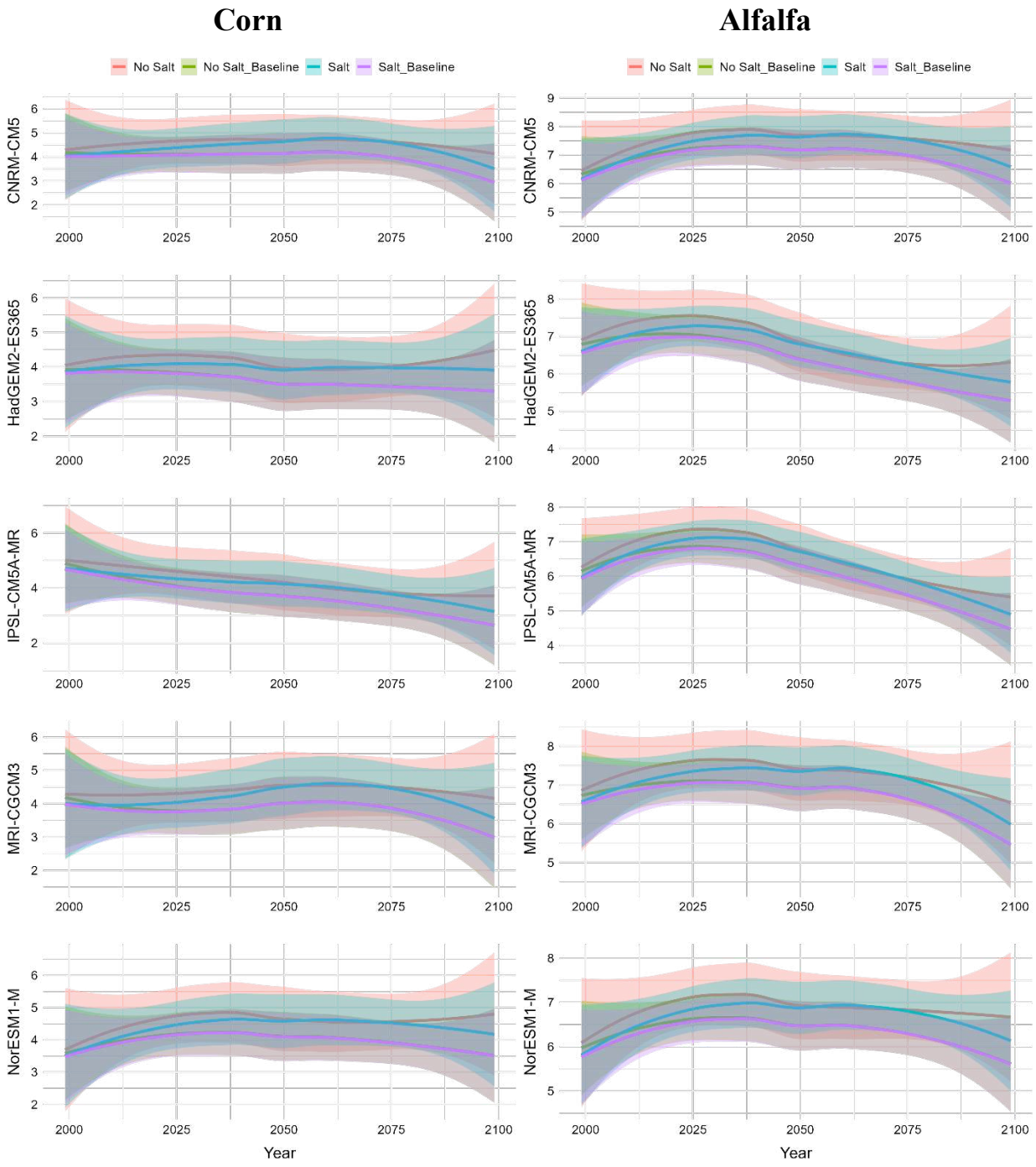


**Figure A.3.8** Plots above show corn and alfalfa yields, under the salinity stress, five GCM climate model, RCP8.5, and the irrigation practice scenario (1) 20% increase in irrigation efficiency and 20% reduction in irrigation water loss relative to baseline by the year 2100.

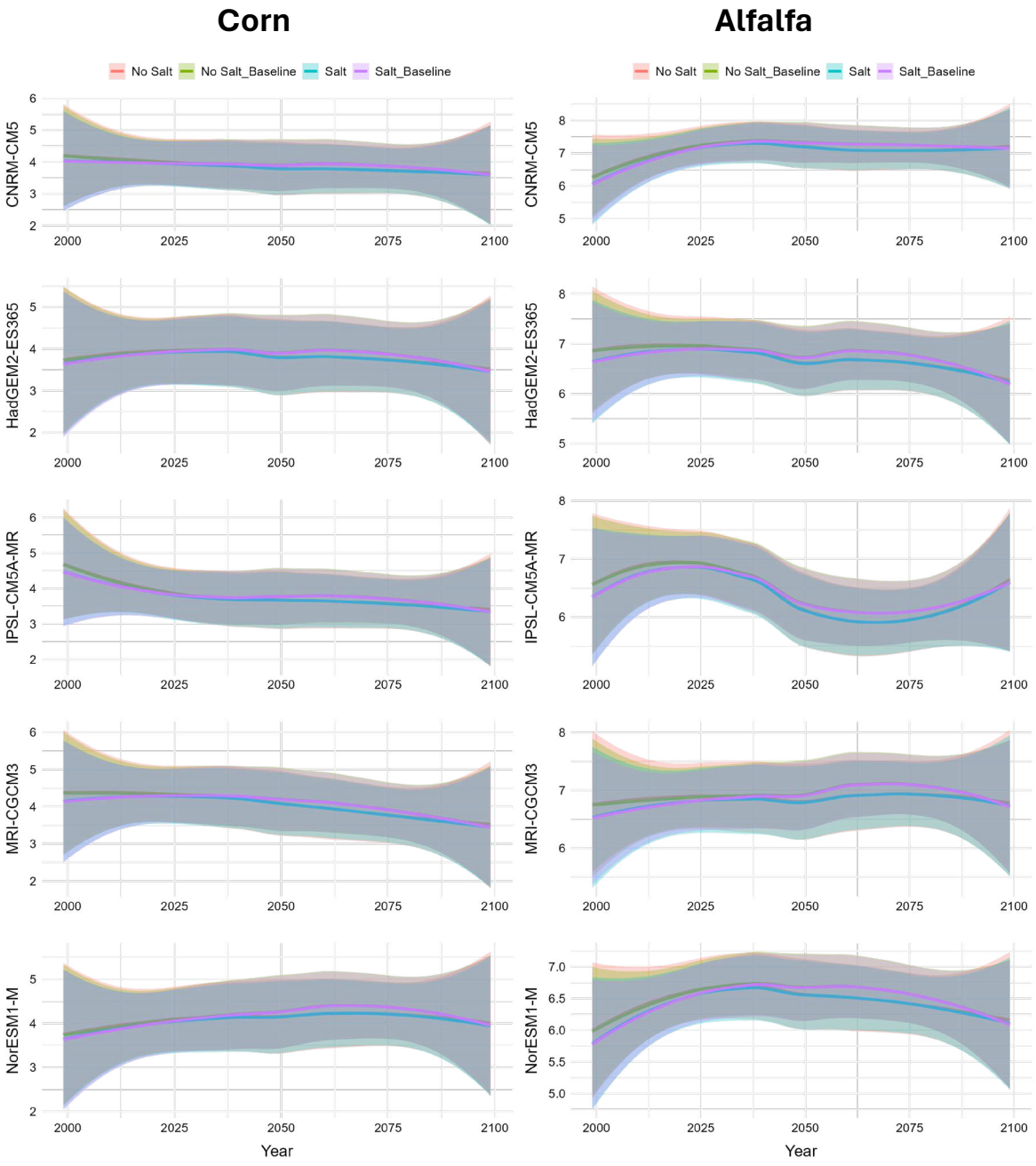


**Figure A.3.9** Plots above show corn and alfalfa yields, under the salinity stress, five GCM climate model, RCP4.5, and the irrigation practice scenario (2) 5% increase in irrigation efficiency and 5% reduction in irrigation water loss relative to baseline by the year 2100.

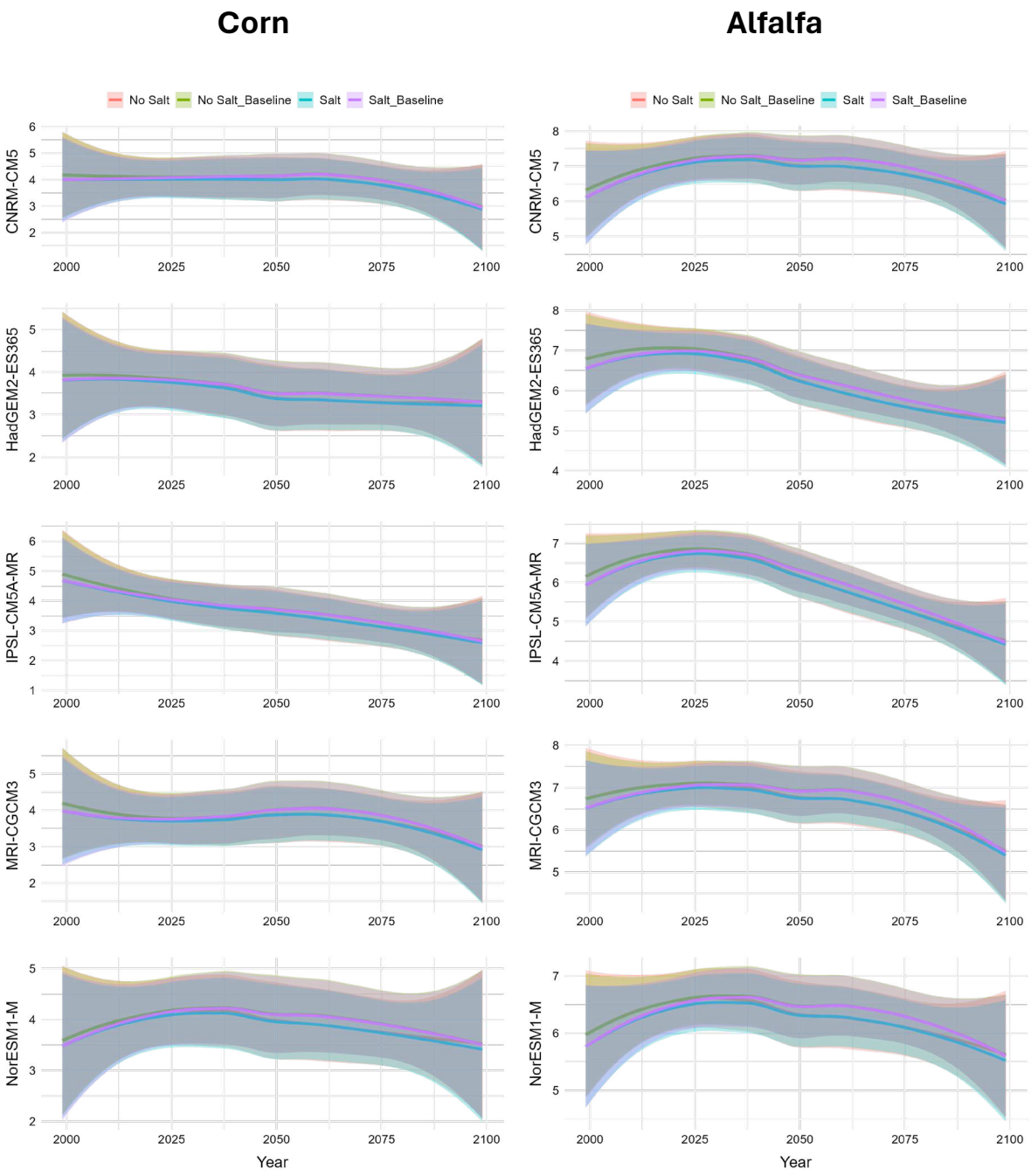


**Figure A.3.10** Plots above show corn and alfalfa yields, under the salinity stress, five GCM climate model, RCP8.5, and the irrigation practice scenario (2) 5% increase in irrigation efficiency and 5% reduction in irrigation water loss relative to baseline by the year 2100.

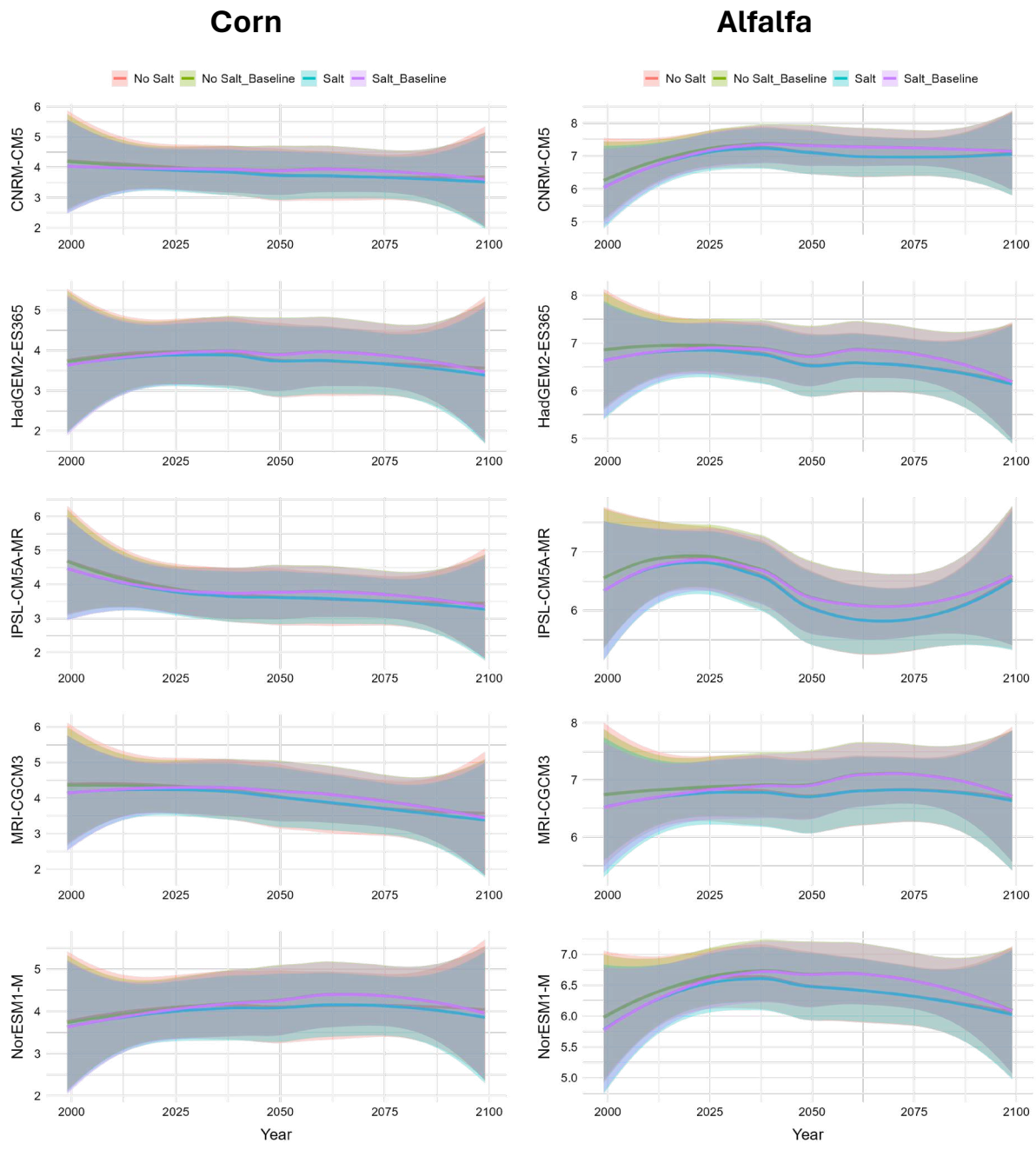


**Figure A.3.11** Plots above show corn and alfalfa yields, under the salinity stress, five GCM climate model, RCP4.5, and the irrigation practice scenario (2) 10% increase in irrigation efficiency and 10% reduction in irrigation water loss relative to baseline by the year 2100.

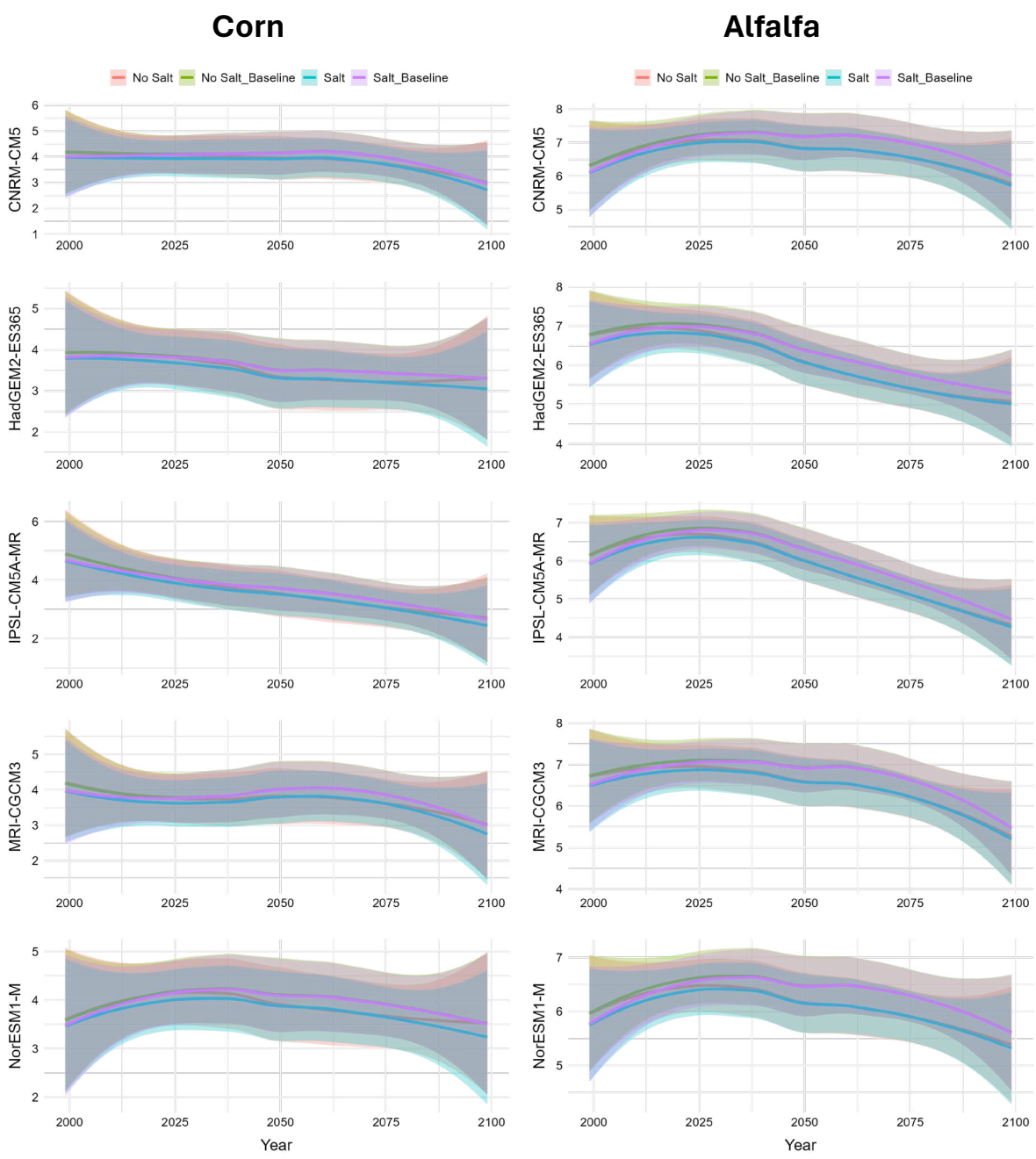


**Figure A.3.12** Plots above show corn and alfalfa yields, under the salinity stress, five GCM climate model, RCP8.5, and the irrigation practice scenario (2) 10% increase in irrigation efficiency and 10% reduction in irrigation water loss relative to baseline by the year 2100.

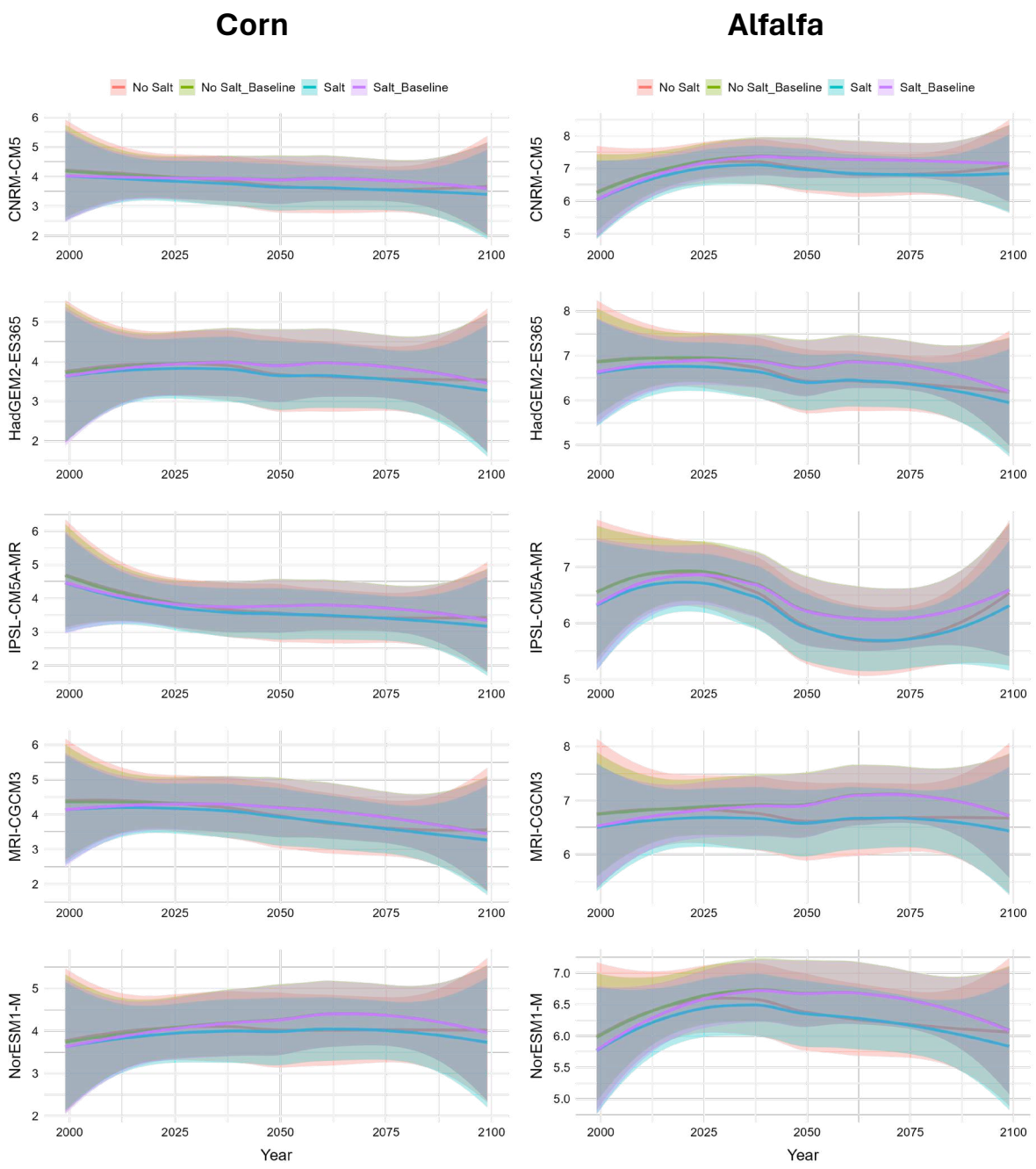


**Figure A.3.13** Plots above show corn and alfalfa yields, under the salinity stress, five GCM climate model, RCP4.5, and the irrigation practice scenario (2) 15% increase in irrigation efficiency and 15% reduction in irrigation water loss relative to baseline by the year 2100.

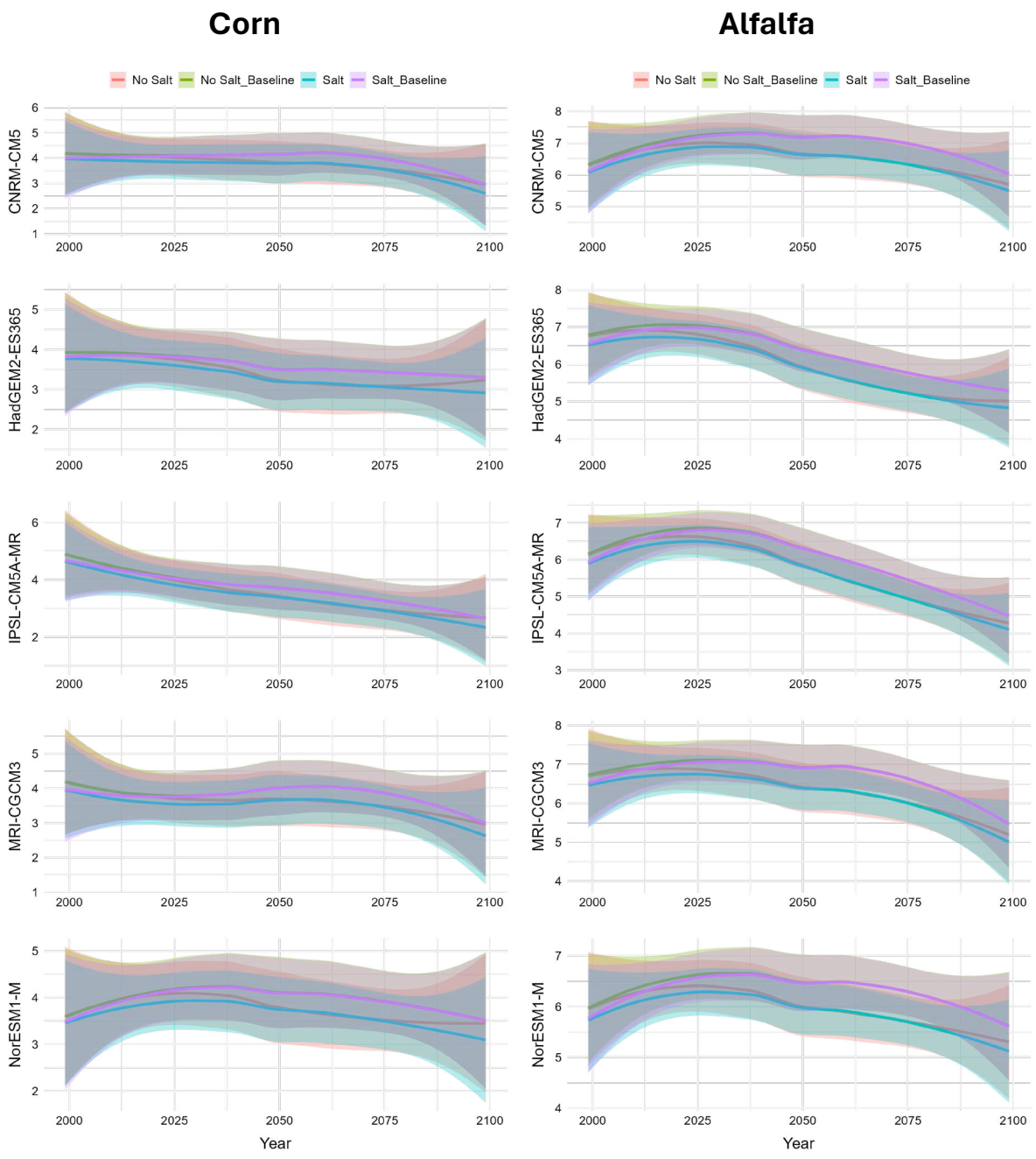


**Figure A.3.14** Plots above show corn and alfalfa yields, under the salinity stress, five GCM climate model, RCP8.5, and the irrigation practice scenario (2) 15% increase in irrigation efficiency and 15% reduction in irrigation water loss relative to baseline by the year 2100.

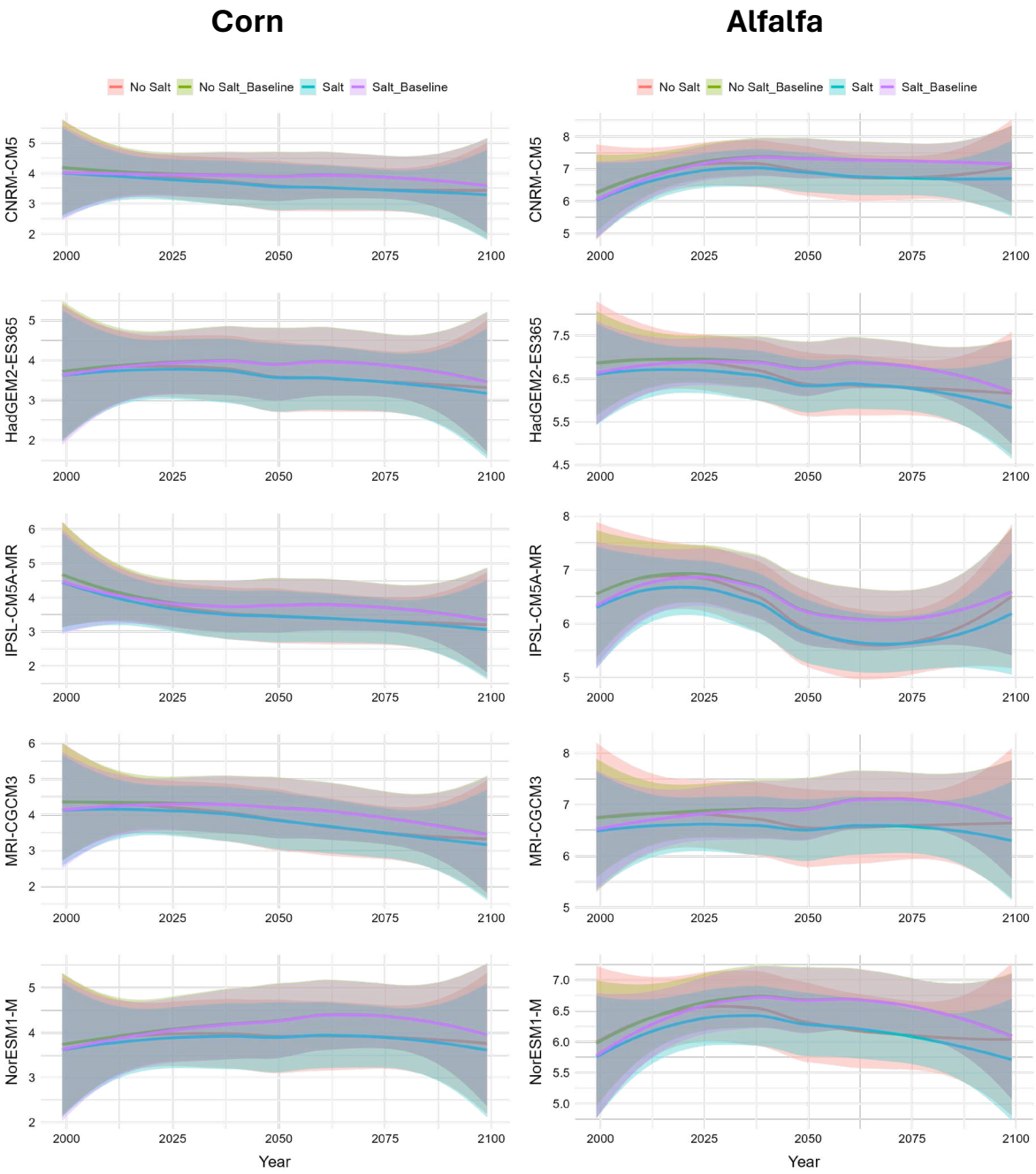


**Figure A.3.15** Plots above show corn and alfalfa yields, under the salinity stress, five GCM climate model, RCP4.5, and the irrigation practice scenario (2) 20% increase in irrigation efficiency and 20% reduction in irrigation water loss relative to baseline by the year 2100.

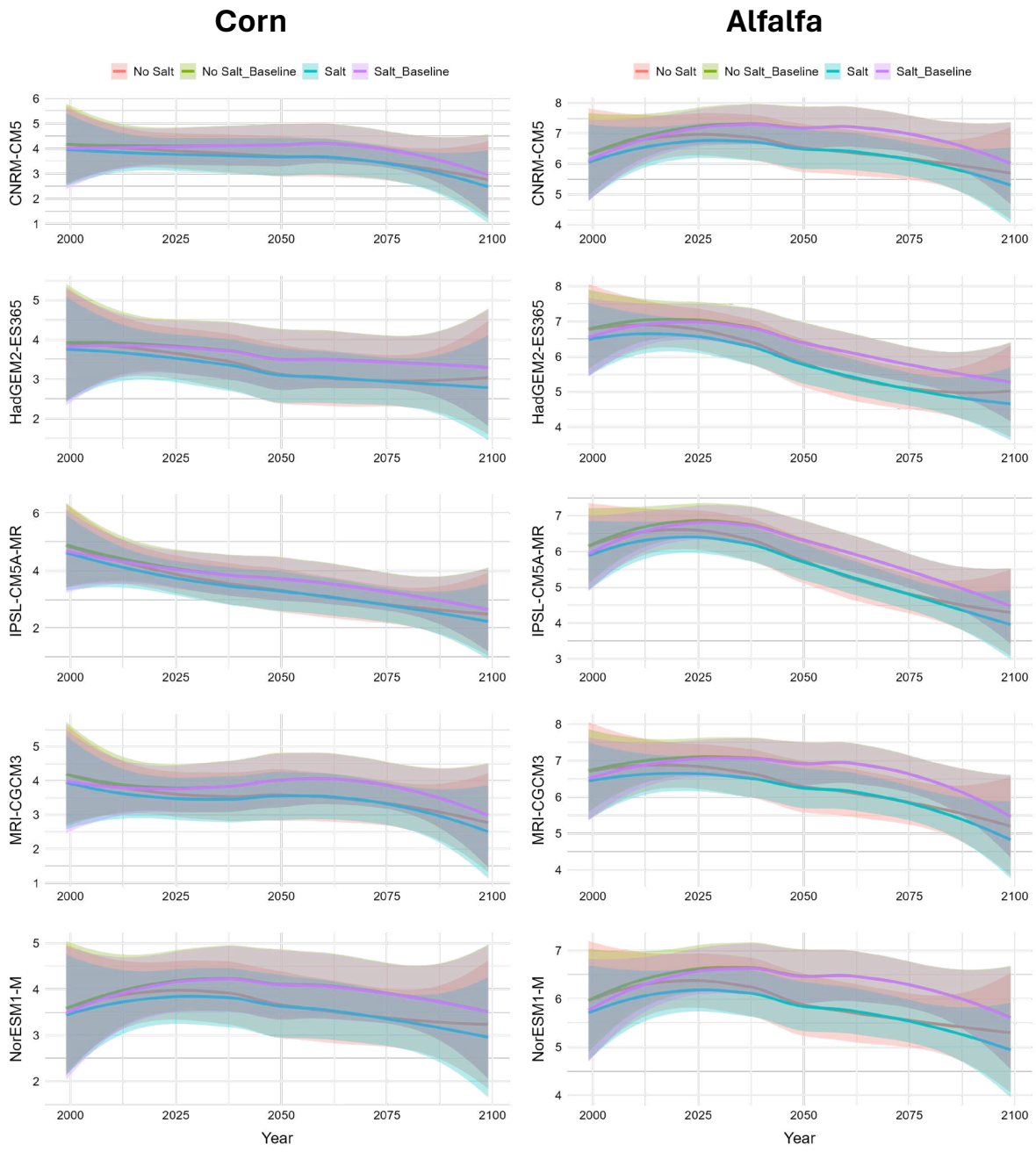


**Figure A.3.16** Plots above show corn and alfalfa yields, under the salinity stress, five GCM climate model, RCP8.5, and the irrigation practice scenario (2) 20% increase in irrigation efficiency and 20% reduction in irrigation water loss relative to baseline by the year 2100.